Title
Platelet Contributions to Cardiovascular Remodeling in Chronic Kidney Disease

Author
Velasquez-Mao, Aaron Jeffrey

Publication Date
2021

Peer reviewed|Thesis/dissertation

Platelet Contributions to Cardiovascular Remodeling in Chronic Kidney Disease

by

Aaron Jeffrey Velasquez-Mao

A dissertation submitted in partial satisfaction of the

requirements for the degree of

Joint Doctor of Philosophy

with University of California, San Francisco

in

Bioengineering

in the

Graduate Division

of the

University of California, Berkeley

Committee in charge:

Professor Moriel H. Vandsburger, Chair
Professor Nicholas T. Ingolia
Professor Tamara Alliston, UCSF

Fall 2021

Abstract

Platelet Contributions to Cardiovascular Remodeling in Chronic Kidney Disease

by

Aaron Jeffrey Velasquez-Mao

Joint Doctor of Philosophy in Bioengineering

University of California, Berkeley and University of California, San Francisco

Professor Moriel H. Vandsburger, Chair

Chronic kidney disease (CKD) patients on hemodialysis (HD) suffer elevated mortality from cardiovascular disease (CVD) linked to accumulating uremic toxicity. Recent findings in cardiac MRI indicate earlier fibrosis and hypertrophy in CKD patients, challenging the traditional belief that cardiorenal syndrome develops secondary to uremia and hypervolemia, inciting the need to re-explore CVD pathogenesis as a result of CKD. Platelets present a promising link between CKD and CVD as rich sources of tissue regulators that are abnormally stimulated during HD. However, while activation of circulating platelets by receptor binding and subsequent coagulation events are defined by a well characterized physiological response, the mechanobiology of platelet degranulation is comparatively unexplored. I hypothesized that the observed early cardiac remodeling in HD patients is in part caused by HD-aggravated platelet dysregulation leading to non-uremic circulatory imbalances. To test this, I proposed 1) characterizing the effects of HD on platelets and the circulating proteome, 2) mechanistically studying platelet activation in response to the fluidic stimulus of depressurization experienced by frictional loss along the HD flow circuit, and 3) visually observing fibrotic developments in cardiac tissues in vitro as a result of contact with platelets of varying dysregulation.

In the first study, plasma and platelets from end stage renal disease (ESRD) patients before and after HD were profiled for proteome and transcriptome growth factors (PDGF, FGF, EGF), proteolytic regulators (MMPs, TIMPs), coagulative factors (vWF, PAF, PF4), cardiac indicators (BNP, TPO, TXA_2), and inflammatory markers (CRP, TNFα, IL1b) to examine HD-modulation of platelet effects beyond thrombotic activation. Elevation of plasma proteolytic regulators, fibrotic factors, and corresponding platelet RNA transcripts revealed uniquely pro-fibrotic platelet phenotypes in ESRD patients during HD. Correlations against prior time on dialysis (HD vintage) and blood flow rate (BFR) indicated worsening dysfunction with longer HD vintage and faster prescribed BFR, particularly characterized by preferentially enhanced translation and secretion of matrix metalloproteinases (MMP), tissue inhibitors of MMPs (TIMP), and

inflammatory cytokines. Compensatory mechanisms of increased platelet growth factor synthesis with acute plasma MMP and TIMP increases show short-term mode-switching between dialysis sessions leading to long-term pro-fibrotic bias. Chronic pro-fibrotic adaptation of platelet synthesis was observed through changes in differential secretory kinetics of heterogeneous granule subtypes. Chronic and acute platelet responses to HD describe contributions to a pro-fibrotic milieu in ESRD.

In the second study, platelets from healthy and HD (pre- and post-treatment) donors were cyclically depressurized in static suspension to mimic the precipitous and repetitive pressure drops across the hemodialysis flow circuit. Platelet activation was measured by integrin complexing of the traditional coagulative indicator glycoprotein αIIbβ3 (PAC1) and expression of the granule surface receptor P-selectin (CD62P). The progressive increase in CD62P with no changes in PAC1 over pressure-cycling duration regardless of uremia signifies that hydrostatic depressurization involves a novel agonist-free mechanism leading to platelet degranulation as a unique case in which CD62P and PAC1 do not interchangeably indicate platelet activation. Subsequent stimulation using ADP further suggests that sustained depressurization regimens desensitize integrin αIIbβ3 activation. Variability in platelet response caused by uremia and CKD were observed by elevated baseline PAC1 in pre-dialysis samples, PAC1 retention after ADP exposure, and maximum CD62P with ADP independent of pressure. Theory for hydrostatic pressure-induced degranulation circumventing integrin-initiated signal transduction is presented based on the Starling Equation.

In the third study, induced pluripotent stem cell derived cardiomyocyte tissues were cultured with plasma and platelets from hemodialysis donors pre- and post-filtration, healthy donor plasma and platelets, and continuation media. Spontaneously contracting tissues from all test groups were visually analyzed daily for changes in troponin muscular network and functional contractile output and lysed after 28 days of culture for matricellular protein composition. Cardiac tissues developed more fibrotic phenotypes in dialysis derived media, with amplified compositional and structural changes by refreshed post-dialysis platelets over exhausted and uremic pre-dialysis platelets, illustrating a direct link bridging platelet dysfunction to the clinical outcomes of deteriorative cardiac fibrogenesis observed in the REMODELING clinical trial. Separately, healthy plasma and platelets enhanced cardiac maturity, suggesting promising implications for the tissue engineering toolbox.

Collectively, these studies depict how platelets contribute to CVD progression in CKD. The identification of unique pro-fibrotic platelet phenotypes in ESRD independent of uremic state, a novel mechanism of platelet degranulation independent of chemical stimulus, and direct visual observation of platelet-dependent cardiovascular remodeling establish a distinct pathway explaining the manifestation of uremic cardiomyopathy independent of hemodynamic overload. Future use of platelets as therapeutic agents and diagnostic tools for left ventricular remodeling, microvascular dysfunction, and myocardial interstitial fibrosis could aid the prevention of congestive heart failure.

Dedicated to the one who sleeps at my feet

Her eyes concealing nothing

Plagued by nothing

My best friend

Red

Acknowledgements

I am deeply grateful to everyone who has mentored and supported me along this journey. Natalie, who was there for me when I witnessed a traumatic shooting, forced me to go to the ER when I was attacked by raccoons, and took care of me when I got hit by a car. My PI, Dr. Moriel Vandsburger, who believed in me, gave me a problem to become passionate about, and trusted me with the resources to do the science I cared most about. Drs. Dorian Liepmann, Steve Conolly, Nick Ingolia, Ruth Dubin, and Tamara Alliston for their generosity and mentorship that made me a better scientist. Drs. Tamara Alliston and D'Anne Duncan at UCSF for supporting me in my first year transition to the Bay Area. My undergraduate mentors Drs. Jeffrey Jacot, Guy Genin, Elliot Elson, and Veronique Kugener who gave me a chance to prove myself. Drs. Chris Tsao and Behzad Babaei, who as graduate students mentored and inspired me to pursue research during my bachelor degree. Dr. Mary West who taught me how to use the proteomics, microscopy, and flow cytometry equipment in the QB3 core facilities. Dr. Paul Lum who helped me navigate the microfabrication equipment in the BNC.

I also want to acknowledge my funding sources through the UCSF IMSD Fellowship, the NSF GRFP, and the Lewis Scholar Award. It has been an immense honor to be a part of these cohorts, and as with all listed above, I hope I have made you proud.

Contributions

My work is co-authored with the following on previous and upcoming manuscripts, comprising chapters 2 through 4 of this dissertation.

Velasquez-Mao AJ, Velasquez MA, Hui Z, Armas-Ayon D, Wang J, Vandsburger MH. Hemodialysis exacerbates proteolytic imbalance and pro-fibrotic platelet dysfunction. Scientific reports. 2021 Jun 3;11(1):1-4.

Velasquez-Mao AJ, Velasquez MA, Vandsburger MH. Cyclical depressurization degranulates platelets in an agonist-free mechanism of platelet activation. In review.

Velasquez-Mao AJ, Ayala C, Lam B, Velasquez MA, Vandsburger MH. Plasma and platelet culture of iPSC-derived cardiomyocytes: tracking cardiac tissue remodeling by hemodialysis patient blood. In submission.

Table of Contents

List of Figures

List of Tables

List of Abbreviations

ACD-A	Anticoagulant Citrate Dextrose Solution, Solution A
ADMA	asymmetric dimethylarginine
ADP	adenosine diphosphate
AGEs	advanced glycosylation end products
ANOVA	analysis of variance
ATP	adenosine triphosphate
B2M	beta-2-microglobulin
BCA	bicinchoninic acid
BFR	blood filtration rate
BPA	bisphenol A
BSL2	biosafety level 2
CD62P	P-Selectin
CF	cardiac fibroblast
CKD	chronic kidney disease
CM	cardiomyocyte
CRP	c-reactive protein
CRS	cardiorenal syndrome
CTGF	connective tissue growth factor
cTn	cardiac troponin
CVD	cardiovascular disease
ECM	extracellular matrix
EDTA	ethylenediaminetetraacetic acid
EGF	epidermal growth factor
ELISA	enzyme-linked immunoassay
ESRD	end stage renal disease
FAP	fibroblast activation protein
FGF	fibroblast growth factor
FSC	forward-scatter
FWHM	full-width at half max
GAPDH	glyceraldehyde 3-phosphate dehydrogenase
GF	growth factor
GFP	green fluorescent protein
GFR	glomerular filtration rate
GP	glycoprotein
HD	hemodialysis
hESC	human embryonic stem cells
IFNγ	interferon gamma
IGF1	insulin-like growth factor 1
IL1β	interleukin 1 beta
iPSC	induced pluripotent stem cells
IRB	Institutional Review Board
IS	indoxyl sulfate
KDIGO	Kidney Disease: Improving Global Outcomes
LAP	latency-associated peptide
LDL	low-density lipoprotein
LVH	left ventricular hypertrophy
MK	megakaryocytes
MMP	matrix metalloproteinases
NIDDK	National Institute of Diabetes and Digestive and Kidney Diseases
NO	nitrous oxide
NTpBNP	N-terminal prohormone of brain natriuretic peptide
PAC1	activated GPIIb/IIIa integrin complex
PAF	platelet-activating factor
PAN	polyacrylonitrile
PCR	polymerase chain reaction
pCS	p-cresol sulfate
PDGF	platelet-derived growth factor
PDGFRA	platelet-derived growth factor receptor A
PE	polyethylene
PES	polyethersulfone
PF4	platelet factor 4
PGE1	prostaglandin E1
PGI2	prostacyclin
POSTN	periostin
PPBP	pro-platelet basic protein
PRP	platelet-rich plasma
PTH	parathyroid hormone
PVC	polyvinyl chloride
PVDF	polyvinylidene fluoride
RAAS	renin–angiotensin–aldosterone system
RGD	Arg-Gly-Asp
ROCK	rho kinase
ROS	reactive oxygen species
RT	room-temperature
SDS	sodium dodecyl sulfate
SSC	side-scatter
TCF21	transcription factor 21
TGFβ1	transforming growth factor beta-1
TIMP	tissue inhibitor of MMP
TNFR1	tumor necrosis factor receptor 1
TNFα	tumor necrosis factor alpha
TPO	thrombopoietin
TX	thromboxane
USRDS	United States Renal Data System
vWF	von Willebrand Factor
WB	western blot
WISP1	WNT1-inducible-signaling pathway protein 1
β-TG	beta-thromboglobulin

Chapter 1

Introduction

Chronic Kidney Disease

Chronic kidney disease (CKD) is a global public health problem, characterized by progressive loss of kidney function culminating in end stage renal disease (ESRD). In the United States, CKD has an estimated prevalence of 15%, based on the USRDS 2020 Annual Data Report conducted by the NIDDK, and a 5-year survival rate on dialysis of 35% that decreases to 25% in diabetic CKD[1,2]. CKD most greatly affects the elderly population, with a 9% prevalence in adults below the age of 65 that increases to 39% above the age of 65. However, other risk factors include sex, race, diabetes, hypertension, cardiovascular disease, and body mass index. While prevalence has remained relatively stable for the past two decades, the shifting distribution towards stage 3 CKD according to the National Health & Nutrition Examination Surveys and disproportionately high incidence in black communities make understanding CKD pathogenesis and related mortalities increasingly urgent sociomedical issues.

The kidneys essentially function to eliminate waste from the blood stream while stabilizing circulating water and solute concentrations. The structure of the nephron, the basic renal filtration unit, enables diffusive concentration gradients and high surface area for active transport. In CKD, damage occurs in the glomeruli, at the capillary interface. Sustained pressurization by hypertension, diabetes, and elevated blood sugar, decreased perfusion by severe dehydration or episodes of shock, and the accumulation and deposition of amyloids, lipids, and granulomas can all contribute to glomerular injury. Ordinarily, the glomeruli have an exceptional range of pressure autoregulation, including by nervous regulation of arteriole constriction and humoral regulation by the renin-angiotensin-aldosterone system (RAAS). As a result, measurable increases in plasma urea and creatinine are typically not significantly damaging until there is a 50% or greater reduction in filtration rate[3]. However, sustained pressurization concurrent to clogging at the glomerular capillaries results in compensatory hyperfiltration leading to long term damage. CKD etiology is observed by progressive dysfunction that manifests by obstructive capillary damage, hypertrophy of the epithelium, and focal segmental glomerular sclerosis which all act to increase filtration resistance.

CKD diagnosis is stratified by albuminuria levels and glomerular filtration rate (GFR), estimated by serum creatinine, age, weight, and sex. Albuminuria indicates protein leakage from glomerular injury, while creatinine, a metabolic waste product from creatine phosphate, reliably correlates to volumetric flow through the glomeruli as a small molecule that is exclusively passively transported[4]. **Figure 1.1** depicts prognosis of CKD by GFR and albuminuria measurements.

Prognosis of CKD by GFR and albuminuria categories: KDIGO 2012				Persistent albuminuria categories Description and range		
				A1	A2	A3
				Normal to mildly increased	Moderately increased	Severely increased
				< 30 mg/g < 3 mg/mmol	30–300 mg/g 3–30 mg/mmol	> 300 mg/g > 30 mg/mmol
GFR categories (ml/min/1.73 m²) Description and range	G1	Normal or high	≥ 90			
	G2	Mildly decreased	60–89			
	G3a	Mildly to moderately decreased	45–59			
	G3b	Moderately to severely decreased	30–44			
	G4	Severely decreased	15–29			
	G5	Kidney failure	< 15			

Figure 1.1. Prognosis of CKD by GFR and albuminuria measurements. From [4], Kidney Disease: Improving Global Outcomes (KDIGO) CKD Work Group, 2012. Green: low risk of CKD. Yellow: moderately increased risk. Orange: high risk. Red: very high risk.

CKD is stratified by five stages. Stage 1 CKD consists of kidney damage with normal or increased GFR (>90 mL/min/1.73 m 2). Stage 2 consists of mild reduction in GFR (60-89 mL/min/1.73 m^2). Stage 3a consists of moderate reduction in GFR (45-59 mL/min/1.73 m^2). Stage 3b consists of moderate reduction in GFR (30-44 mL/min/1.73 m^2). Stage 4 consists of severe reduction in GFR (15-29 mL/min/1.73 m^2). Stage 5 consists of kidney failure (GFR < 15 mL/min/1.73 m^2)[4]. Dialysis is typically initiated upon diagnosis of ESRD at stages 4 or 5.

Other markers of CKD severity include low levels of bicarbonate (HCO_3) which indicates malnutrition and reduced metabolism, high levels of c-reactive protein (CRP) which indicates oxidative damage and inflammation, and low vitamin D which is produced in the kidneys[5,6]. Separately, low vitamin D, or calcifediol, is associated with CKD-mineral and bone disorder because of its intricate relationship in regulating vascular solubility of calcium and phosphate with parathyroid hormone (PTH) and fibroblast growth factor 23 (FGF23). Dysregulation of these factors leads to vascular calcification, a major contributor to various cardiovascular diseases.

Therapeutic options for CKD are extremely limited, consisting of either renal transplant or dialysis. Considering the shortage of transplant donors, dialysis is in most cases the only viable solution for disease management. Among dialysis options, hemodialysis is more frequently used over peritoneal dialysis[1]. While median overall survival of hemodialysis (37 months) exceeds that of peritoneal dialysis (20 months), the lack of randomized clinical trials, existence of conflicting studies, and biases caused by access and education render comparison inconclusive[7]. Because hemodialysis is more frequently used over peritoneal dialysis at approximately 9:1, studies herein are designed to focus on the former.

Cardiorenal Syndrome

Cardiovascular disease (CVD) rather than renal failure is the predominant cause of death in CKD patients. CVD is present in a majority of patients on dialysis, and CVD related mortalities are 20 times more frequent than the general population[8]. Among CKD-CVD, hypertension presents in 90% of patients, left ventricular hypertrophy presents in 70%, coronary artery disease presents in 40%, and 35% have an ischemic event. This effect, similar to CKD-caused bone disorders, of chronic dysfunction of the kidneys causing acute or chronic dysfunction of the cardiovascular system is defined by cardiorenal syndrome (CRS).

The pathophysiology of CRS is multiform and complex[9]. From a purely uremic standpoint, sodium and water overload from reduced filtration causes peripheral and pulmonary edema, hypertension, and cardiac congestion. Metabolic acidosis by the accumulation of phosphates, sulfates, and organic anions can lead to poor nitrogen balance, protein degradation, and amino acid oxidation as well as bone mineral loss, which can in turn further disrupt mineral metabolism as observed in the calcifediol-PTH-FGF23 dysregulation of renal bone disease. Hyperphosphatemia causes vascular calcification and stiffening. Reduced secretion of renal factors like erythropoietin causes anemia, muscle weakness, and atrophy.

The buildup of retained toxins, oxidative stress, chronic inflammation, and vascular remodeling constitute a worsening cycle of accumulating toxicity[9]. Urea degrades to cyanate, which reacts with amine groups to break down the gastrointestinal epithelium to cause inflammation, oxidizes low-density lipoprotein (LDL) to reduce tissue elasticity, accelerates amyloid production from albumin, and carbamylates erythropoietin to drive anemia. Other uremic retention compounds like p-cresol sulfate (pCS) and indoxyl sulfate (IS) comprise a group of molecules called advanced glycosylation end products (AGEs) formed by Maillard reactions that trigger intra-cellular events leading to oxidation and inflammation[10]. pCS induces endothelial cell dysfunction via rho-kinase toxicity, while IS can trigger a chronic immune response. Oxidative stress by reactive oxygen species (ROS) like asymmetric dimethylarginine (ADMA) causes endothelial damage. Because the kidneys are an important source of antioxidant enzymes, accumulation of ROS leads to impairment of nitrous oxide (NO), a key inhibitor of platelet activation at vascular walls. Chronic inflammation by reduced NO and accumulation of

inflammatory cytokines increases platelet and leukocyte reactivity driving localized vascular remodeling[11]. Accumulation of ROS, inflammatory products, and uremic toxins prime the vasculature for remodeling and calcification. The overcompensatory production of FGF23 by osteocytes unregulated by Klotho induces hyperphosphatemia, while accumulation of PTH and deficiency of calcifediol increases blood calcium. Acidosis reduces protein-calcium binding, finally leading to a combination of Ca^{2+} and PO_4^{3-} in calcium deposition[12].

The many mechanisms driving cardiovascular remodeling culminate in heart failure by arrhythmias, congestion, and ischemia. Hyperkalemia alters cardiomyocyte action potential effecting polarization and conduction abnormalities that cause sinus tachycardia and bradycardia, idioventricular rhythm, and 1st-, 2nd-, and 3rd-degree heart block[13]. Macrovascular calcification and ventricular hypertrophy exacerbate hemodynamic overload leading to diastolic dysfunction[14]. Furthermore, a reinforcing cycle of microvascular dysfunction and myocardial interstitial fibrosis reduce coronary perfusion, enhancing all of the above[15,16]. Among these, the leading cause of death in uremic cardiomyopathy is congestive heart failure at 31% prevalence, with 50/50 categorizations of dilated and hypertrophic cardiomyopathies[17]. In essence, myocardial thickening and septal wall stiffening are thought to lead to chronic weakening of the heart with fluid overload.

Recent studies have found that left ventricular hypertrophy develops independent of hydrodynamic overload[18]. This concept of early onset of CVD before CKD progression to ESRD is reflected by how patients with relatively high GFR are significantly more likely to die of CVD than reach stage 4 CKD. Technological advances in cardiac MRI sensitivity through creatinine tracking by CEST-MRI have enabled early detection of cardiac fibrosis in the low stage CKD population[19]. These findings motivate further investigation into the non-uremic mechanisms driving CVD in CKD.

Platelet Biology

Platelets may explain the missing links regarding CVD development in early CKD and accelerated CVD progression from HD because of their role in tissue regulation and adaptation to chronic stimuli. Fragmented from megakaryocytes (MK) residing in the bones and lungs, platelets contain mRNAs and ribosomes and shift their transcriptomes and proteomes in response to activation[20,21]. Ordinary functions include wound healing by clot formation, leukocyte recruitment by cytokine and microvesicle secretion, and angiogenic matrix remodeling at sites of vascular injury[22]. However, platelets have recently garnered attention for their roles aiding tumorigenesis, endothelial injury, and systemic fibrosis by non-traditional mechanisms of dysfunction. In the progression of cancer, platelet coagulation is exploited to shroud tumor cells from immune response, while growing evidence of “tumor conditioning” of platelets utilizes their reservoirs of angiogenic proteins to aid tumor vascularization[23]. Aberrant adhesion to leukocytes forming heterotypic aggregates causes pathogenic adhesion to vascular endothelial

walls, aiding the propagation and progression of arterial atherosclerotic disease[24]. Finally, growing recognition of their immune regulation and storage of bioactive molecules involved in tissue injury and remodeling makes them suspect in vasculopathy, autoimmunity, and fibrogenesis observed in systemic sclerosis[25]. Because hemodialysis induces both hypersensitivity and thrombocytopenia in platelets[26], these same principles of non-traditional platelet dysfunction may be reasonable to apply in the pathogenesis of CVD in CKD.

To understand the basis of platelet dysfunction and phenotypic adaptation requires understanding of platelet physiology. Platelets are simple relative to eukaryotic cells as anucleate discs, approximately 2μm in diameter that circulate in the bloodstream for 5-9 days before clearance. Platelet structure is visible by cryo-electron microscopy in **Figure 1.2**[27]. Of particular note are the open canalicular system, dense tubular system, and cytoskeletal structures as enactors of active export, and alpha, delta, and gamma granules as storage for secreted factors. Platelets additionally contain ribosomes for protein translation and RNA derived from MK in the bones and lungs[28] that are protected until use in protein production[21].

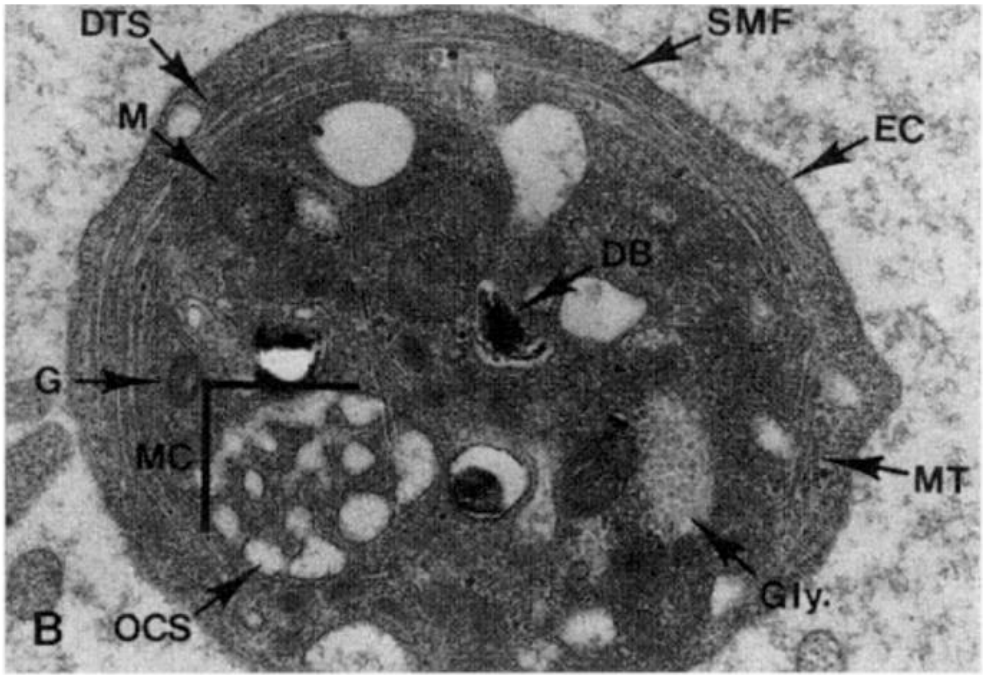

Figure 1.2. Platelet structure by cryo-electron microscopy. From [27], George M Rodgers, Clinical Obstetrics and Gynecology, 1999. (M) Mitochondria, (DTS) Dense tubular system, (SMF) Submembrane filaments, (EC) Exterior coat glycocalyx, (DB) Delta granules, (MT) Circumferential microtubules, (Gly) Glycogen, (OCS) Open canalicular system, (MC) Membrane complex, (G) Alpha granules.

In their classic function of hemostasis, platelets first recruit to the site of vascular rupture to form a plug and next build a longer lasting fibrin network[29]. Upon exposure of basal matrix in endothelial damage, platelets adhere by integrin activation of glycoproteins Ib to von Willebrand Factor (vWF) and exposed Arg-Gly-Asp (RGD) sites on collagen and IIbIIIa to fibrin and other platelets. Simultaneously, the intrinsic and extrinsic pathways of coagulation are initiated by basal matrix collagen exposure activating Factor XII and endothelial signaling by the release of tissue factor, respectively. Platelet activation and adhesion is a self-amplifying process driven by the release of additional coagulation and platelet recruiting factors, culminating in the generation of active thrombin, which cleaves soluble fibrinogen into insoluble fibrin monomers to form a mesh in secondary hemostasis. It is the dysfunction of platelet recruiting and granule secretory mechanisms that may produce off-target effects leading to tissue dysregulation.

Upon degranulation, which occurs as a result of the coagulation cascade, signal transduction, and physical stimuli, platelets release growth factors, cytokines, and tissue regulators with broad systemic effects[22]. Among secreted factors, platelet-derived TIMPs and MMPs modulate matrix composition and structure, platelet derived growth factor (PDGF) stimulates fibrotic proliferation, and beta-thromboglobulin (β-TG) recruits fibroblasts[30,31]. Observed external presentation of P-Selectin on platelets after HD indicates elevated degranulation and suggests the involvement of adaptive responses in transcriptomic and translative regulation[32].

Hemodialysis in Platelet Dysfunction

Although hemodialysis is the prevailing renal replacement therapy, it is an independent risk factor for CVD mortality[33]. During dialysis, platelets commonly become dysfunctional, leading to excessive bleeding and inappropriate clotting[26]. While platelet counts have been measured to fall during the first 30 minutes of hemodialysis, they recover to or slightly overshoot pre-dialysis levels by the end of dialysis[34]. Considering ordinary MK number in bone marrow[35], this recovery is attributed to platelet reticulation by thrombopoiesis, or platelet renewal. Thus, shortened platelet life cycles and iatrogenic stimulation during dialysis may contribute to long term population-level adaptation in platelet genesis contributing to behavioral dysfunction.

Uremia itself inhibits ordinary platelet function by the accumulation of ions and phosphates. Increased plasma calcium and uremic toxins like phenolic acid directly inhibit calcium and ADP mediated receptor binding to prevent aggregation[36]. Uremic platelets further exhibit metabolic changes like reduced granule serotonin, an increased ATP/ADP ratio, and impaired synthesis of thromboxane which together reduce platelet recruiting in thrombotic amplification[37]. However, the reversal of these phenotypes with dialysis indicate a transient mechanism of dysfunction.

Hemodialysis removes uremic solutes and excess water by the countercurrent exchange of externally circulating blood against dialysate containing water, electrolytes, and salt. Uremic solutes are categorized by small (< 500 Da), middle (0.5 - 15 KDa), and large (>15 KDa)

molecules, cleared at rates determined by dialyzer filter porosity. Growing recognition of the hazards of middle and large solute accumulation and retrospective findings of higher overall survival with higher flux hemodialysis have contributed to a trend of greater large solute removal in hemodialysis prescription[38]. Beta-2-microglobulin (B2M) is now included on dialyzer data sheets as a 12 KDa surrogate marker for filtration of inert middle molecule retention proteins. Physiologically, more recent super high-flux dialyzer filters having porosities of 65 KDa more closely resemble actual glomerular filtration, whereas previous low flux and high flux filters have porosities of 3 KDa and 15 KDa. However, true physiological filtration preceding excretion of solutes involves multitude processes of reabsorption post-glomerular filtration, like how albumin (67 KDa) is almost completely reabsorbed in the proximal tubule.

Biocompatibility poses another significant hurdle in hemodialysis. Precise manufacturing of hollow fiber pore structures and sterilization of external units designed for contact with blood require trade-offs between chemistry considerations and blood reactivity. Antiquated use of plasticizers like bisphenol A (BPA) in polycarbonate housings and polysulfone membranes, exposed hydroxyl groups in cellulose, phthalates in polyvinyl chloride (PVC) and polyethylene (PE) tubing, and sterilization by ethylene oxide have caused a multitude of adverse effects including by anaphylaxis, complement activation, and oxidative stress. While these are no longer used, modern dialyzers, made slightly more inert by use of materials like polyacrylonitrile (PAN) and polyethersulfone (PES), still exhibit interfacial problems by membrane fouling, platelet activation, and leukocyte response[39].

Fluid Dynamics as Physical Agonists

Beyond chemical activation and inhibition of platelets during uremia and dialysis, physical stimuli also induce the activation signaling cascade. Microbubbles and high shear rates in the HD circuit are known platelet physical activators by causing interfacial adhesion and increased receptor-agonist kinetics[40,41]. The generation of gas microemboli by pressure gradients and turbulent flow can cause huge physiological damage in circulation by lodging in capillaries, resulting in ischemia, complement activation, and inflammation. Energetics at the gas-liquid interface induce protein conformation changes that expose binding sites that promote platelet aggregation, while direct conformation changes of platelet surface receptors promote the cascade of integrin signal transduction. High shear implicit in the high volumetric flow rates required of ultrafiltration causes platelet rolling that increases the effective receptor density of binding glycoproteins (primarily Ib and IIbIIIa). Shear of large proteins like vWF, which ranges in size from 500 to 20,000 KDa, exposes binding sites for platelet adhesion. However, while shear is the traditional physical agonist of interrogation in hemodialysis, its specific effects on platelets beyond binding have proven limited.

The effects of pressure on platelets however are relatively unstudied. Research in decompression sickness has found that platelet aggregation is induced by the application of negative pressure

and reversibly inhibited by hydrostatic pressurization using inert gas[42,43]. Coincidentally, the hemodialysis flow circuit is characterized by rapid changes in pressure, particularly from 150mmHg to 5mmHg between dialyzer entry and venous return[44]. Should this precipitous depressurization also induce platelet degranulation in addition to aggregation, this physical mechanism may contribute to platelet dysfunction leading to cardiotoxic non-uremic imbalance.

Works Cited

1. United States Renal Data System. 2020 USRDS Annual Data Report: Epidemiology of kidney disease in the United States. National Institutes of Health, National Institute of Diabetes and Digestive and Kidney Diseases, Bethesda, MD, 2020.
2. Hill NR, Fatoba ST, Oke JL, Hirst JA, O'Callaghan CA, Lasserson DS, Hobbs FR. Global prevalence of chronic kidney disease–a systematic review and meta-analysis. PloS one. 2016 Jul 6;11(7):e0158765.
3. Khan Academy. Renal Physiology. Accessed 2019.
4. Kidney Disease: Improving Global Outcomes (KDIGO) CKD Work Group. KDIGO 2012 Clinical Practice Guideline for the Evaluation and Management of Chronic Kidney Disease. Kidney Int 2013; 3 Suppl: 1–150.
5. Clase CM, Kiberd BA, Garg AX. Relationship between glomerular filtration rate and the prevalence of metabolic abnormalities: results from the Third National Health and Nutrition Examination Survey (NHANES III). Nephron Clinical Practice. 2007;105(4):c178-84.
6. Navaneethan SD, Schold JD, Arrigain S, Jolly SE, Jain A, Schreiber Jr MJ, Simon JF, Srinivas TR, Nally Jr JV. Low 25-hydroxyvitamin d levels and mortality in non–dialysis-dependent CKD. American journal of kidney diseases. 2011 Oct 1;58(4):536-43.
7. Sens F, Schott-Pethelaz AM, Labeeuw M, Colin C, Villar E. Survival advantage of hemodialysis relative to peritoneal dialysis in patients with end-stage renal disease and congestive heart failure. Kidney international. 2011 Nov 1;80(9):970-7.
8. Cozzolino M, Mangano M, Stucchi A, Ciceri P, Conte F, Galassi A. Cardiovascular disease in dialysis patients. Nephrology Dialysis Transplantation. 2018 Oct 1;33(suppl_3):iii28-34.
9. Arora, Pradeep. Chronic Kidney Disease. Medscape. Jul 17, 2018. https://emedicine.medscape.com/article/238798-overview
10. Lekawanvijit S. Cardiotoxicity of uremic toxins: a driver of cardiorenal syndrome. Toxins. 2018 Sep;10(9):352.
11. Fassett RG, Venuthurupalli SK, Gobe GC, Coombes JS, Cooper MA, Hoy WE. Biomarkers in chronic kidney disease: a review. Kidney international. 2011 Oct 2;80(8):806-21.

12. Jimbo R, Kawakami-Mori F, Mu S, Hirohama D, Majtan B, Shimizu Y, Yatomi Y, Fukumoto S, Fujita T, Shimosawa T. Fibroblast growth factor 23 accelerates phosphate-induced vascular calcification in the absence of Klotho deficiency. Kidney international. 2014 May 1;85(5):1103-11.
13. Parham WA, Mehdirad AA, Biermann KM, Fredman CS. Hyperkalemia revisited. Texas Heart Institute Journal. 2006;33(1):40.
14. Wang X, Shapiro JI. Evolving concepts in the pathogenesis of uraemic cardiomyopathy. Nature Reviews Nephrology. 2019 Mar;15(3):159-75.
15. Radhakrishnan A, Pickup LC, Price AM, Law JP, Edwards NC, Steeds RP, Ferro CJ, Townend JN. Coronary microvascular dysfunction: a key step in the development of uraemic cardiomyopathy?. Heart. 2019 Sep 1;105(17):1302-9.
16. González A, Schelbert EB, Díez J, Butler J. Myocardial interstitial fibrosis in heart failure: biological and translational perspectives. Journal of the American College of Cardiology. 2018 Apr 17;71(15):1696-706.
17. Harnett JD, Foley RN, Kent GM, Barre PE, Murray D, Parfrey PS. Congestive heart failure in dialysis patients: prevalence, incidence, prognosis and risk factors. Kidney international. 1995 Mar 1;47(3):884-90.
18. Edwards NC, Moody WE, Chue CD, Ferro CJ, Townend JN, Steeds RP. Defining the natural history of uremic cardiomyopathy in chronic kidney disease: the role of cardiovascular magnetic resonance. JACC: Cardiovascular Imaging. 2014 Jul 1;7(7):703-14.
19. Stromp, T. A. et al. Quantitative Gadolinium-Free Cardiac Fibrosis Imaging in End Stage Renal Disease Patients Reveals A Longitudinal Correlation with Structural and Functional Decline. Sci. Rep. 8, 1–10 (2018).
20. Weyrich, Andrew S., et al. "Protein synthesis by platelets: historical and new perspectives." Journal of Thrombosis and Haemostasis 7.2 (2009): 241-246.
21. Mills, Eric W., Rachel Green, and Nicholas T. Ingolia. "Slowed decay of mRNAs enhances platelet specific translation." Blood 129.17 (2017): e38-e48.
22. Golebiewska, Ewelina M., and Alastair W. Poole. "Platelet secretion: From haemostasis to wound healing and beyond." Blood reviews 29.3 (2015): 153-162.
23. Bambace NM, Holmes CE. The platelet contribution to cancer progression. Journal of thrombosis and haemostasis. 2011 Feb;9(2):237-49.
24. Ed Rainger G, Chimen M, Harrison MJ, Yates CM, Harrison P, Watson SP, Lordkipanidzé M, Nash GB. The role of platelets in the recruitment of leukocytes during vascular disease. Platelets. 2015 Aug 18;26(6):507-20.
25. Ntelis K, Solomou EE, Sakkas L, Liossis SN, Daoussis D. The role of platelets in autoimmunity, vasculopathy, and fibrosis: implications for systemic sclerosis. InSeminars in arthritis and rheumatism 2017 Dec 1 (Vol. 47, No. 3, pp. 409-417). WB Saunders.

26. Daugirdas JT, Bernardo AA. Hemodialysis effect on platelet count and function and hemodialysis- associated thrombocytopenia. Kidney International. 2012;82(2):147-157. doi:10.1038/ki.2012.130
27. Rodgers GM. Overview of platelet physiology and laboratory evaluation of platelet function. Clinical obstetrics and gynecology. 1999 Jun 1;42(2):349-59.
28. Lefrançais E, Ortiz-Muñoz G, Caudrillier A, Mallavia B, Liu F, Sayah DM, Thornton EE, Headley MB, David T, Coughlin SR, Krummel MF. The lung is a site of platelet biogenesis and a reservoir for haematopoietic progenitors. Nature. 2017 Apr;544(7648):105-9.
29. Chaudhry, R., Usama, S.M. and Babiker, H.M., 2018. Physiology, coagulation pathways.
30. Murate, Takashi, et al. "The production of tissue inhibitors of metalloproteinases (TIMPs) in megakaryopoiesis: possible role of platelet‐and megakaryocyte‐derived TIMPs in bone marrow fibrosis." British journal of haematology 99.1 (1997): 181-189.
31. Borkham-Kamphorst, Erawan, et al. "Platelet-derived growth factor-D modulates extracellular matrix homeostasis and remodeling through TIMP-1 induction and attenuation of MMP-2 and MMP-9 gelatinase activities." Biochemical and biophysical research communications 457.3 (2015): 307-313.
32. Cases, Aleix, et al. "Platelet activation on hemodialysis: Influence of dialysis membranes." Kidney International Supplement 41 (1993).
33. Hu, J. R. & Coresh, J. The public health dimension of chronic kidney disease: What we have learnt over the past decade. Nephrol. Dial. Transplant. 32, ii113–ii120 (2017).
34. Knudsen F, Nielsen AH, Kristensen SD. The effect of dialyser membrane material on intradialytic changes in platelet count, platelet aggregation,circulating platelet aggregates and antithrombin III.Scand J Urol Nephrol 1985;19: 227–232.
35. Gafter U, Bessler H, Malachi Tet al.Platelet count and thrombopoietic activity in patients with chronic renal failure. Nephron 1987; 45: 207–210.
36. Lutz J, Menke J, Sollinger D, Schinzel H, Thürmel K. Haemostasis in chronic kidney disease. Nephrology Dialysis Transplantation. 2014 Jan 1;29(1):29-40.
37. Di Minno G, Martinez J, McKean ML, De La Rosa J, Burke JF, Murphy S. Platelet dysfunction in uremia. Multifaceted defect partially corrected by dialysis. The American journal of medicine. 1985 Nov 1;79(5):552-9.
38. Palmer SC, Rabindranath KS, Craig JC, Roderick PJ, Locatelli F, Strippoli GF. High‐flux versus low‐flux membranes for end‐stage kidney disease. Cochrane Database of Systematic Reviews. 2012(9).
39. Tony Bouré, Raymond Vanholder; Which dialyser membrane to choose?, Nephrology Dialysis Transplantation, Volume 19, Issue 2, 1 February 2004, Pages 293–296,
40. Barak, Michal, and Yeshayahu Katz. "Microbubbles." Chest 128.4 (2005): 2918-2932.
41. Hosseinzadegan, H., and D. K. Tafti. "Mechanisms of platelet activation, adhesion, and aggregation." Thrombosis and Haemostasis: Research 1.2 (2017): 1-6.

42. Murayama M. Ex vivo human platelet aggregation induced by decompression during reduced barometric pressure, hydrostatic, and hydrodynamic (Bernoulli) effect. Thrombosis research. 1984;33(5):477-485.
43. Pickles DM, Ogston D, Macdonald AG. Effects of hydrostatic pressure and inert gases on platelet aggregation in vitro. Journal of Applied Physiology. 1990;69(6):2239-2247. doi:10.1152/jappl.1990.69.6.2239.
44. Ronco, Claudio, et al. "Effects of a reduced inner diameter of hollow fibers in hemodialyzers." Kidney international 58.2 (2000): 809-817.

Chapter 2

Hemodialysis exacerbates proteolytic imbalance and pro-fibrotic platelet dysfunction

Introduction

Chronic kidney disease (CKD) is characterized by progressive loss of kidney function culminating in end stage renal disease (ESRD). Although hemodialysis (HD) is the prevailing renal replacement therapy, it is an independent risk factor for cardiovascular disease (CVD) mortality[1–6] beyond the traditional risk factors of diabetes, hypertension, lipoprotein levels, and smoking[7]. Potential causes of CVD-related mortality in patients with ESRD include coronary artery disease, vascular calcification with sustained local and systemic inflammatory and pro-osteogenic upregulation[5], and uremic cardiomyopathy characterized by left ventricular hypertrophy, focal scarring, and diffuse interstitial fibrosis[8–11]. Further, mitochondrial disease[12,13] secondary to CKD[14,15] is linked to endothelial dysfunction and extracellular matrix (ECM) remodeling. Recent studies have revealed diffuse myocardial fibrosis in response to initiation of HD[16]. Non-invasive imaging studies demonstrate correlations between cardiac fibrosis and imbalanced plasma proteolytic regulators, particularly tissue inhibitors of matrix metalloproteinases (TIMPs) TIMP1 and TIMP2, in ESRD patients[17]. In parallel, plasma biomarkers for endothelial dysfunction, oxidative stress, and inflammation[3,18,19] indicate CKD progression and cardiovascular decline. Uremic retention compounds inadequately removed during HD have been identified as potential toxins driving the aforementioned pathological processes[6,20–22]. However, cardiotoxicity from circulatory waste accumulation alone insufficiently explains the scope of adverse cardiovascular events and multi-organ fibrosis observed in HD patients, considering lower incidence in peritoneal dialysis patients[23] despite similar residual toxin retention.

Platelets derive secretomes from megakaryocyte upregulation prior to fragmentation and shift patterns of synthesis and secretion in response to activation[24]. Prior to fragmentation, megakaryocytes differentially sort mRNA into platelets with selective emphasis on MMP and TIMP transcripts[25]. HD aberrantly and repetitively stimulates platelets[26], however prior studies of platelets during HD and anti-platelet therapy trials focus on acute thrombus formation[27]. While thrombogenic platelet responses in HD are mitigated with anti-thrombotic agents, concomitant modulations of platelet secretion of factors implicated in tissue regeneration, fibrotic diseases, and cardiovascular stiffening[28] remain poorly understood. Additionally, megakaryocyte-driven fibrosis may be stimulated by HD-induced release of compounds known to be inadequately removed during HD[29]. The combination of acute changes in platelet physiology and chronic adaption of platelet formation may serve as a potential mechanism underlying the development of multi-organ fibrosis and endothelial dysfunction in ESRD patients following initiation of HD.

In these experiments, we recruited ESRD patients on routine hemodialysis from DaVita clinics in the Oakland, CA area. Blood samples were obtained immediately before and after HD. Healthy controls were recruited for comparison. We quantified differences in circulating concentrations of proteolytic regulators, growth factors (GF), clotting factors, cardiovascular indicators, and inflammatory indicators in healthy versus HD patient blood and further measured changes in HD patients pre- versus post-treatment. Because of differences observed in MMPs and TIMPs between healthy and HD patient blood considering familiar differences observed in GF, cardiovascular, and inflammatory levels, we characterized platelet secretomes to determine contributions from HD. Our findings suggest acute and sustained adaptations in platelet protein synthesis and secretion from HD treatment leading to progressively pro-fibrotic behaviors. This shift in platelet phenotype may contribute to enhanced tissue remodeling in HD patients beyond conventional processes of hypertrophy, leading to heightened frequency of adverse cardiovascular outcomes.

Methods

Study Recruitment

HD blood samples were collected immediately before vascular access and after tubing removal from patients at DaVita facilities in Berkeley and Oakland. All patients were dialyzed using NIPRO single-use, hollow-fiber ELISIO filters. Control blood samples from healthy adults with no history of smoking, drug abuse, current medications, or comorbidities were drawn at the University of California, Berkeley Tang Center. Given variability between manufacturers of ELISA tests, control samples were used to provide ranges of normal values for each assay. Patient samples were processed immediately after HD sessions, and control samples were processed immediately after collection. Demographics, documented causes of renal failure, comorbidities, and comedications are summarized in **Tables 2.1** and **2.2**. No differences were found among plasma or platelet measurements owing to ethnicity or vascular access as assessed by ANOVA. Participants provided informed consent under protocols approved by the U.C. Berkeley IRB and in compliance with the Declaration of Helsinki. All methods were performed in accordance with the relevant guidelines and regulations therein.

Plasma and Platelet Isolation

Blood samples were collected in ACD-A Vacutainers and sterile-processed by combination with inhibitor cocktail (20μM PGE1, 6mM acetylsalicylic acid, and 400mM EDTA at 1:200 dilution), centrifugation at 200g, and drip filtration through an Acrodisc WBC Isolation Syringe filter. Remaining erythrocyte and leukocyte contamination was immunoprecipitated by anti-CD235a and anti-CD45 conjugated Dynabeads. Platelets and plasma were separated by centrifugation at 2000g. Plasma was aliquoted and stored at -80°C for up to 1 month. Platelets were lysed in Trizol and stored at -80°C for up to 1 month.

Table 2.1. Patient Demographics (n=56)	
Age, years - median (range)	61.905 (23.83-85.25)
Gender ratio - [male/female]	32/24
Pre-Dialysis Weight, kg - median (range)	79.65 (49.6-160.7)
Post-Dialysis Weight, kg - median (range)	78.35 (48.7-158.9)
Height, cm - median (range)	167.65 (150-185.5)
Ethnicity	
African American	29
Asian American	7
Caucasian	13
Hispanic	7
Prior time on dialysis, months - median (range)	39.417 (1.97-221.77)
Filter surface area, m2 - [1.5/1.7/1.9]	22/29/5
Vascular Access - [shunt/fistula/catheter]	14/33/9
Cause of renal failure	
Hypertension	37
Diabetes mellitus	25
Polycystic kidney disease	1
IgA Nephropathy	1
Analgesics	0
MPGN	0
Unknown	14
Comorbidities	
Anemia	16
Hyperlipidemia	10
CHF	7
Hepatitis	6
Hypothyroidism	5
Medication	
Lipid-lowering drugs	20
Platelet inhibitor	12
RAS Inhibitors	10
Coumarin derivatives	2
None	11
Unknown	15

Table 2.2. Healthy Demographics (n=25)	
Age, years - median (range)	53.92 (45.33-76.17)
Gender ratio - [male/female]	16/9
Weight, kg - median (range)	71.2 (45.36-113.4)
Height, cm - median (range)	175.26 (154.94-187.96)
Ethnicity	
African American	0
Asian American	5
Caucasian	18
Hispanic	2

Enzyme Immunoassay Kits for Plasma Proteomics

Plasma protein concentrations were measured using pre-made ELISA and Luminex assay kits per manufacturers' directions (**Table 2.3**). Samples were tested in duplicate within the same assay, leading to exclusion of measurements with CV% greater than 30%. Three plates were used per marker. Some samples were re-tested across assay kits for validation. Entire assay kits were excluded from control-HD comparison based on a combination of CV% of inter-assay replicates, three-sample Kruskal-Wallis, and two-sample Kolmogorov-Smirnov tests ($p \leq 0.05$). Absorbance measurements were interpolated to a 5-parameter logistic standard curve using Matlab. For intra-HD change analysis, if either pre- or post- measurement was invalidated or fell outside of test ranges, both measurements were excluded.

Quantitative PCR for Platelet Lysate

Platelet RNA was extracted from Trizol by phase-separation with chloroform and precipitation by isopropanol. The RNA pellet was washed with 75% ethanol, reformed by centrifugation (7500g/ 4°C), and dissolved in nuclease-free water after decanting. Samples were purified using Qiagen RNA Cleanup Kits. cDNA was synthesized using Superscript IV Vilo Master Mix according to RNA concentrations measured by Qubit Fluorometer and probed using TaqMan primers (**Table 2.4**), with TaqMan Fast Advanced Master Mix. Primer amplification was performed in a QuantStudio 3 Real-Time PCR System. Paired PCR samples with Ct values above 38 were excluded.

Table 2.3. Enzyme Immunoassay Kits used for Plasma Measurements.

Protein	Classification	Manufacturer	Detection range	Dilution
11TXB2	Cardiovascular indicator	Elabsci (E-EL-H0207)	15.6-1,000 pg/mL	1:1, 1:6
CRP	Inflammatory indicator	ThermoFisher (EPX01A-10288-901)	5.66-5800 pg/mL	1:500
CTGF	Growth factor	Cloud-Clone (SEA010Hu)	7.8-500 pg/mL	1:1, 1:2
EGF	Growth factor	Cloud-Clone (SEA560Hu)	3.9-250 pg/mL	1:2, 1:4
FGF2	Growth factor	Cloud-Clone (CEA551Hu)	12.4-1,000 pg/mL	1:1
GAPDH	Cardiovascular indicator	ThermoFisher (EPX01A-12154-901)	244-250,000 pg/mL	1:1
IFNγ	Inflammatory indicator	ThermoFisher (EPX01A-10228-901)	12-11,925 pg/mL	1:1
IGF1	Growth factor	Cloud-Clone (SEA050Hu)	156-10,000 pg/mL	1:50, 1:100
IL1β	Inflammatory indicator	ThermoFisher (EPX01A-10224-901)	2.14-8,750 pg/mL	1:1
LAP (TGFβ1)	Growth factor	ThermoFisher (BMS2065)	156-10,000 pg/mL	1:2.5, 1:25
MMP2	Proteolytic regulation	ThermoFisher (EPX03A-10829-901)	36-146,700 pg/mL	1:25, 1:50
MMP3	Proteolytic regulation	ThermoFisher (EPX03A-10829-901)	18-18,125 pg/mL	1:25, 1:50
MMP9	Proteolytic regulation	ThermoFisher (EPX03A-10829-901)	0.72-2,950 pg/mL	1:25, 1:50
MMP13	Proteolytic regulation	ThermoFisher (EPX01A-12131-901)	7.08-29,000 pg/mL	1:1
MMP14	Proteolytic regulation	Wuhan (EH0369)	31-2,000 pg/mL	1:2, 1:6
NTpBNP	Cardiovascular indicator	Wuhan (EH0350)	39-2,500 pg/mL	1:1, 1:2
PAF	Clotting Factor	Elabsci (E-EL-H2199)	78.1-5,000 pg/mL	1:6
PDGFB	Growth factor	RayBiotech (ELH-PDGFBB-1)	1-400 pg/mL	1:1, 1:2
PDGFD	Growth factor	Cloud-Clone (SEC919Hu)	12.5-800 pg/mL	1:1
PF4	Clotting Factor	ThermoFisher (EHPF4)	20.58-15,000 pg/mL	1:100, 1:200
PGI2	Cardiovascular indicator	Blue Gene (ABIN771046)	25-500 pg/mL	1:1
PPBP (βTG)	Growth factor	ThermoFisher (EHPPBP)	4.1-1,000 pg/mL	1:600, 1:5,000
TIMP1	Proteolytic regulation	ThermoFisher (EPX01A-12018-901)	146-150,000 pg/mL	1:20, 1:50
TIMP2	Proteolytic regulation	ThermoFisher (EHTIMP2)	1.6-1,200 pg/mL	1:300
TIMP3	Proteolytic regulation	Cloud-Clone (SEA129Hu)	150-10,000 pg/mL	1:1, 1:4
TNFR1	Inflammatory indicator	ThermoFisher (EPX01A-10203-901)	189-774,400 pg/mL	1:1
TPO	Cardiovascular indicator	ThermoFisher (EPX01A-12161-901)	94-96,275 pg/mL	1:1
vWF	Clotting Factor	ThermoFisher (EPX040-10825-901)	0.00244-2.5 %plasma	1:500

*Kits not purchased from ThermoFisher were purchased through Antibodies-Online.

Table 2.4. Primers used for PCR.

RNA Target	Details	Accession #	Assay ID (Thermo)
EGF	Growth factor	NM_001178130.2, NM_001178131.2, NM_001963.5	Hs01099990_m1
FGF2	Growth factor	NM_002006.4	Hs00266645_m1
GAPDH	Metabolic indicator	NM_002046.5, NM_001256799.2, NM_001289745.1, NM_001289746.1	Hs02786624_g1
IFNγ	Inflammatory cytokine	NM_000619.2	Hs00989291_m1
IGF1	Growth factor	NM_000618.4, NM_001111283.2, NM_001111284.1	Hs01547656_m1
IL1β	Inflammatory cytokine	NM_000576.2	Hs01555410_m1
MMP1	Proteolytic regulation	NM_001145938.1 NM_002421.3	Hs00899658_m1
MMP2	Proteolytic regulation	NM_004530.5, NM_001127891.2, NM_001302508.1, NM_001302510.1, NM_001302509.1	Hs01548727_m1
MMP3	Proteolytic regulation	NM_002422.4	Hs00968305_m1
MMP9	Proteolytic regulation	NM_004994.2	Hs00957562_m1
MMP13	Proteolytic regulation	NM_002427.3	Hs00942584_m1
MMP14	Proteolytic regulation	NM_004995.3	Hs01037003_g1
MMP24	Proteolytic regulation	NM_006690.3	Hs00198580_m1
P2RY12	Loading Control	NM_022788.4 NM_176876.2	Hs01881698_s1
PAFAH2	Clotting factor	NM_000437.3	Hs00166473_m1
PDGFB	Growth factor	NM_002608.3, NM_033016.3	Hs00966522_m1
PDGFD	Growth factor	NM_025208.4, NM_033135.3	Hs00228671_m1
PF4	Clotting factor	NM_002619.3	Hs00427220_g1
PPBP	Growth factor	NM_002704.3	Hs00234077_m1
TBXAS1	Clotting factor	NM_001061.4, NM_030984.3, NM_001130966.2, NM_001166253.1, NM_001166254.1, NM_001314028.1	Hs01022706_m1
TGFβ1	Growth factor	NM_000660.5	Hs00998133_m1
TIMP1	Proteolytic regulation	NM_003254.2	Hs01092512_g1
TIMP2	Proteolytic regulation	NM_003255.4	Hs00234278_m1
TIMP3	Proteolytic regulation	NM_000362.4	Hs00165949_m1
TNFα	Inflammatory cytokine	NM_000594.3	Hs00174128_m1
vWF	Clotting factor	NM_000552.4	Hs01109446_m1

Gray = Ct values detected were above cutoff threshold.

Western Blots for Platelet Lysate

Protein was precipitated from Trizol using acetone at -20°C followed by centrifugation (12000g/ 4°C). The protein pellet was washed with 0.3M guanidine hydrochloride in 95% ethanol and 100% ethanol before dissolution in 3% SDS in ultrapure water. Solubilized protein was aliquoted and stored for single use at -20°C for up to 1 month, according to concentrations measured by BCA assay. Protein samples were denatured by LDS and reduced, electrophoresed at 20µg loads, and transferred to PVDF membranes by Power Blotter. Membranes were probed for one target by iBind Flex, stripped and re-probed for loading control, and discarded. Target bands were

detected using SuperSignal West Pico, SuperSignal West Femto, and SuperSignal Enhancer where appropriate. Membranes were imaged using a ChemiDoc XRS. Band densitometry was performed using ImageJ. Antibodies used are listed in **Table 2.5**.

Table 2.5. Antibodies used for WB.

Protein Target	Classification	Manufacturer
CTGF	Pro-fibrotic	ThermoFisher (MA5-26817, 31430)
EGF	Fibro-protective	ThermoFisher (M805, 31430)
FGF2	Fibro-protective	ThermoFisher (MA5-15276, 31430)
GAPDH	Metabolic activity	ThermoFisher (MA5-15738, 31430)
IGF1	Pro-fibrotic	ThermoFisher (MA1-088, 31430)
LAP (TGFβ1)	Pro-fibrotic	ThermoFisher (MA5-17186, 31430)
MMP1	Proteolytic regulation	ThermoFisher (MA1-771, 31430)
MMP14	Proteolytic regulation	ThermoFisher (PA5-13183, 31460)
MMP2	Proteolytic regulation	ThermoFisher (MA1-772, 31430)
MMP24	Proteolytic regulation	ThermoFisher (PA5-51333, 31460)
MMP3	Proteolytic regulation	ThermoFisher (MA5-17123, 31430)
MMP9	Proteolytic regulation	ThermoFisher (MA1-12895, 31430)
PDGFB	Pro-fibrotic	ThermoFisher (PA5-19524, 31460)
PDGFD	Pro-fibrotic	ThermoFisher (40-2100, 31460)
PF4	Activation indicator	ThermoFisher (MA5-23926, 31430)
PPBP	Pro-fibrotic	ThermoFisher (PA5-51254, 31460)
TIMP1	Proteolytic regulation	ThermoFisher (MA1-773, 31430)
TIMP2	Proteolytic regulation	ThermoFisher (MA1-774, 31430)
TIMP3	Proteolytic regulation	ThermoFisher (PA5-26133, 31460)
TNFR1	Activation indicator	ThermoFisher (MA5-23706, 31430)
14-3-3y	Loading control	ThermoFisher (MA1-16587, 31430)
Goat Anti-Mouse IgG, HRP		ThermoFisher (31430)
Goat Anti-Rabbit IgG, HRP		ThermoFisher (31460)

Statistics

HD versus control plasma measurement distributions were compared by two-sample t test, assuming unequal variance and two tails. Intra-HD plasma relative protein changes, platelet RNA changes, and PL protein changes were assessed by one-sample t test using two tails. Linear dependencies were assessed by multiple linear regression (MLR), and unique linear dependencies to individual predictors were assessed by Pearson correlation. **Figures 2.4-2.7** tabulate correlation coefficients for manually grouped comparisons and are automatically colored according to predictive strength p, with raw data plots for significant correlations depicted in **Figures 2.8-2.10**. Significance in all cases was determined by $p \leq 0.05$. Figure error bars represent 95% confidence intervals. Box and whisker plots represent sample quartiles.

Results

I. Hemodialysis patient plasma is proteolytically dysregulated and pro-fibrotic

HD patient plasma indicated broadly elevated proteolytic activity and regulation, a pro-fibrotic GF profile, cardiac stress, and elevated systemic inflammatory response compared to healthy plasma (**Figure** 2.**1**). Concentrations of four matrix metalloproteinases (MMPs: MMP2, MMP3, MMP9, MMP14) and two tissue inhibitors of MMPs (TIMPs: TIMP1, TIMP2) were significantly elevated in dialysis patients both before and after HD compared to control values (**Figure** 2.**1A**). In contrast, plasma levels of growth factors were more nuanced (**Figure** 2.**1B**), with fibroblast growth factor two (FGF2) levels significantly below and insulin like growth factor 1 (IGF1) concentrations significantly above control levels. Platelet derived growth factor (PDGF) D concentrations pre-HD trended higher than control levels and were significantly elevated in post-HD plasma, while neither pre- nor post-HD PDGFB levels significantly differed from controls. In agreement with prior studies[30–33], inflammation and cardiovascular stress measured uniformly higher in dialysis patients, shown by N-Terminal Prohormone of Brain Natriuretic Peptide (NTpBNP), C-reactive protein (CRP), tumor necrosis factor receptor 1 (TNFR1), and interleukin 1 beta (IL1β) as shown in **Figure** 2.**1C**. Broad elevation of MMPs and TIMPs support enhanced tissue remodeling as an adaptive response to HD. Further, the widely sustained elevation of plasma MMPs and TIMPs post-treatment suggests a pathogenesis that is insufficiently cleared and potentially exacerbated by HD. Given prior findings that FGF2 reduces structural damage in CKD[34], while elevated IGF1 correlates to systemic sclerosis[35], these results suggest a pro-fibrotic phenotype in HD patient plasma. Further, given the key role PDGFs play in the genesis of vascular lesions, elevated chronic PDGFD and minor PDGF increases post-HD may contribute to a homeostatic shift toward tissue stiffening in HD patients[36]. This link between proteolytic dysregulation and fibrosis in HD patients is further supported by the mechanistic induction of TIMPs and attenuation of MMPs by PDGFs[37]. No differences were observed between dialysis patient and control plasma for the TGFβ precursor latency associated peptide (LAP), pro-platelet basic protein (PPBP)/ Beta-Thromboglobulin (βTG), Platelet-Activating Factor (PAF), Von Willebrand Factor (vWF), platelet factor 4 (PF4), Glyceraldehyde 3-Phosphate Dehydrogenase (GAPDH), Thrombopoietin (TPO), thromboxane metabolite (TXM) 11TXB2, and Interferon-γ (IFNγ). For vasodilator Prostaglandin I2 (Prostacyclin; PGI2) no difference was observed between pre-HD and healthy control levels, though post-HD levels were significantly suppressed (**Figure 2.2**).

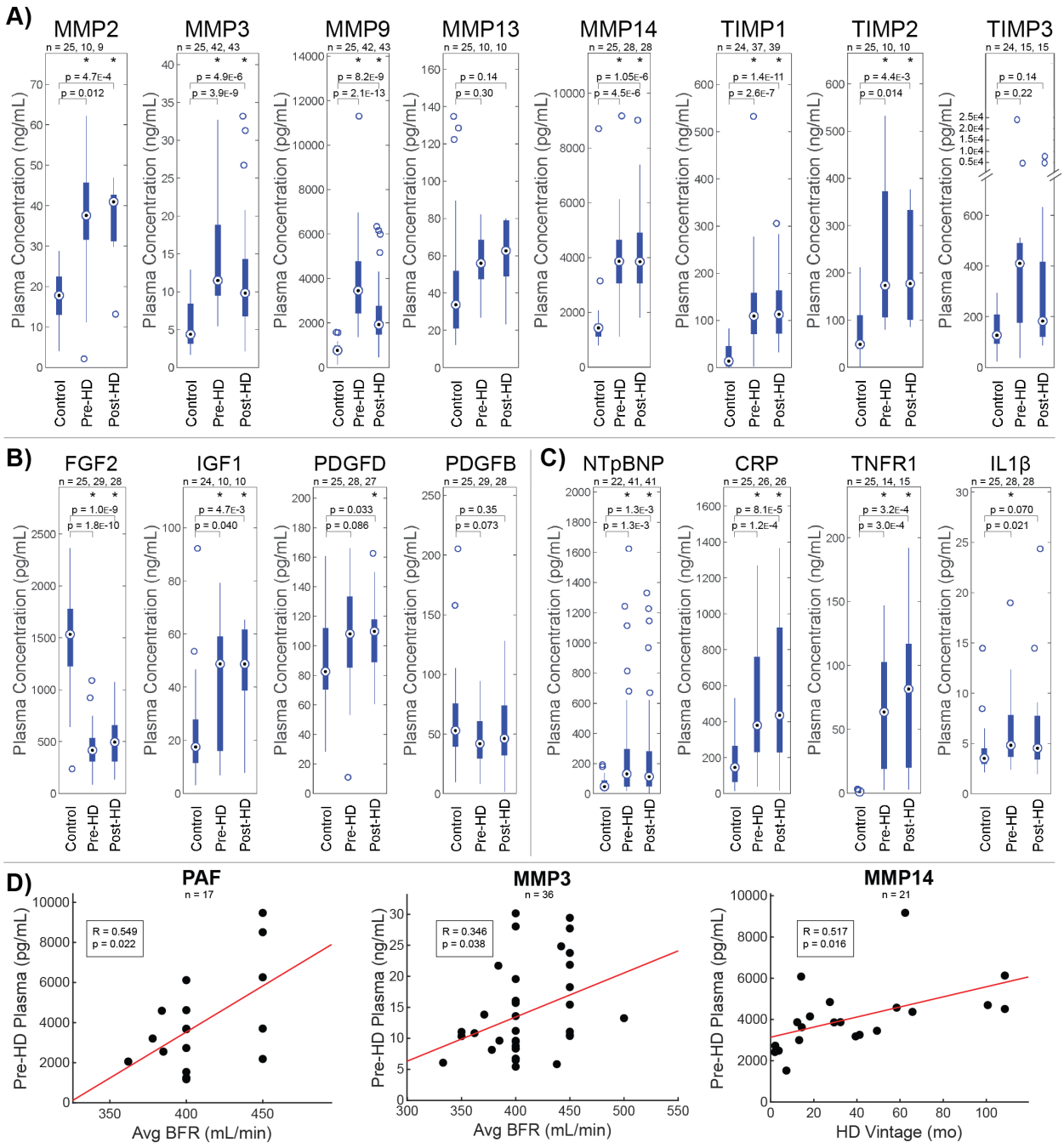

Figure 2.1. Hemodialysis patient plasma is characterized by proteolytic dysregulation and pro-fibrotic indicators. Comparison of plasma concentrations of (**A**) MMPs and TIMPs, (**B**) growth factors, and (**C**) inflammatory and cardiovascular markers between healthy control and pre-dialysis or post-dialysis samples as measured by ELISA and compared by t test. *$p < 0.05$. Box and whisker plots represent quartiles. (**A**) Concentrations of four MMPs (MMP2, MMP3, MMP9, MMP14) and two TIMPs (TIMP1, TIMP2) were significantly elevated in dialysis patients both before and after HD compared to healthy controls. (**B**) Significantly depressed FGF2 and significantly elevated IGF1 in dialysis patients indicate a pro-fibrotic circulatory

phenotype. (**C**) Natriuretic peptides and inflammatory markers are elevated in dialysis patients as established indicators of adverse cardiovascular outcomes. (**D**) Significant Pearson correlations ($p < 0.05$) between pre-dialysis plasma concentrations and treatment parameters blood flow rate (BFR) and dialysis vintage. Positive relationships against PAF and MMPs support worsening proteolytic and coagulative dysfunctions with BFR and Vintage. Figure was prepared in Matlab R2019 (Mathworks, Nattick MA, mathworks.com).

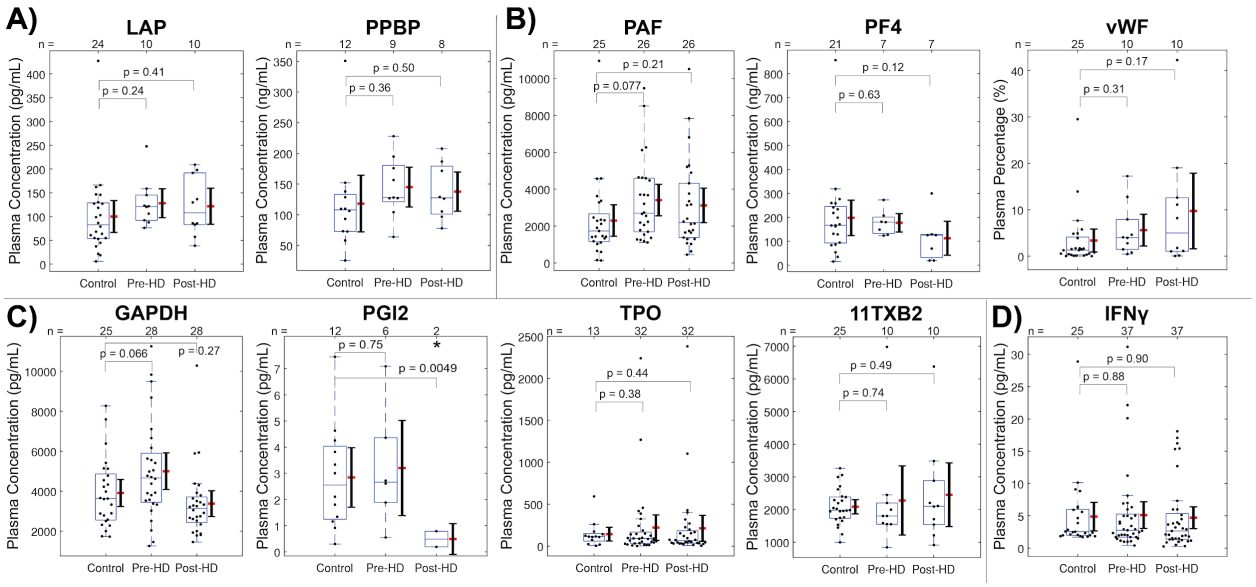

Figure 2.2. Biomarkers exhibiting comparable dialysis-to-control plasma ranges. Comparison of plasma concentrations of (**A**) growth factors, (**B**) clotting factors, (**C**) cardiovascular indicators, and (**D**) inflammatory cytokines between healthy control and pre-dialysis or post-dialysis samples as measured by ELISA and compared by t test. *$p < 0.05$. Box and whisker plots represent quartiles. Adjacent ranges represent mean (red) ± 95% confidence interval. (**C**) Post-dialysis PGI2 levels were significantly depressed compared to healthy controls.

II. Intra-dialysis changes reveal reduced MMP and heightened TIMP1 plasma levels

The impacts of single HD sessions on circulatory biomarker accumulation were assessed by relative changes in paired plasma samples from dialysis patients pre- and post-treatment. One-sample t tests indicated plasma protein concentrations likely to change iatrogenically on average. Post-HD plasma indicated lower proteolytic activity, higher proteolytic inhibition, higher clot sensitivity, and lower glycolytic enzyme levels compared to paired pre-HD samples.

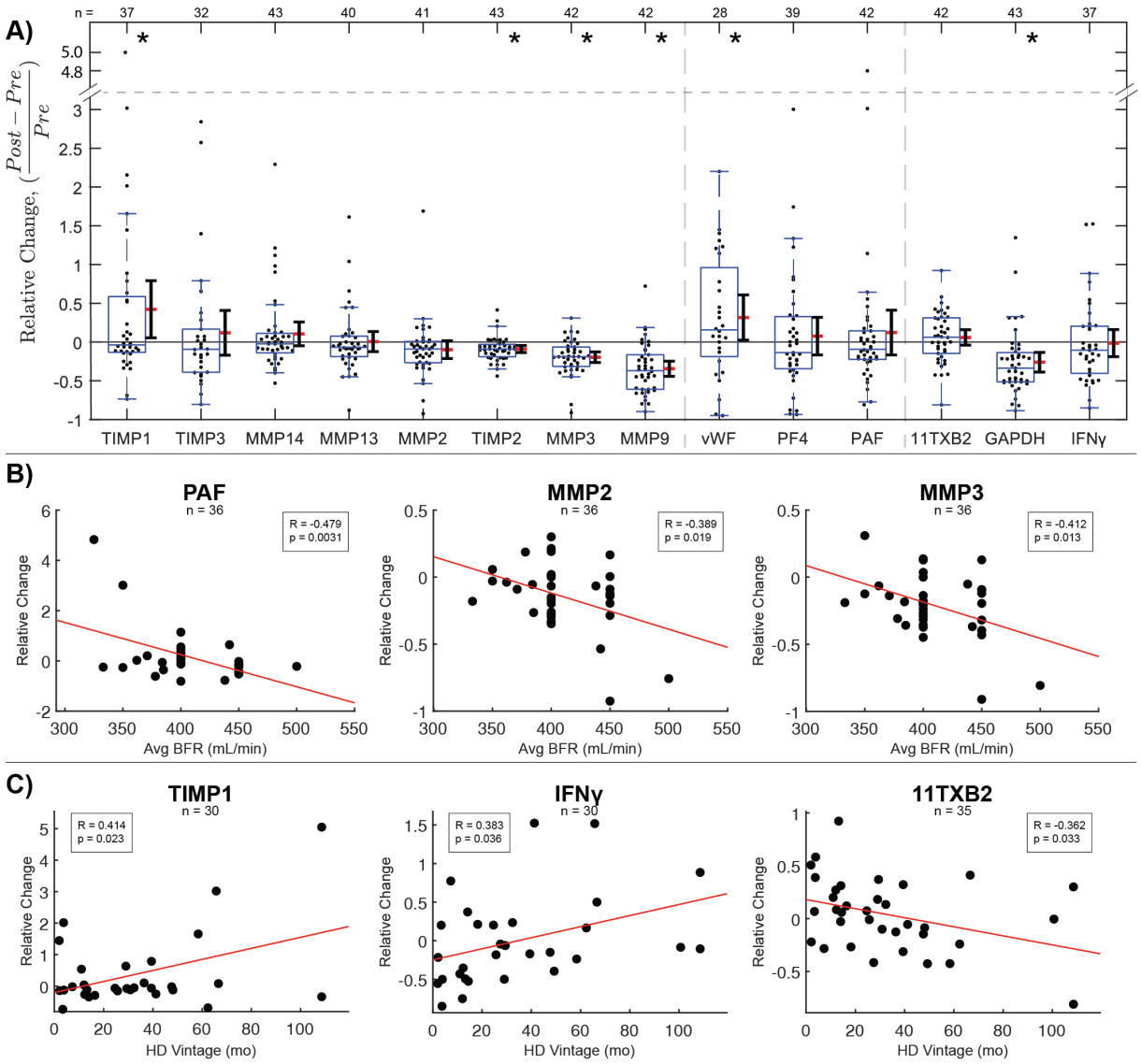

Figure 2.3. Intra-dialysis changes reveal MMP clearance and acute TIMP1 elevation that increases in severity with dialysis vintage. (**A**) Relative changes in paired plasma samples from dialysis patients pre- and post-treatment as measured by ELISA. Significant intra-dialysis increases were observed in proteolytic regulator TIMP1 and clotting factor vWF. Significant decreases were observed in TIMP2, proteases MMP3 and MMP9, and oxidative stress indicator GAPDH. Statistical significance was assessed using one-sample t test. *$p < 0.05$. Box and whisker plots represent quartiles. Adjacent ranges represent mean (red) ± 95% confidence interval. (**B** and **C**) Significant Pearson correlations ($p < 0.05$) between intra-dialysis plasma protein changes and BFR or Vintage, respectively. Negative relationships against PAF and MMPs show clearance with increasing BFR. Positive relationships against TIMP1 and cytokine IFNγ support increasing proteolytic inhibition and immune reactivity with Vintage, while decreasing thromboxane metabolite with Vintage reflects progression of coagulative dysfunction. Figure was prepared in Matlab R2019 (Mathworks, Nattick MA, mathworks.com).

Significant intra-dialytic changes were found in 2 MMPs (MMP3, MMP9), 2 TIMPs (TIMP1, TIMP2), no GFs, 1 clotting factor (vWF), 1 cardiovascular indicator (GAPDH), and no inflammatory indicators (**Figure 2.3**). All measured proteases and proteolytic regulators decreased in a majority of HD patients, reflecting typical protein removal effects by mechanisms like membrane adsorption. However, TIMP1 significantly increased on average. Considering TIMP2, MMP3, and MMP9 significantly decrease on average, this isolates TIMP1 as a molecule that is acutely secreted into plasma during dialysis. In particular, an increased ratio of TIMP1 to MMP9 post-dialysis may link HD to increased tissue fibrosis and systemic stiffening characteristic of cardiorenal syndrome. In contrast, relative changes among measured growth factors were not statistically significant. FGF2, PDGFB, IGF1, and Connective Tissue Growth Factor (CTGF) increased in a majority of patients during HD sessions, while epidermal growth factor (EGF), LAP, PDGFD, and PPBP decreased in a majority of sessions (**Figure 2.4**). Among measured clotting factors, vWF levels significantly increased on average. Among cardiovascular and inflammatory indicators, GAPDH significantly decreased on average. In parallel, 11TXB2 and CRP increased in a majority of sessions, while Thrombopoietin (TPO), NTpBNP, PGI2, TNFR1, TNFα, IFNγ, and IL1β decreased in a majority of sessions, with no significant paired average changes (**Figure 2.4**).

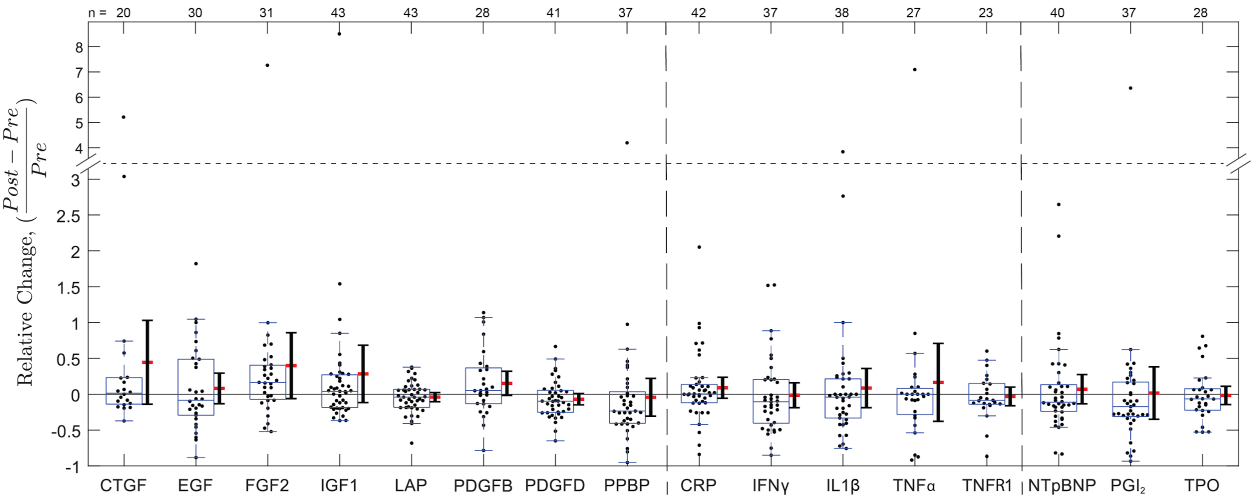

Figure 2.4. Plasma biomarker levels unchanged by single dialysis sessions. Relative changes in paired plasma samples from dialysis patients pre- and post-treatment as measured by ELISA. Statistical significance was assessed using one-sample t tests. *$p < 0.05$. Box and whisker plots represent quartiles. Adjacent ranges represent mean (red) ± 95% confidence interval.

III. Plasma proteolytic imbalance worsens with dialysis vintage and faster blood flow rate

Pre-treatment levels of all proteins measured were compared simultaneously by multivariate linear regression (MLR) against patient age, HD Vintage defined as the number of months of regular HD treatment prior to collection, average HD blood flow rate (BFR), sex, and weight to determine potential targets and patient predictors of cyclical dialytic stress (**Table 2.6**). Plasma levels of PAF correlated uniquely to BFR against all patient predictors (p=0.017) (**Figure 2.1D**), elevations of which may contribute to the development of microvascular dysfunction[38] and amplification of leukocyte-induced microvascular alterations through enhanced platelet recruitment[39]. Separately, MMP3 correlated uniquely to BFR (p=0.025) and MMP14 correlated uniquely to HD Vintage (p=0.038) against all patient predictors, indicating increasingly disturbed proteolytic balance.

Table 2.6. P-values of independent patient predictors of biomarker measurements by multiple linear regression.

Y	Independent Predictors of Y				
	BFR	Vintage	Age	Sex	Weight
PAF (Plasma)	0.017	0.11	0.16	0.55	0.59
MMP3 (Plasma)	0.025	0.64	0.38	0.60	0.82
MMP14 (Plasma)	0.12	0.038	0.31	0.25	0.88
PAF (ΔPlasma)	0.018	0.066	0.83	0.15	0.10
MMP2 (ΔPlasma)	0.058	0.55	0.45	0.29	0.70
MMP3 (ΔPlasma)	0.020	0.33	0.67	0.24	0.046
TIMP1 (ΔPlasma)	0.081	0.027	0.42	0.96	0.71
IFNg (ΔPlasma)	0.81	0.043	0.70	0.35	0.72
TX11B2 (ΔPlasma)	0.27	0.032	0.44	0.54	0.61
PAFAH2 (ΔRNA)	0.72	0.00019	0.16	0.83	0.37
MMP3 (WB)	0.046	0.63	0.089		
TIMP2 (WB)	0.18	0.012	0.41		
PPBP (WB)	0.90	0.021	0.31		

Relative plasma changes intra-HD compared to treatment parameters indicated effects and predictors of protein removal and accumulation (**Table 2.6**). Among simultaneously compared patient predictors, BFR correlated negatively against ΔPAF (p=0.018) and ΔMMP2 (p=0.058) (**Figure 2.3B**), while ΔMMP3 was predicted by both BFR (p=0.020) and weight (p=0.046)

(**Figure SF3**), reflecting acute effects of increasing prescribed HD speed. HD Vintage uniquely predicted positive ΔIFNγ (p=0.043), Δ11TXB2 (p=0.032), and ΔTIMP1 (p=0.027), reflecting both acute changes during dialysis and longer-term chronic adaptations to repeated dialysis exposure (**Figure 2.3C**). Positive correlations between BFR and pre-treatment PAF and MMPs suggest increasing BFR may aid short-term clearance while also contributing to long-term dysfunction. However, increasing IFNγ and decreasing 11TXB2 with vintage imply chronically enhanced inflammatory sensitivity and platelet dysfunction in response to prolonged HD treatment. The combination of chronically elevated plasma TIMP1 levels in HD patients (**Figure 2.1A**), further acute elevation in response to dialysis (**Figure 2.3A**), and positive correlation to dialysis vintage suggests both acute and chronic adaptations that enhance MMP inhibition and fibrotic ECM deposition[40].

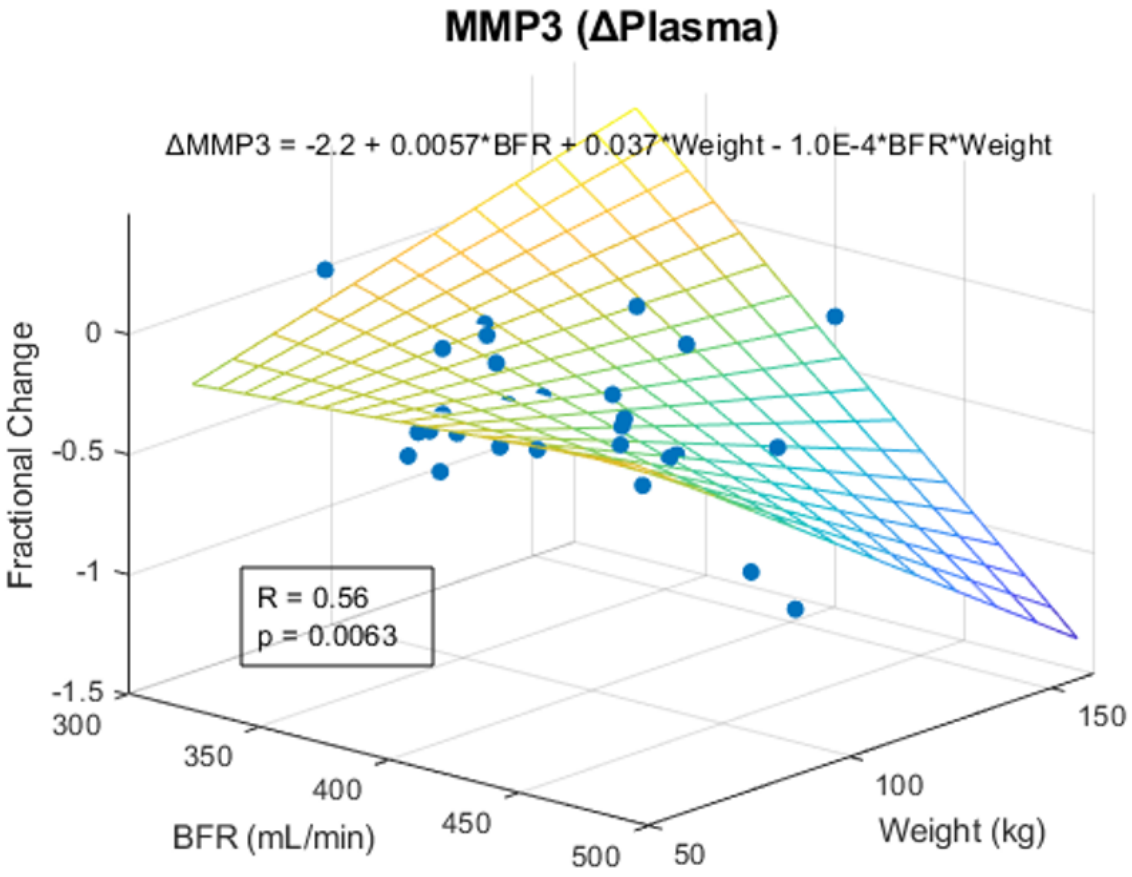

Figure 2.5. Multiple linear regression of blood flow rate and patient weight to intra-dialysis changes of plasma MMP3. Significant multivariate correlation of plasma ΔMMP3 to blood flow rate and patient weight, subtracting interactions between predictors.

IV. Intra-dialysis platelet transcriptome changes reflect long-term drivers of dysfunction

Platelet lysate (PL) from pre- and post-HD blood samples were assessed for relative RNA changes to examine chronic effects on platelet function between treatment sessions. PCR analysis revealed greater average RNA content in post-HD platelets for all secreted biomarkers relative to generic platelet Purinergic Receptor P2Y12 (P2RY12) (**Figure 2.6A**). This is consistent with expected platelet turnover, increasing overall RNA reserves. However, disproportionate intra-HD changes between markers reveal selective degradation following translation[41,42] and upregulation in megakaryocytes prior to fragmentation[25], neglecting endogenous uptake mechanisms[43]. Significant increases were found in 2 growth factors (EGF, PPBP), 2 clotting factors (PF4, vWF), and 1 metabolic indicator (GAPDH). Among growth factor RNAs, increased EGF and PPBP may signify enhanced regenerative and fibrotic potential, while the majority decreases observed for FGF2, PDGFB, PDGFD, and TGFβ1 signify stimulated depletion without compensatory upregulation in new platelets. Among clotting factor RNAs, significant increases measured for PF4 and vWF indicate platelet hypersensitization, while the majority decreases observed for PAF RNA may presage a pathway to long-term dysfunction. While no significant intra-HD changes were found in MMPs or TIMPs, MMP1 decreased while all 3 measured TIMP transcripts increased in a majority of patients, indicating preferential TIMP upregulation. The multi-modal distribution of TIMP1 changes reveals patient subsets exhibiting either depleted or highly upregulated TIMP1 RNA. Because of patient differences in rates of platelet renewal, this could signify that HD stimulates both TIMP1 translation in existing platelets and upregulation in subsequent platelet production. The parallel significant increase in GAPDH represents the increased metabolic capacity of platelets upon renewal. When correlated simultaneously against patient predictors by multivariate linear regression, Vintage uniquely predicted ΔPAFAH2 RNA (p=1.9E-4) (**Table 2.6**). Increasing intra-dialytic PAF upregulation (R = 0.861, p = 9.2E-6) (**Figure 2.6B**) supports altered platelet translative potential leading to clotting dysfunction with long-term HD. These results imply that beyond RNA renewal effects of chronically shortened platelet life cycles, megakaryocytes may respond to iatrogenic stress by shifting platelet protective and translative behaviors.

V. Platelet secretomes shift with dialysis vintage

To determine intra-dialytic effects on platelet activity, blood was re-sampled from 12 HD patients for platelet proteomic analysis (**Figure 2.6C**). Among measured MMPs, TIMPs, and GFs for paired pre- and post-HD samples, one significant decrease was observed in connective tissue growth factor (CTGF), signifying a case in which granule-mediated secretion outpaces production. While relative platelet lysate protein changes generally showed high variability,

MMP3 correlated positively to BFR (p=0.046) (**Table 2.6**), signifying net synthesis accompanying platelet renewal (**Figure 2.6D**). TIMP2 correlated negatively to Vintage (p=0.012) (**Table 2.6**), suggesting depletion after long-term HD, while PPBP correlated positively to Vintage (p=0.021) (**Table 2.6**), revealing enhanced production of fibrotic molecules (**Figure 2.6E**). Collectively, these suggest that faster BFR increases platelet proteolytic capabilities, and that long-term HD patients develop pro-fibrotic platelets.

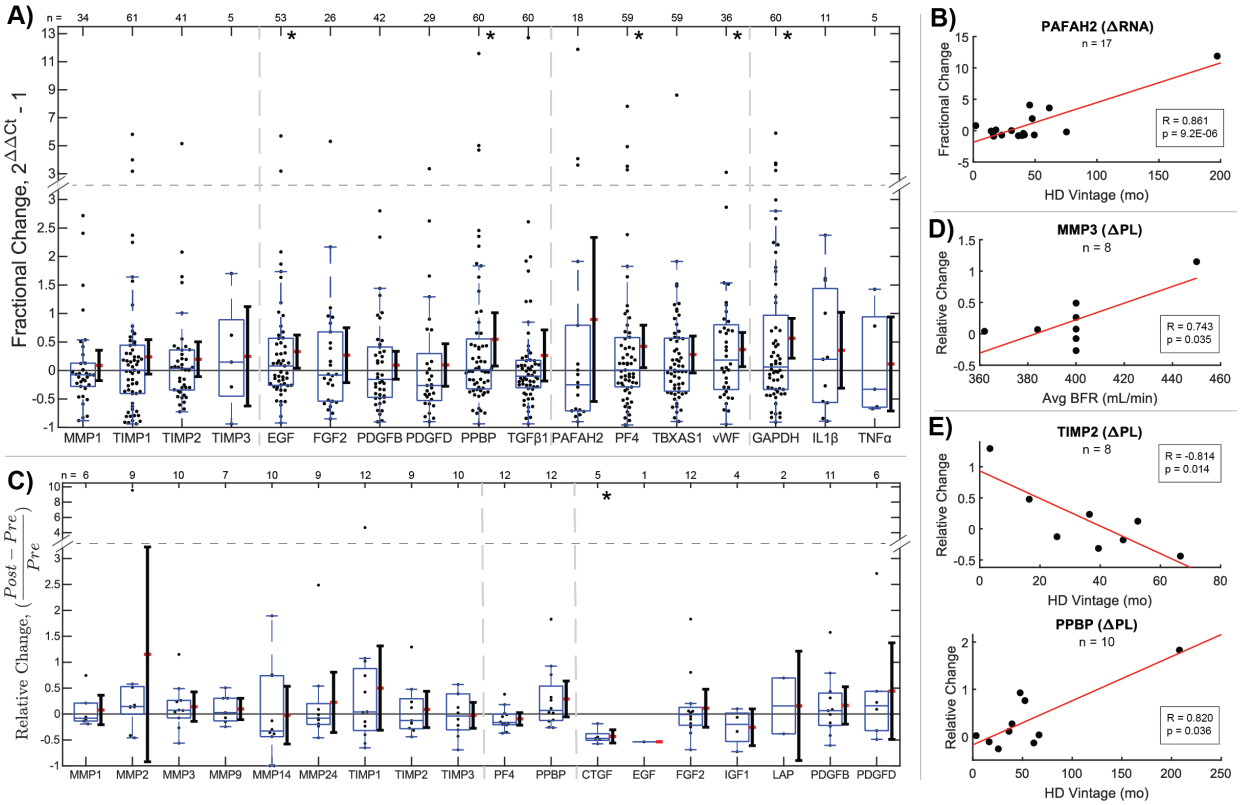

Figure 2.6. Intra-dialysis platelet transcriptome and secretome changes reflect long-term drivers of dysfunction. (**A**) Relative changes in paired platelet lysate RNA composition in dialysis patients pre- and post-treatment as measured by qPCR. Disproportionate increases in transcripts post-dialysis show selective upregulation of TIMPs and MMP1 degradation in a majority of patients. Fibro-protective EGF, pro-fibrotic PPBP, clotting factors PF4 and vWF, and GAPDH significantly increased by t test, reflecting changes affecting a diverse set of mechanisms. *p < 0.05. Box and whisker plots represent quartiles. Adjacent ranges represent mean (red) ± 95% confidence interval. (**B**) A significant Pearson correlation ($p < 0.05$) shows increasing capacity for PAF production with Vintage. (**C**) Relative changes in paired platelet lysate protein composition in pre- and post-treatment as measured by Western Blot. Statistical significance was assessed by one-sample t test. *p < 0.05. (**D** and **E**) Significant Pearson correlations ($p < 0.05$) between intra-dialysis platelet lysate secretome changes and BFR or Vintage, respectively. The positive relationship between MMP3 and BFR supports acute proteolytic enhancement in platelets, while reduction in MMP1 and TIMP2 with Vintage supports sensitization of MMP and

TIMP secretion. The positive relationship between PPBP and Vintage reflects the impact of progressive platelet dysfunction on tissue dysregulation. Prepared in Matlab R2019.

VI. Elevated activation and inflammatory state indicate platelet dysfunction

Plasma measurements revealed chronic accumulation of MMPs and TIMPs and acutely heightened TIMP1, while disproportionate changes in the platelet secretome revealed altered protein synthesis between HD sessions. However, further examination of platelet secretome correlations to plasma clotting, inflammatory, and cardiovascular regulators revealed fundamental behavioral adaptations to HD (**Figure 2.7**). In aggregate, these findings reveal accelerated platelet turnover with enhanced translative capacity, augmented proteolytic enzyme translation and secretion, elevated platelet inflammatory and regenerative response, platelet dysfunction in patients with attenuated native platelet inhibition, and further evidence of worsening dysfunction with faster BFR and longer Vintage.

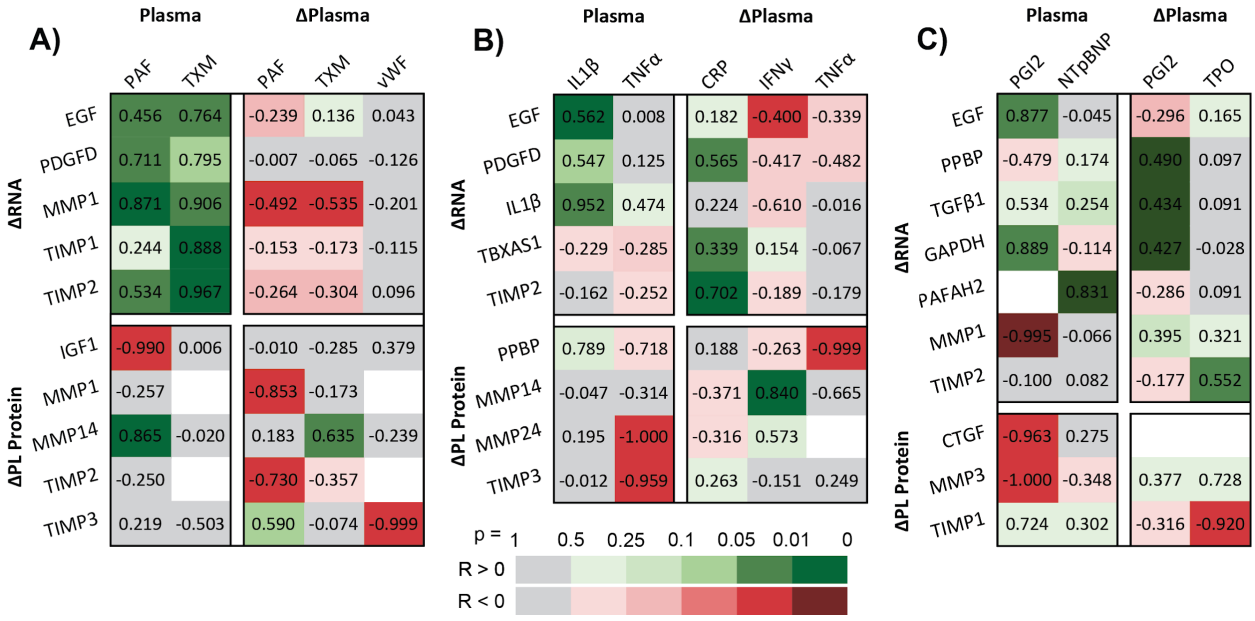

Figure 2.7. Elevated platelet activation, inflammatory state, and cardiovascular stress indicate platelet dysfunction. Pearson correlation coefficients, R, of intra-dialysis platelet lysate RNA or protein relative changes against pre-dialysis plasma protein levels or intra-dialysis plasma relative changes, categorized by interpreted effects on platelets caused by (**A**) coagulative and (**B**) inflammatory indicators. (**A**) Platelet ΔRNA correlates positively to pre-dialysis levels of coagulative indicators and negatively to intra-dialysis protein changes, revealing targets of selective megakaryocyte upregulation and stimulated synthesis during dialysis. Platelet proteome correlations to plasma support acute MMP and TIMP exocytosis during dialysis and elevated chronic membrane-type MMP14 presentation with plasma levels of platelet activators. Increasing acute MMP and TIMP ΔRNA with increasing chronic plasma indicators, coupled

with decreasing ΔRNA with increasing acute Δplasma indicators attributed to translation and degradation support MMPs and TIMPs as platelet-mediated targets causing dysfunction. (**B**) Platelet secretome correlations to chronic levels and acute changes in plasma inflammatory markers show platelet contributions to inflammatory and regenerative response. EGF is chronically enhanced and acutely synthesized, while IL1β is chronically amplified in platelets. Meanwhile, PDGFD, TIMP2, and TBXAS1 RNA are protected with acute inflammation. Membrane-type MMPs appear to be chronically suppressed and acutely enhanced, while TIMP3 synthesis is chronically suppressed and PPBP is acutely secreted. (**C**) Platelet inhibition by PGI_2 protects RNA from translation as shown by positive correlations against EGF, GAPDH, PPBP, and TGFβ1 transcripts and negative correlations against granule CTGF and MMP3. PAFAH2 upregulation correlates to plasma NTpBNP, showing platelet dysfunction with chronic cardiac strain. Platelet renewal is shown by TIMP2 RNA increases and granule TIMP1 decreases with plasma TPO. Figure was prepared in Matlab R2019 and Microsoft Excel v2020.

Table 2.7. Multiple linear regression of plasma clotting factors to MMP and TIMP upregulation in platelets.

Predictor(s)	R^2	Adjusted R^2	P-value
A = PAF (Plasma), B = 11TXB2 (Plasma), C = PAF (ΔPlasma), D = 11TXB2 (ΔPlasma)			
y = MMP1 (ΔRNA). y = -0.93 + 2.0E-4*A + 7.6E-5*B			
A+B	0.91	0.85	0.027
A	0.76	0.73	0.00050
B	0.82	0.78	0.013
y = TIMP2 (ΔRNA). y = -0.93 + 3.3E-5*A + 7.2E-4*B - 1.0*C - 2.5*D			
A+B+C+D	0.98	0.93	0.044
A+B+C	0.94	0.89	0.022
A+B+D	0.97	0.95	0.0076
A+C+D	0.58	0.46	0.028
B+C+D	0.98	0.95	0.0061
A+B	0.94	0.92	0.0032
A+C	0.45	0.35	0.039
A+D	0.44	0.34	0.040
B+C	0.94	0.91	0.0038
B+D	0.97	0.96	0.00080
C+D	0.11	0.023	0.31
A	0.28	0.23	0.049
B	0.94	0.92	0.0004

C	0.07	0.025	0.22
D	0.093	0.049	0.16

i. Chronic elevation of platelet activators accelerates platelet turnover and enhances overall translative capacity, while acute elevation preferentially augments MMP/TIMP translation and secretion

Platelet secretome correlations to plasma measurements of clotting factors connect platelet activation with both long- and short-term changes in transcriptomic potential and secretory behavior (**Figure 2.7A**). Multiple positive correlations between RNA and pre-HD plasma clotting factor levels reveal selective growth factor, MMP1, and TIMP upregulation upon platelet renewal for patients with chronic elevation of PAF and TXM. In parallel, negative RNA correlations to acute plasma clotting factor changes show selective translation and degradation of MMP1 RNA with iatrogenic clotting. Negative platelet lysate IGF1 and positive MMP14 correlations to pre-HD plasma PAF reveal heighted platelet sensitization to granule secretion and membrane-MMP presentation. Finally, correlations between the change in platelet lysate (ΔPL) and plasma (Δplasma) clotting factors similarly show MMP and TIMP secretion and MMP14 presentation with acute clotting. When collectively applied as predictors of platelet activity, multivariate linear regression reveals that pre-HD clotting factor elevation of PAF and TXM indicate MMP1 upregulation ($R^2 = 0.91$, $p = 0.027$), while pre-HD elevation and intra-HD clearance of PAF and TXM indicate TIMP2 upregulation ($R^2 = 0.98$, $p = 0.044$) (**Table 2.7**).

Table 2.8. Multiple linear regression of platelet upregulation to acute inflammation.

Predictor(s)	R^2	Adjusted R^2	P-value
A = PDGFD (ΔRNA), B = TBXAS1 (ΔRNA), C = TIMP2 (ΔRNA)			
y = CRP (ΔPlasma). y = -0.15 - 0.012*A + 0.14*B + 0.34*C			
A+B+C	0.87	0.82	0.00070
A+B	0.40	0.30	0.048
A+C	0.86	0.83	0.00010
B+C	0.55	0.50	0.00040
A	0.32	0.27	0.028
B	0.11	0.09	0.035
C	0.49	0.47	0.0002

ii. Inflammatory elevation accompanies amplified platelet inflammatory and regenerative response

Inflammatory cytokines influence the platelet secretome in dialysis patients (**Figure 2.7B**). Platelet EGF and IL1β RNA increased with plasma IL1β, while EGF RNA was translated and degraded with plasma ΔIFNγ, showing regenerative and inflammatory contributions with

systemic inflammation. Conversely, positive PDGF-DD, TIMP2, and thromboxane (TX) RNA correlations to acute plasma ΔCRP suggest that acute inflammation suppresses translation and degradation of pro-fibrotic RNA (R^2 = 0.87, p = 0.0007) (**Table 2.8**). Whereas clotting factor elevation predicted platelet MMP/TIMP production and secretion, inflammatory elevation predicted growth factor amplification and production. Elevated plasma TNFα accompanied reduced ΔMMP24 and ΔTIMP3, suggesting reduced MMP/TIMP production. Degranulation with acute inflammation is observed by presentation of MMP14 and depletion of PPBP.

iii. Patients with higher native platelet inhibition show lower platelet dysfunction

Platelet correlations to cardiovascular markers validate known regulatory and dialytic effects (**Figure 2.7C**). Platelet dysfunction is observed by increasing PAF RNA with plasma NTpBNP. TIMP2 RNA upregulation and PL TIMP1 depletion with plasma ΔTPO shows selective TIMP renewal with platelet turnover. Positive RNA correlations to plasma PGI2 and ΔPGI2 validate platelet inhibition of RNA translation and degradation, though minimal improvement in adjusted R^2 is observed by multiplexing RNA predictors against plasma PGI2 (**Table 2.9**). Finally, platelet MMP1 RNA, MMP3 and CTGF production are attenuated by higher plasma PGI2. Thus, normal restorative platelet inhibition indicates lower platelet dysfunction.

Table 2.9. Multiple linear regression of platelet upregulation to plasma PGI2 levels.

Predictor(s)	R^2	Adjusted R^2	P-value
A = EGF(ΔRNA), B = GAPDH (ΔRNA)			
y = PGI2 (Plasma). y = 1.8 + 0.90*A + 0.79*B			
A+B	0.82	0.70	0.078
A	0.77	0.71	0.022
B	0.79	0.74	0.018
A = PDGFD (ΔRNA), B = TBXAS1 (ΔRNA), C = TIMP2 (ΔRNA)			
y = PGI2 (ΔPlasma). y = -0.14 + 0.29*A + 0.16*B + 0.07*C			
A+B+C	0.28	0.21	0.015
A+B	0.24	0.20	0.0088
A+C	0.27	0.23	0.0053
B+C	0.24	0.19	0.012
A	0.24	0.22	0.0021
B	0.19	0.17	0.0073
C	0.18	0.16	0.0094

iv. Faster BFR and longer HD Vintage exacerbate platelet dysfunction

Comparisons of platelet RNA and protein levels against clotting factors indicate broader effects of BFR and Vintage on long-term platelet translation and secretion. Faster BFR

increasingly stimulates platelet dysfunction, shown by comparison of pre-HD plasma PAF to BFR (**Figure 2.1D**) by multivariate linear regression. Similarly, stimulation of platelet RNA renewal and degranulation with plasma clotting factor elevation depict a mechanism of increasingly stimulated platelet dysfunction with BFR (**Figure 2.7A**). Decreasing plasma ΔPAF and ΔTXM with both higher BFR and Vintage, respectively (**Figures 2.3B&C**), and increasing ΔMMP1 RNA and PL ΔMMPs and ΔTIMPs with decreasing ΔPAF and ΔTXM (**Figure 2.7A**) show preferential augmentation of platelet MMPs and TIMPs with increasing BFR and Vintage. Further, platelet-driven mechanisms causing tissue dysregulation appear to extend between HD sessions, shown by the significant relative increases in clotting factor RNA post-HD. Thus, in addition to directly enhancing platelet PAF RNA (**Figure 2.6B**), faster BFR and longer Vintage may cause platelet behavioral adaptations that reduce regenerative contributions and disrupt proteolytic balance.

VII. Hemodialysis shifts platelet function from regenerative to pro-fibrotic

Platelet correlations to circulating clotting, inflammatory, and cardiovascular factors indicate worsening dysfunction with accelerated platelet turnover, subdued acute phase response, cardiac stress markers, and attenuated platelet inhibition. In parallel, secretome correlations to fibrotic and regenerative factors reveal distinct modes of platelet behavior and suggest a chronic shift toward a pro-fibrotic mileu. Increasingly pro-fibrotic platelets with proteolytic circulation and decreasingly pro-fibrotic platelets with regenerative circulation show two sides of the same coin. Regenerative feedback responses to fibrotic activity and vice versa show short-term mode-switching between HD sessions. Inverse proportionalities between heterogeneous granule proteins and proteases illustrate a long-term mechanism accounting for shifts in production.

i. Perturbed plasma proteolytic balance is associated with pro-fibrotic platelets with enhanced MMP/TIMP production and secretion

Increasing granule MMPs and TIMPs with increasing pro-fibrotic RNA identify platelet populations with enhanced fibrotic contributions (**Figure 2.8A**). Granule MMPs and TIMPs increased with fibrotic GF, MMP, and TIMP RNA, while membrane-type MMPs increased with clotting factor RNA. Platelet TGFβ1, TIMP1, and PPBP upregulation predicted stored MMP1 (R^2 = 0.88, p = 0.043) and MMP2 (R^2 = 0.92, p = 0.0033) concentrations (**Table 2.10**). Increasingly pro-fibrotic platelet transcriptomes are also identified by acute plasma MMP and TIMP increases (**Figure 2.8B**). Fibrotic GF, TIMP, and TX transcripts increased with acute increases in plasma TIMPs (R^2 = 0.45, p = 0.025) (**Table 2.11**), while PAF RNA increased with acute increases in plasma MMPs (R^2 = 0.60, p = 0.026) (**Table 2.12**). The self-amplifying cycle of fibrotic transcript upregulation and protein synthesis with acute proteolytic imbalance is further supported by observations of enhanced platelet MMP/TIMP production and secretion (**Figure 2.8C**), shown by increases in platelet lysate MMP/TIMP with chronic plasma TIMP

elevation (R^2 = 0.79, p = 0.043) and decreases in platelet lysate MMP/TIMP with acute plasma TIMP elevation (R^2 = 0.79, p = 0.043) (**Table 2.13**).

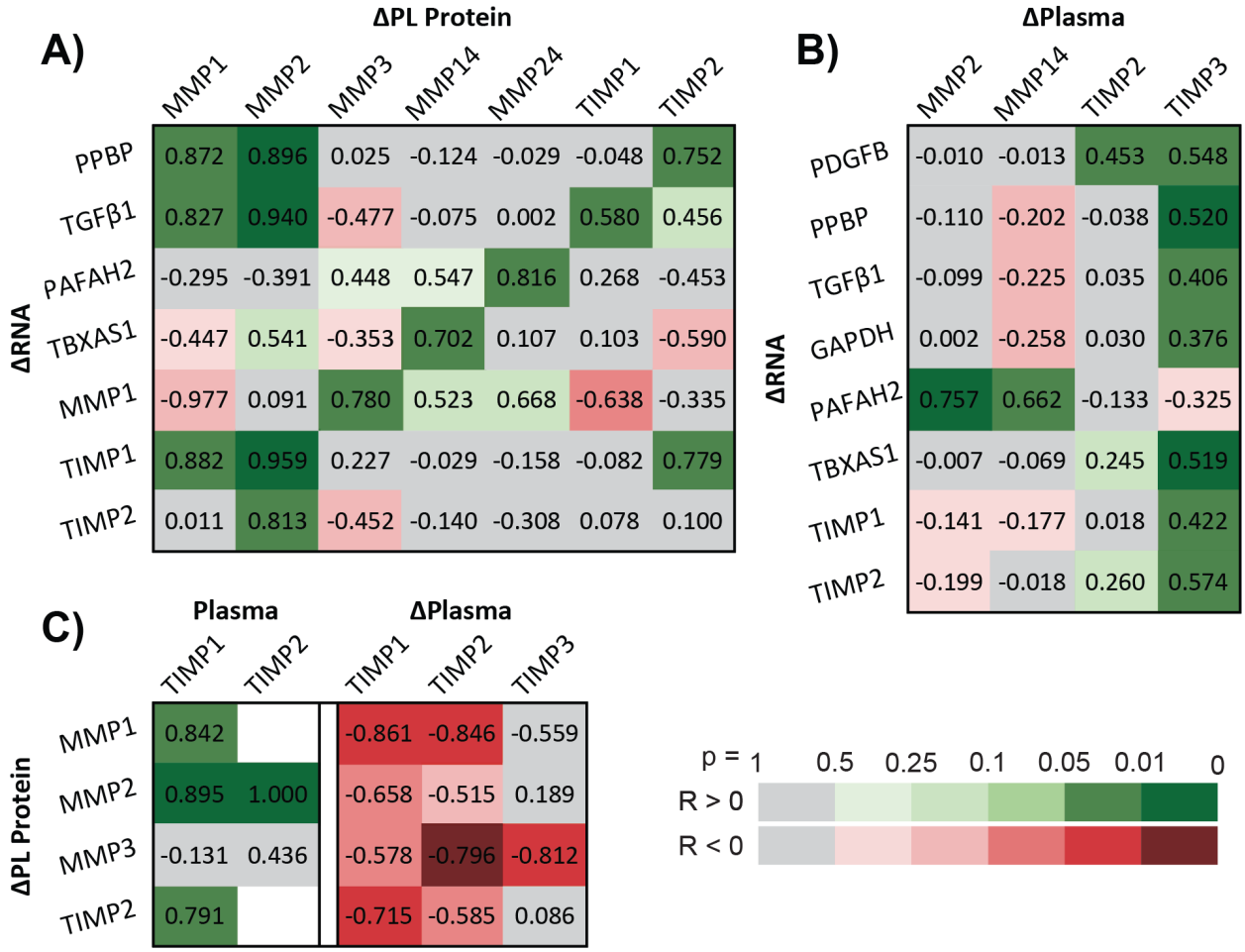

Figure 2.8. Pro-fibrotic platelet secretomes correlate to elevated plasma MMPs and TIMPs. Pearson correlation coefficients, R, of fibrotic platelet (**A**) ΔRNA against platelet ΔMMPs and ΔTIMPs, (**B**) ΔRNA against plasma ΔMMPs and ΔTIMPs, and (**C**) Δprotein against plasma TIMPs and ΔTIMPs. (**A**) Platelets with acutely enhanced MMP and TIMP secretomes have amplified transcripts for MMPs, TIMPs, platelet activators, and other fibrotic factors. (**B**) Patients presenting acute plasma MMP and TIMP increases have platelets exhibiting greater RNA for fibrotic factors. (**C**) Chronic plasma TIMP elevation accompanies greater platelet production of MMPs and TIMPs, and increased intra-dialysis MMP and TIMP secretion. Figure was prepared in Microsoft Excel v2020 (Microsoft Corp. www.microsoft.com)..

Table 2.10. Multiple linear regression of fibrotic upregulation to platelet MMP levels.

Predictor(s)	R^2	Adjusted R^2	P-value
A = TGFb1 (ΔRNA), B = TIMP1 (ΔRNA), C = PPBP (ΔRNA)			
y = MMP1 (ΔPL). y = -0.45 - 0.81*A + 0.64*B			
A+B	0.88	0.79	0.043
A	0.68	0.61	0.042
B	0.78	0.72	0.020
y = MMP2 (ΔPL). y = 0.75 + 1.0*A + 1.7*B - 0.29*C			
A+B+C	0.92	0.88	0.0033
A+B	0.92	0.90	0.00050
A+C	0.88	0.85	0.0015
B+C	0.92	0.89	0.00050
A	0.88	0.87	0.00020
B	0.92	0.91	0.000043
C	0.80	0.78	0.0011

Table 2.11. Multiple linear regression of fibrotic upregulation to intra-dialysis plasma TIMP changes.

Predictor(s)	R^2	Adjusted R^2	P-value
A = PPBP, B = TGFb1, C = GAPDH, D = TBXAS1, E = TIMP1 (ΔRNA)			
y = TIMP3 (ΔPlasma). y = 0.13 + 0.21*A + 0.038*B - 0.091*C + 0.36*D + 0.20*E			
A+B+C+D+E	0.45	0.32	0.025
A+B+C+D	0.43	0.32	0.016
A+B+C+E	0.40	0.29	0.020
A+B+D+E	0.44	0.33	0.013
A+C+D+E	0.45	0.35	0.010
B+C+D+E	0.41	0.30	0.021
A+B+C	0.31	0.22	0.033
A+B+D	0.41	0.33	0.0075
A+B+E	0.28	0.20	0.042
A+C+D	0.43	0.35	0.0058
A+C+E	0.39	0.31	0.0084
A+D+E	0.44	0.36	0.0048
B+C+D	0.33	0.24	0.028

B+C+E	0.37	0.29	0.013
B+D+E	0.41	0.32	0.0086
C+D+E	0.39	0.31	0.0093
A+B	0.27	0.22	0.020
A+C	0.3	0.24	0.013
A+D	0.41	0.36	0.0023
A+E	0.28	0.23	0.015
B+C	0.21	0.15	0.055
B+D	0.33	0.27	0.0098
B+E	0.21	0.15	0.051
C+D	0.29	0.23	0.017
C+E	0.35	0.3	0.0047
D+E	0.39	0.33	0.0029
A	0.27	0.24	0.0046
B	0.16	0.13	0.032
C	0.14	0.11	0.049
D	0.27	0.24	0.0055
E	0.18	0.15	0.023

Table 2.12. Multiple linear regression of plasma MMP changes to platelet PAF upregulation.

Predictor(s)	R^2	Adjusted R^2	P-value
A = MMP2 (ΔPlasma), B = MMP14 (ΔPlasma)			
y = PAFAH2 (ΔRNA). y = 0.14 + 1.4*A + 0.66*B			
A+B	0.60	0.50	0.026
A	0.57	0.53	0.0070
B	0.44	0.38	0.026

Table 2.13. Multiple linear regression of platelet MMPs and TIMPs to plasma TIMP elevation.

Predictor(s)	R^2	Adjusted R^2	P-value
A = MMP2 (ΔPL), B = MMP3 (ΔPL), C = TIMP2 (ΔPL)			
y = TIMP1 (Plasma). y = 1.4E5 + 3.8E4*A + 2.3E4*C			
A+C	0.79	0.69	0.043
A	0.80	0.77	0.0011
C	0.63	0.57	0.011
y = TIMP2 (ΔPlasma). y = -0.021 - 0.22*B - 0.15*C			
B+C	0.70	0.58	0.050
B	0.63	0.59	0.0059
C	0.34	0.25	0.098

ii. Higher plasma levels of fibro-protective GFs correlate to lower fibrotic and higher regenerative contributions by platelets

Higher plasma levels of regenerative growth factors indicated platelets with decreasing fibrotic contributions (**Figure 2.9A**). Plasma FGF2 correlated to reduced RNA for inflammatory IL1β and fibrotic TGFβ1.Platelet production and secretion of fibrotic CTGF and TIMP1 decreased with plasma FGF2 and IGF1, indicated by negative correlations to pre-HD levels and positive correlations to intra-HD changes. Using MLR, TGFβ1 RNA retention and reduced PL CTGF and TIMP1 predicted plasma FGF2 levels (R^2 = 1.0, p = 0.0021) (**Table 2.14**). Further, platelet TIMP1 was predicted by plasma IGF1 depression pre-HD, accumulation intra-HD, and FGF2 clearance (R^2 = 1.0, p = 0.036) (**Table 2.14**). However, unlike FGF2, plasma IGF1 correlated to increased platelet MMP1 RNA. Finally, clotting factor translation was reduced with ΔEGF, shown by TX RNA preservation.

Table 2.14. Multiple linear regressions of plasma growth factors to platelet fibrotic production.

Predictor(s)	R^2	Adjusted R^2	P-value
A = TGFβ1 (ΔRNA), B = CTGF (ΔPL), C = TIMP1 (ΔPL)			
y = FGF2 (Plasma). y = -1387 + 774*A - 4981*B - 84*C			
A+B+C	1.0	1.0	0.0021
A+B	0.94	0.88	0.059
A+C	0.80	0.60	0.200
B+C	0.89	0.78	0.11
A	0.18	0.14	0.030
B	0.86	0.81	0.023
C	0.78	0.70	0.048
A = IGF1 (Plasma), B = FGF2(ΔPlasma), C = IGF1 (ΔPlasma)			
y = TIMP1 (ΔPL). y = 2.2 - 3.8E-5*A - 3.3*B + 3.2*C			
A+B+C	1	1	0.036
A+B	0.95	0.89	0.053
A+C	0.96	0.93	0.036
B+C	0.91	0.87	0.0075
A	0.82	0.76	0.035
B	0.91	0.89	0.001
C	0.8	0.78	0.0001

iii. Acute elevation in fibrotic activity and PDGFs accompany a regenerative platelet response between treatment sessions

Acute enhancements in platelet secretome growth factors to acute plasma increases in fibrotic activity suggest short-term behavioral adaptations between HD sessions (**Figure 2.9B**). Increased fibro-protective RNA (FGF2 and EGF) with fibrotic plasma (MMP9, ΔPPBP, and ΔTIMP3) shows a regenerative shift post-HD. This is supported by platelet IGF1 and PDGF retention with plasma ΔMMPs and ΔTIMPs. FGF2 upregulation with ΔPDGFD and retention with pre-HD PDGFD demonstrate a case of fibrotic enhancement of regenerative potential. In fact, multivariate linear regression revealed that plasma MMP9, PDGFD, and PPBP positively predict FGF2 upregulation (R^2 = 0.76, p = 0.015) (**Table 2.15**). Further feedback activity is observed by secretome correlations to PDGFs (**Figure 2.9C**). As expected, PDGFB RNA decreases as plasma levels increase because of translation followed by degradation. Other platelet lysate correlations to plasma PDGFs show platelet depletion of PF4, retention of MMP3 and TIMP3, and acutely stimulated production of membrane-type MMPs.

Table 2.15. Multiple linear regression of plasma fibrotic factors to platelet growth factor upregulation.

Predictor(s)	R^2	Adjusted R^2	P-value
A = MMP9 (Plasma), B = PDGFD (ΔPlasma), C = PPBP (ΔPlasma)			
y = FGF2 (ΔRNA). y = -0.37 + 9.9E-5*A + 0.92*B +1.1*C			
A+B+C	0.76	0.65	0.015
A+B	0.43	0.32	0.047
A+C	0.57	0.47	0.023
B+C	0.69	0.61	0.0092
A	0.33	0.28	0.026
B	0.3	0.24	0.042
C	0.36	0.29	0.041

iv. Secretome correlations support pro-fibrotic physiological adaptations in platelets

Platelet behavioral adaptations may be explained in part by selective differences in granule activity (**Figure 2.9D**). Decreasing platelet lysate MMP9 and increasing platelet lysate PPBP with increasing EGF RNA show an inverse trade-off between producing proteases and other alpha granule proteins. Further, plasma PPBP was accompanied by reduced protease secretion, observed by platelet lysate MMP2 retention, and increased alpha-granule production elsewhere, observed by TIMP3 and PDGFB synthesis. Thus, increasingly regenerative platelet

phenotypes may be characterized by disproportionate growth factor accumulation and protease attenuation. Conversely, increasingly fibrotic platelets may present with protease accumulation and heterogenic alpha granules with pro-fibrotic disproportion.

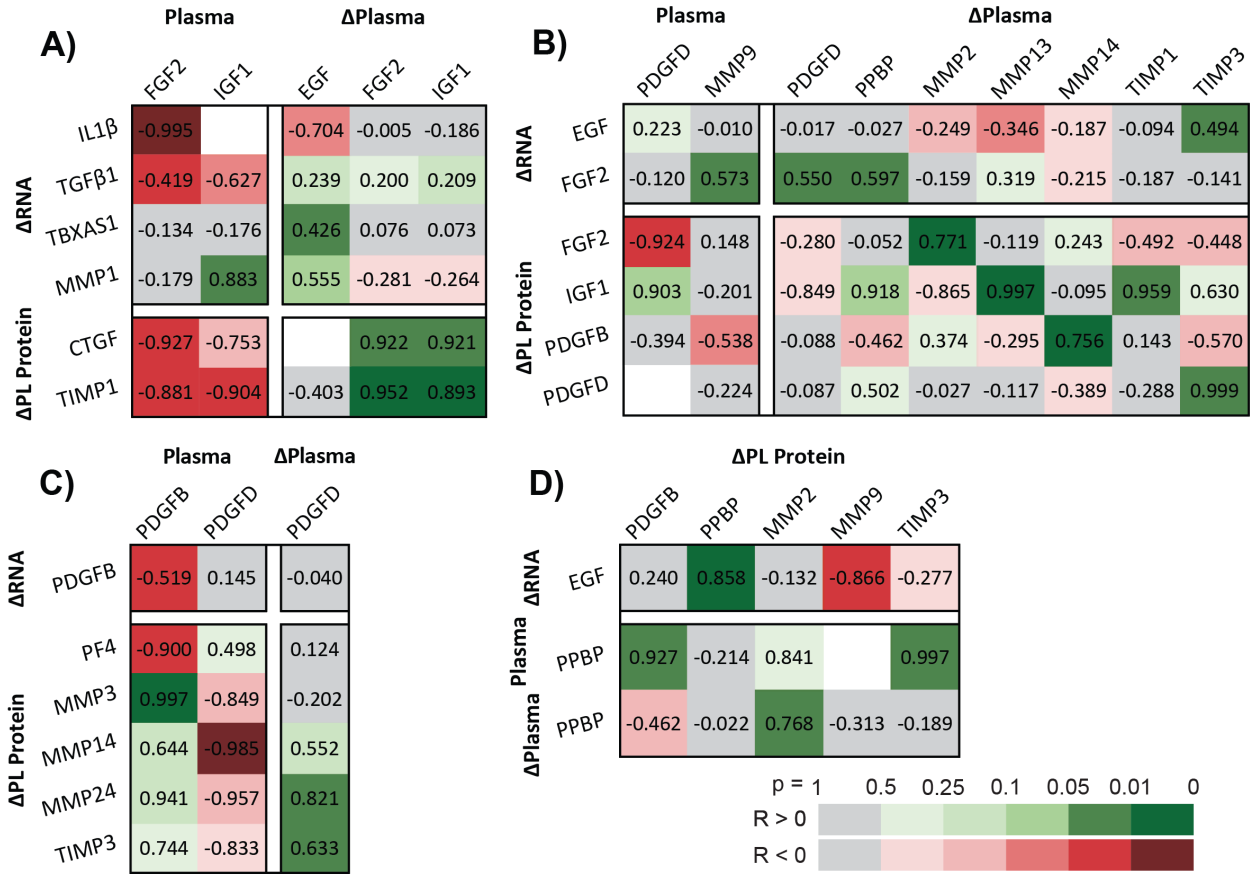

Figure 2.9. Growth factor and proteolytic trends suggest a chronic shift in platelet function from regenerative to pro-fibrotic. Pearson correlation coefficients, R, of intra-dialysis platelet lysate RNA or protein relative changes against pre-dialysis plasma protein levels or intra-dialysis plasma relative changes, categorized by interpreted effects on platelets caused by (**A**) growth factors, (**B**) fibrotic activity, and (**C**) PDGFs. (**A**) Higher plasma levels of regenerative growth factors indicated platelets with decreasing fibrotic contributions. Chronic fibro-protective FGF2 plasma elevation correlated to lower fibrotic molecule production and RNA, and acute plasma FGF2 elevation correlated to fibrotic molecule retention. Plasma EGF reduces TBXAS1 translation, while IGF1 shows mixed effects including MMP1 amplification. (**B**) Compensatory mechanisms are observed by acute enhancement of regenerative factors with acute plasma fibrotic activity, showing transient mode-switching between dialysis sessions. Growth factor RNA and protein synthesis accompany acute plasma MMP and TIMP increases. Plasma PDGFD elevation accompanies FGF2 RNA upregulation and protection. (**C**) PDGF feedback shows an

example of fibrotic enhancement of regenerative potential. PDGFB RNA decreases with increasing plasma PDGFB levels, showing degradation after translation and secretion. Rising PDGF levels accompany decreased granule PF4, TIMP3 and MMP3 retention, and acutely stimulated presentation of membrane-MMPs. (**D**) Correlations among alpha-granule proteins and proteases elucidate physiological adaptations contributing to pro-fibrotic or fibro-protective functions. Decreasing MMP9 and increasing PPBP in platelets with increasing EGF RNA show a trade-off in differential alpha-granule filling behaviors. Acute plasma PPBP elevation, which showed to accompany regenerative RNA enhancement, correlated to MMP2 retention. Figure was prepared in Microsoft Excel v2020 (Microsoft Corp. www.microsoft.com).

Correlation Plots - Raw Data

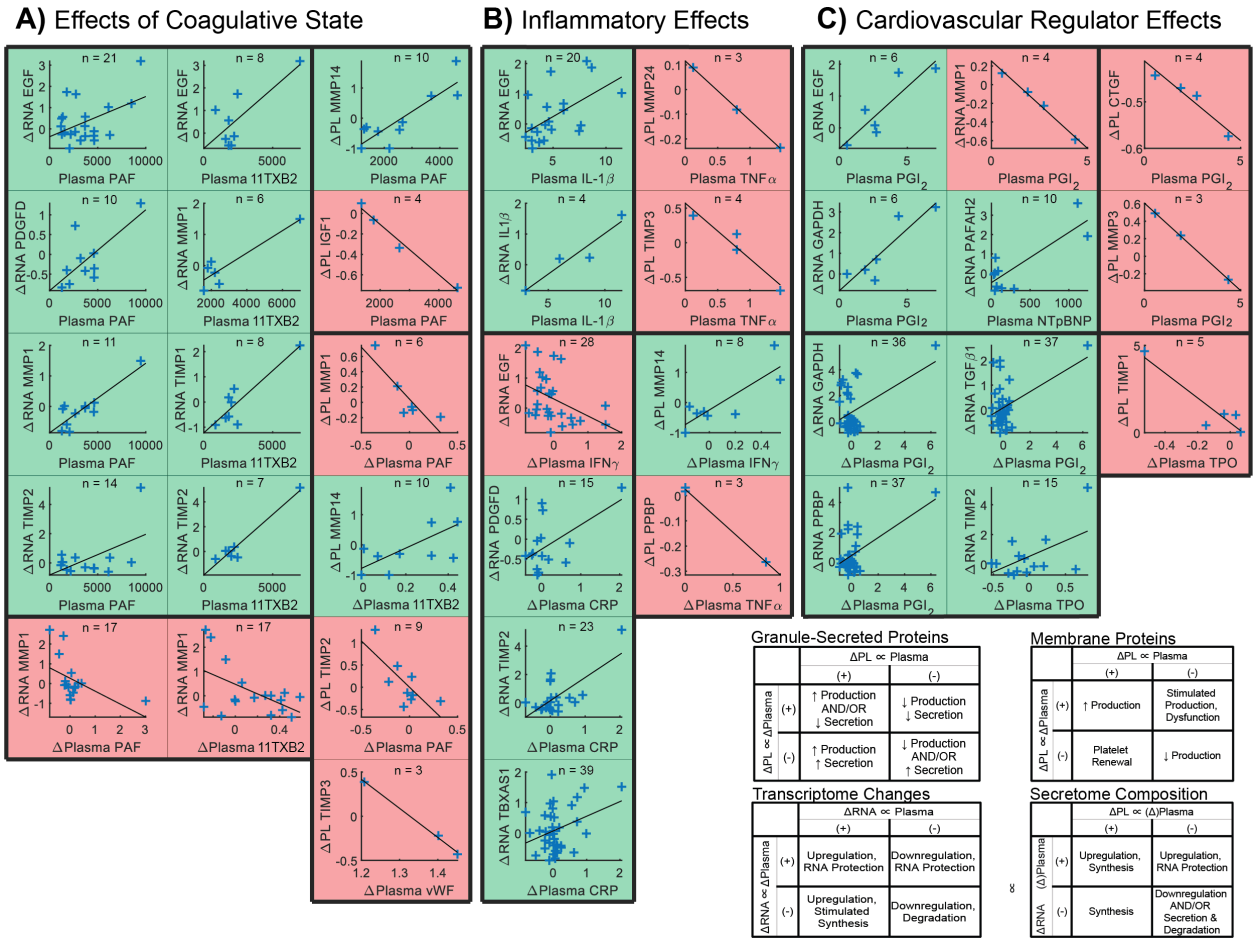

Figure 2.10. Significant Pearson correlations for Figure 2.7. ($p < 0.05$) Intra-dialysis platelet lysate RNA or protein relative changes against pre-dialysis plasma protein levels or intra-dialysis plasma relative changes, categorized by interpreted effects on platelets caused by (**A**) coagulative, (**B**) inflammatory, and (**C**) cardiovascular indicators.

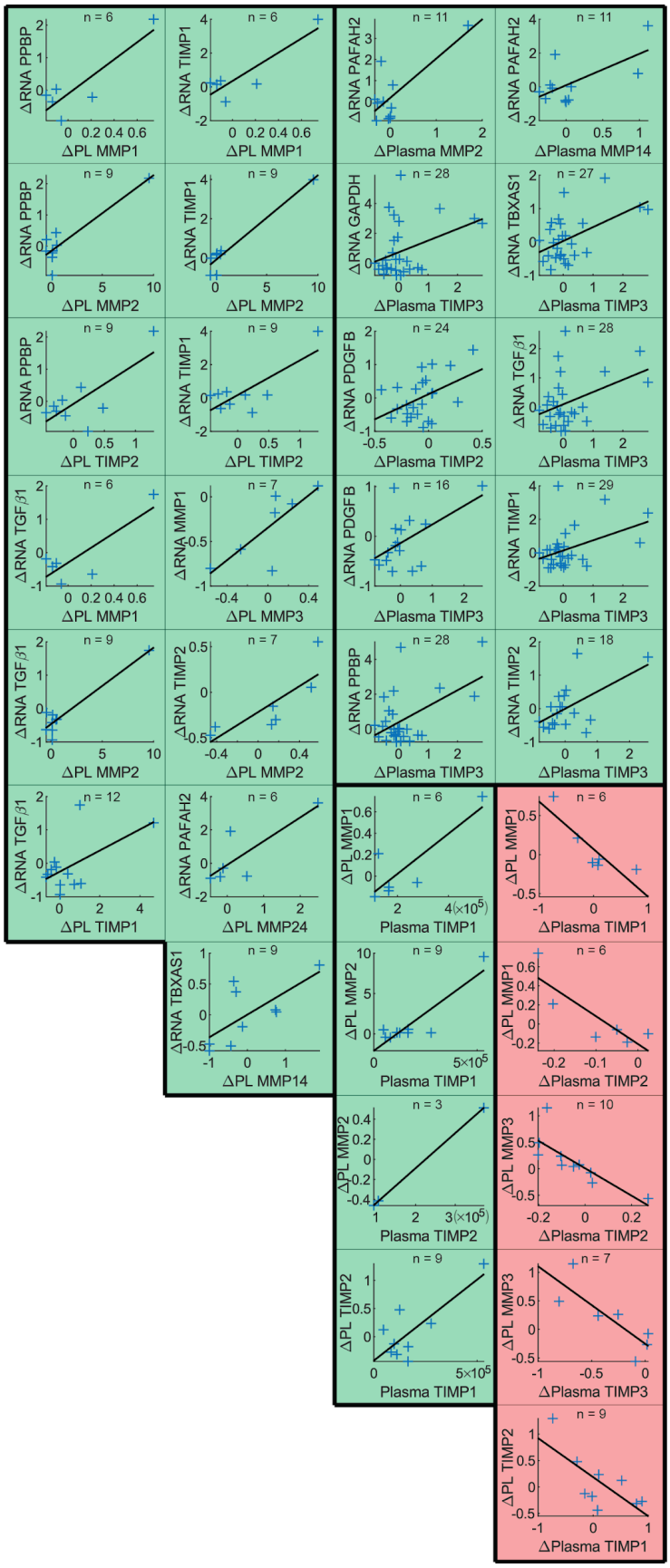

Figure 2.11. Significant Pearson correlations for Figure 2.8. ($p < 0.05$) Platelet ΔRNA against platelet Δprotein, platelet ΔRNA against Δplasma, and platelet Δprotein against plasma or Δplasma.

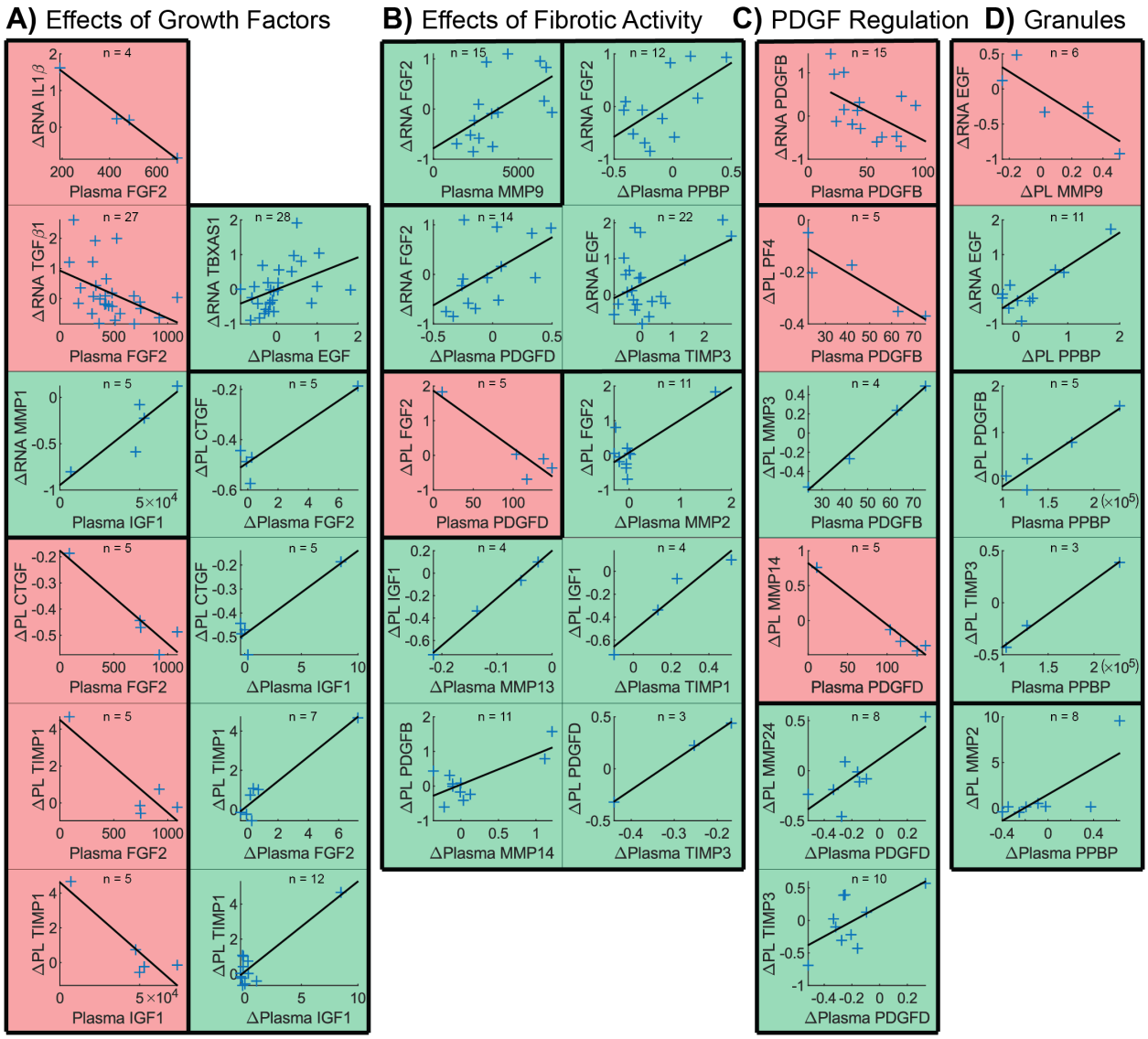

Figure 2.12. Significant Pearson correlations for Figure 2.9. ($p < 0.05$) Intra-dialysis platelet lysate RNA or protein relative changes against pre-dialysis plasma protein levels or intra-dialysis plasma relative changes, categorized by interpreted effects on platelets caused by (**A**) growth factors, (**B**) fibrotic activity, and (**C**) PDGFs. (**D**) Correlations amongst alpha-granule and lysosome proteins elucidate physiological adaptations contributing to pro-fibrotic or fibro-protective functions.

Discussion

Many plasma biomarker measurements reported in this study mirror prior findings in HD patients demonstrating effects of uremia[10,18,19,22], acute inflammatory response[30–32], cardiovascular risk through mechanical strain and oxidative stress[33,44], coagulative dysfunction[26], and microvascular damage and systemic fibrosis[28,29,34–38,45]. Comparison of these measurements to prescribed dialysis metrics and quantitative platelet characterization yield novel insights into a circulatory environment in HD patients that is characterized by profound shifts in ECM homeostasis, microvascular damage, and platelet function. First, chronic plasma elevation of MMPs and TIMPs, insufficient removal by dialysis, and disproportionate acute TIMP1 enhancement characterize dysregulated ECM homeostasis. These symptoms accompany enhanced production and secretion of MMPs and TIMPs by platelets, illustrating a vicious cycle of dysregulation. Second, depressed FGF2[34,45], elevated IGF1[35], and elevated PDGFD[37] in plasma indicate high risk for microvascular damage and fibrosis, supported by increasing platelet contributions of pro-fibrotic TIMP1, CTGF, and TGFβ1 with decreasing plasma FGF2 and increasing MMP1 RNA with plasma IGF1. Third, platelet secretome correlations reveal adaptive mechanisms that enhance cardiovascular risk. Elevated NTpBNP, which implies cardiovascular strain, indicated greater platelet coagulation, while elevated clotting markers accompanied preferential MMP and TIMP translation and secretion. This pro-fibrotic platelet dysfunction decreased with native platelet inhibition, increasing inflammatory response, and regenerative GF circulation. Contrarily, acute increases in plasma fibrotic activity and PDGFs elicited a reduced pro-fibrotic platelet response in the short-term. Finally, differences between rates of platelet-released factors demonstrate chronic adaptations affecting differential secretory kinetics of alpha-granule subtypes, known to be heterogenous and specialized for inflammatory, immune, and tissue regulatory functions beyond hemostasis[46].

Heightened BFR has been linked to increased HD patient hospitalization and mortality in studies comparing dialysis service providers and national standards[47,48], however underlying mechanisms are generally unexplored. The correlations observed in this study between platelet function, HD filtration rate and secondary effects of high-BFR reveal potential deregulatory mechanisms of increasing BFR. HD patients prescribed higher BFR had higher pre-HD plasma PAF and MMP3 levels despite higher post-HD clearance of PAF, MMP2, and MMP3. In platelets, higher BFR enhanced both PAF RNA and intracellular MMP3. Consequently, PAF and MMP enhancement in plasma correlated to higher overall platelet RNA with emphasis on fibrotic transcripts and augmented MMP translation and secretion. Similar trends were observed against HD Vintage, with increasing PAF RNA, PPBP synthesis, and platelet MMP1 and TIMP2 secretion over time. Thus, while coagulative reactivity has been shown to remain consistent throughout individual HD sessions[49], platelet behaviors beyond coagulation may naturally change with longer prior time on dialysis, and increasing BFR may exacerbate pathogenesis by accentuated repetitive and excessive stimulation of platelets during therapy. Increasing plasma PAF with BFR and platelet RNA content may be of particular significance in driving microvascular damage not only in the

direct promotion of leukocyte activation[38], but also indirectly by bridging leukocyte-endothelial adhesion by P-selectin presentation which is enhanced by degranulation[39]. Chronic change in platelet function considering no acute change in coagulation may in part be explained by receptor shedding, given long-term accumulation of MMPs in spite of intra-HD clearance[50]. Importantly, pharmacological targeting of the sequalae of endothelial dysfunction including multi-organ fibrosis[14,51–53] (NCT02285920) and mitochondrial dysfunction[54,55] is an emerging paradigm to reduce cardiovascular mortality among HD patients. Our data suggest that HD-induced dysfunctional platelets likely contribute to the milieu of imbalanced plasma growth factors and proteolytic dysregulation that influence remodeling of endothelium and ECM in ESRD patients.

This study utilized a small patient sample size and did not examine whether similar changes are observed in CKD patients not on dialysis, or those on peritoneal dialysis. While these would have been interesting avenues to explore, the Covid-19 pandemic limited the ability to acquire additional data from this high-risk patient population. High variability in data sample sizes particularly for platelet transcriptome and proteome biomarkers, measurement distributions in Pearson correlations not spread widely over one axis, and ethnic incongruity between control and patient demographics may limit validity of deductions. Further, the large range of prior times on dialysis may introduce variability in acute biological response owing to the degree of tissue changes that may have already occurred. Future studies could provide greater mechanistic insight by performing media transfer experiments to elucidate platelet-leukocyte interactions. Importantly, these findings suggest that further research into whether methods to reduce platelet dysfunction in HD combined with pharmaceutical therapy using the aforementioned emerging treatments is needed in order to draw mechanistic conclusions.

Works Cited

1. Hu, J. R. & Coresh, J. The public health dimension of chronic kidney disease: What we have learnt over the past decade. *Nephrol. Dial. Transplant.* **32**, ii113–ii120 (2017).
2. Inker, L. A. *et al.* KDOQI US commentary on the 2012 KDIGO clinical practice guideline for the evaluation and management of CKD. *Am. J. Kidney Dis.* **63**, 713–735 (2014).
3. Ravarotto, V., Simioni, F., Pagnin, E., Davis, P. A. & Calò, L. A. Oxidative stress – chronic kidney disease – cardiovascular disease: A vicious circle. *Life Sci.* **210**, 125–131 (2018).
4. de Chickera, S. *et al.* The Risk of Adverse Events in Patients With Polycystic Kidney Disease With Advanced Chronic Kidney Disease. *Can. J. Kidney Heal. Dis.* **5**, 205435811877453 (2018).
5. Benz, K., Hilgers, K. F., Daniel, C. & Amann, K. Vascular Calcification in Chronic Kidney Disease: The Role of Inflammation. *Int. J. Nephrol.* **2018**, (2018).
6. Lekawanvijit, S. Cardiotoxicity of uremic toxins: A driver of cardiorenal syndrome. *Toxins (Basel).* **10**, (2018).

7. Shlipak, M. G. *et al.* Cardiovascular mortality risk in chronic kidney disease: Comparison of traditional and novel risk factors. *J. Am. Med. Assoc.* **293**, 1737–1745 (2005).
8. Mark, P. B. *et al.* Redefinition of uremic cardiomyopathy by contrast- enhanced cardiac magnetic resonance imaging. *Kidney Int.* **69**, 1839–1845 (2006).
9. Radhakrishnan, A. *et al.* Coronary microvascular dysfunction: a key step in the development of uraemic cardiomyopathy? *Heart* **105**, 1302–1309 (2019).
10. Wang, X. & Shapiro, J. I. Evolving concepts in the pathogenesis of uraemic cardiomyopathy. *Nat. Rev. Nephrol.* **15**, 159–175 (2019).
11. Galvan, D. L., Green, N. H. & Danesh, F. R. The Hallmarks of Mitochondrial Dysfunction in Chronic Kidney Disease. *Kidney Int.* **92**, 1051–1057 (2017).
12. Yazdi, P. G., Moradi, H., Yang, J., Wang, P. H. & Vaziri, N. D. Skeletal muscle mitochondrial depletion and dysfunction in chronic kidney disease. *Int. J. Clin. Exp. Med.* **6**, 532–539 (2013).
13. Gioscia-Ryan, R. A. *et al.* Mitochondria-targeted antioxidant (MitoQ) ameliorates age-related arterial endothelial dysfunction in mice. *J. Physiol.* **592**, 2549–2561 (2014).
14. House, A. A. Management of Heart Failure in Advancing CKD : Core Curriculum 2018. *Am. J. Kidney Dis.* **72**, 284–295 (2018).
15. Urakawa, I. *et al.* Klotho converts canonical FGF receptor into a specific receptor for FGF23. *Nature* **444**, 770–774 (2006).
16. Edwards, N. C. *et al.* Defining the natural history of uremic cardiomyopathy in chronic kidney disease: The role of cardiovascular magnetic resonance. *JACC: Cardiovascular Imaging* **7**, 703–714 (2014).
17. Stromp, T. A. *et al.* Quantitative Gadolinium-Free Cardiac Fibrosis Imaging in End Stage Renal Disease Patients Reveals A Longitudinal Correlation with Structural and Functional Decline. *Sci. Rep.* **8**, 1–10 (2018).
18. Fassett, R. G. *et al.* Biomarkers in chronic kidney disease: A review. *Kidney Int.* **80**, 806–821 (2011).
19. Sun, J. *et al.* Biomarkers of cardiovascular disease and mortality risk in patients with advanced CKD. *Clin. J. Am. Soc. Nephrol.* **11**, 1163–1172 (2016).
20. Vanholder, R. *et al.* Review on uremic toxins: Classification, concentration, and interindividual variability. *Kidney Int.* **63**, 1934–1943 (2003).
21. Meert, N. *et al.* Inconsistency of reported uremic toxin concentrations. *Artif. Organs* **31**, 600–611 (2007).
22. Duranton, F. *et al.* Normal and pathologic concentrations of uremic toxins. *J. Am. Soc. Nephrol.* **23**, 1258–1270 (2012).
23. *United States Renal Data System. 2018 USRDS annual data report: End-stage Renal Disease in the United States. Chapter 8: Cardiovascular Disease in Patients with ESRD. National Institutes of Health, National Institute of Diabetes and Digestive and Kidney D*.
24. Weyrich, A. S., Schwertz, H., Kraiss, L. W. & Zimmerman, G. A. Protein synthesis by platelets: Historical and new perspectives. *J. Thromb. Haemost.* **7**, 241–246 (2009).

25. Cecchetti, L. *et al.* Megakaryocytes differentially sort mRNAs for matrix metalloproteinases and their inhibitors into platelets: A mechanism for regulating synthetic events. *Blood* **118**, 1903–1911 (2011).
26. Schoorl, M., Grooteman, M. P. C., Bartels, P. C. M. & Nubé, M. J. Aspects of platelet disturbances in haemodialysis patients. *Clin. Kidney J.* **6**, 266–271 (2013).
27. Summaria, F., Giannico, M. B., Talarico, G. P. & Patrizi, R. Antiplatelet Therapy in Hemodialysis Patients Undergoing Percutaneous Coronary Interventions. *Nephrourol. Mon.* **7**, (2015).
28. Sánchez-González, D. J., Méndez-Bolaina, E. & Trejo-Bahena, N. I. Platelet-rich plasma peptides: Key for regeneration. *Int. J. Pept.* **2012**, (2012).
29. Thachil, J. The lung megakaryocytes and pulmonary fibrosis in systemic sclerosis. *Med. Hypotheses* **72**, 291–293 (2009).
30. Pereira, B. J. G. *et al.* Plasma levels of IL-1β, TNFα and their specific inhibitors in undialyzed chronic renal failure, CAPD and hemodialysis patients. *Kidney Int.* **45**, 890–896 (1994).
31. Zimmermann, J., Herrlinger, S., Pruy, A., Metzger, T. & Wanner, C. Inflammation enhances cardiovascular risk and mortality in hemodialysis patients. *Kidney Int.* **55**, 648–658 (1999).
32. MacDonald, J. H. *et al.* Muscle insulin-like growth factor status, body composition, and functional capacity in hemodialysis patients. *J. Ren. Nutr.* **14**, 248–252 (2004).
33. Zoccali, C. *et al.* Cardiac natriuretic peptides are related to left ventricular mass and function and predict mortality in dialysis patients. *J. Am. Soc. Nephrol.* **12**, 1508–1515 (2001).
34. Villanueva, S. *et al.* Basic fibroblast growth factor reduces functional and structural damage in chronic kidney disease. *Am. J. Physiol. - Ren. Physiol.* **306**, 430–441 (2014).
35. Hamaguchi, Y. *et al.* Elevated serum insulin-like growth factor (IGF-1) and IGF binding protein-3 levels in patients with systemic sclerosis: Possible role in development of fibrosis. *J. Rheumatol.* **35**, 2363–2371 (2008).
36. Bowen-Pope, D. F. & Raines, E. W. History of discovery: Platelet-derived growth factor. *Arterioscler. Thromb. Vasc. Biol.* **31**, 2397–2401 (2011).
37. Borkham-Kamphorst, E., Alexi, P., Tihaa, L., Haas, U. & Weiskirchen, R. Platelet-derived growth factor-D modulates extracellular matrix homeostasis and remodeling through TIMP-1 induction and attenuation of MMP-2 and MMP-9 gelatinase activities. *Biochem. Biophys. Res. Commun.* **457**, 307–313 (2015).
38. Kubes, P., Suzuki, M. & Granger, D. N. Platelet-activating factor-induced microvascular dysfunction: role of adherent leukocytes. *Am. J. Physiol. Liver Physiol.* **258**, G158–G163 (1990).
39. Stokes, K. Y. & Granger, D. N. Platelets: A critical link between inflammation and microvascular dysfunction. *J. Physiol.* **590**, 1023–1034 (2012).

40. Arpino, V., Brock, M. & Gill, S. E. The role of TIMPs in regulation of extracellular matrix proteolysis. *Matrix Biology* (2015). doi:10.1016/j.matbio.2015.03.005
41. Mills, E. W., Green, R. & Ingolia, N. T. Slowed decay of mRNAs enhances platelet specific translation. *Blood* **129**, e38–e48 (2017).
42. Xia, L., Zeng, Z. & Tang, W. H. The Role of Platelet Microparticle Associated microRNAs in Cellular Crosstalk. *Front. Cardiovasc. Med.* **5**, 1–5 (2018).
43. Clancy, L., Beaulieu, L. M., Tanriverdi, K. & Freedman, J. E. The role of RNA uptake in platelet heterogeneity. *Thromb. Haemost.* **117**, 948–961 (2017).
44. Yogalingam, G., Hwang, S., Ferreira, J. C. B. & Mochly-Rosen, D. Glyceraldehyde-3-phosphate dehydrogenase (GAPDH) phosphorylation by protein kinase Cδ (PKCδ) inhibits mitochondria elimination by lysosomal-like structures following ischemia and reoxygenation-induced injury. *J. Biol. Chem.* **288**, 18947–18960 (2013).
45. Bozic, M. *et al.* Association of FGF-2 concentrations with atheroma progression in chronic kidney disease patients. *Clin. J. Am. Soc. Nephrol.* **13**, 577–584 (2018).
46. Heijnen, H. & van der Sluijs, P. Platelet secretory behaviour: As diverse as the granules... or not? *J. Thromb. Haemost.* **13**, 2141–2151 (2015).
47. Dalrymple, L. S. *et al.* Comparison of hospitalization rates among for-profit and nonprofit dialysis facilities. *Clin. J. Am. Soc. Nephrol.* **9**, 73–81 (2014).
48. Foley, R. N. & Hakim, R. M. Why is the mortality of dialysis patients in the United States much higher than the rest of the world? *J. Am. Soc. Nephrol.* **20**, 1432–1435 (2009).
49. Mourikis, P. *et al.* Platelet reactivity in patients with chronic kidney disease and hemodialysis. *J. Thromb. Thrombolysis* **49**, 168–172 (2020).
50. Gardiner, E. E., Al-Tamimi, M., Andrews, R. K. & Berndt, M. C. Platelet receptor shedding. in *Platelets and Megakaryocytes: Volume 3* (eds. Gibbins, J. M. & Mahaut-Smith, M. P.) 321–339 (Springer, 2012). doi:10.1007/978-1-61779-307-3_22
51. Lindberg, K. The kidney is the principle organ mediating klotho effects. *J. Am. Soc. Nephrol.* **25**, 2169–2175 (2014).
52. Maekawa, Y. Klotho protein diminishes endothelial apoptosis and senescence via a mitogen-activated kinase pathway. *Geriatr. Gerontol. Int.* **11**, 510–516 (2011).
53. Hui, H. Klotho suppresses the inflammatory responses and ameliorates cardiac dysfunction in aging endotoxemic mice. *Oncotarget* **8**, 15663–15676 (2017).
54. Jun, M. Antioxidants for chronic kidney disease. *Nephrol.* **18**, 576–578 (2013).
55. Kirkman, D. L., Muth, B. J., Ramick, M. G., Townsend, R. R. & Edwards, D. G. Role of mitochondria-derived reactive oxygen species in microvascular dysfunction in chronic kidney disease. *Am. J. Physiol. Physiol.* **314**, F423–F429 (2017).

Chapter 3

Cyclical depressurization degranulates platelets in an agonist-free mechanism of platelet activation

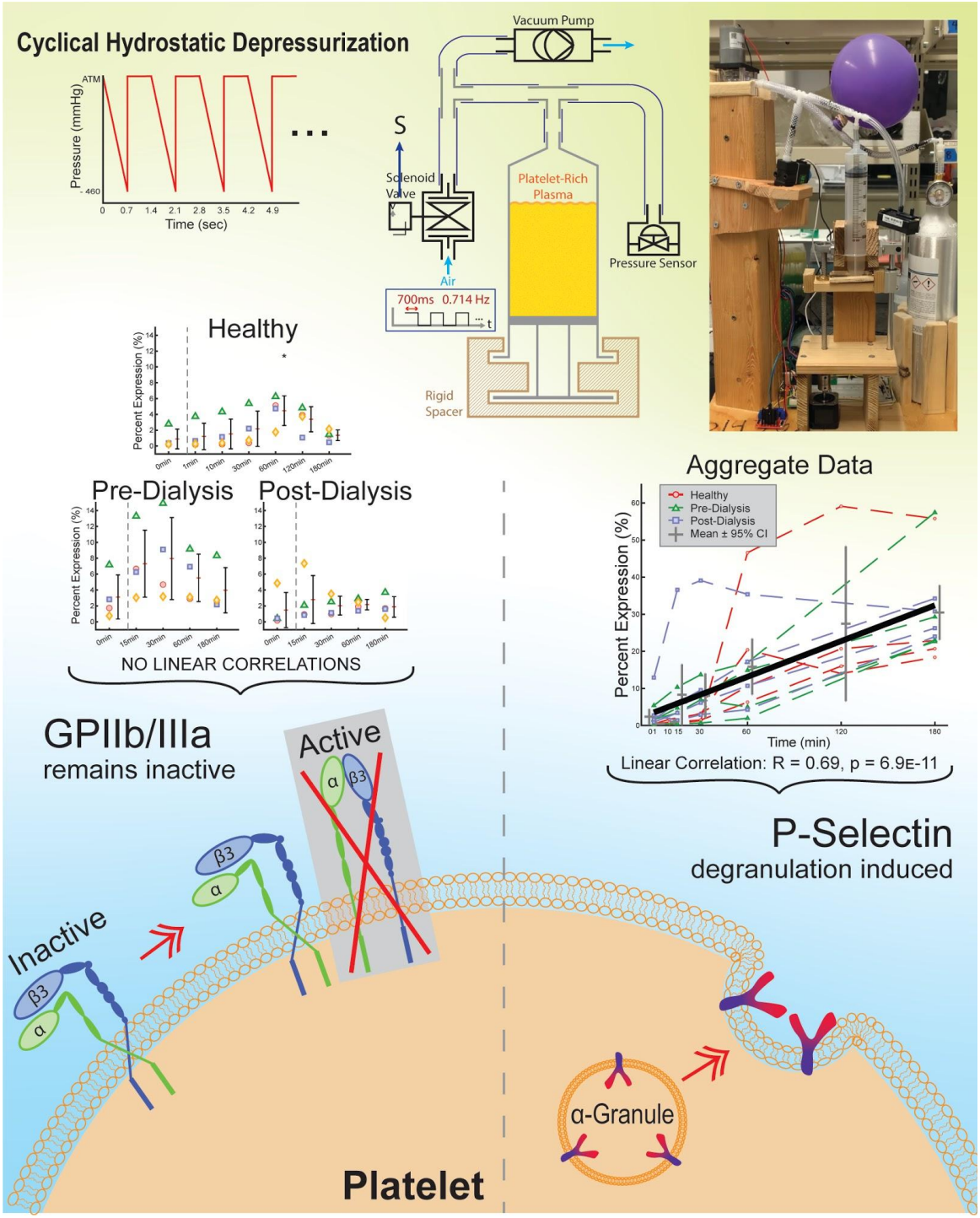

Figure 3.0. Chapter 3 Graphical Abstract.

Introduction

Platelets play a broad role beyond hemostasis as circulating sources of tissue regulatory factors[1]. The contribution to platelet dysfunction by blood filtration therapies like hemodialysis is widely attributed to filter material reactivity and high shear beyond uremia[2,3]. However, these mechanisms activate platelets by receptor adhesion, whether by defective GPIb and GPIIb/IIIa[4], hydrophobic capture[2], or rolling immobilization to RGDS sites on unfurled vWF[5]. Recent hemodialysis findings link chronically pro-fibrotic circulations to increasingly differential platelet granule secretory kinetics[6], amplifying the need to interrogate the drivers and mechanisms of platelet degranulation.

Examining dialysis, the use of hollow microtubes and ultrafiltration produces a flow circuit characterized by rapid and repetitive pressure drops. While receptor-driven signal transduction is well mapped, the effects of non-native pressure cycling present a potential internally-driven alternative that enhances pathological degranulation. Ronco et al measured frictional pressure drops across 200μm diameter hollow fiber dialyzers of up to 200mmHg at a 500mL/min blood flow rate[7]. Interestingly, existing studies on platelets subjected to pressure-based stimulation in isolation are limited. In decompression sickness platelets have heightened reactivity linked to sudden circulatory decompression[8], while the role of platelets in high altitude thrombus formation has long been a topic of debate[9,10]. Hydrostatic decompression induces platelet aggregation during reductions from both atmospheric pressure and high pressurization irrespective of oxygen partial pressure[11], while positive pressure inhibits aggregation[12]. Elsewhere, hydrostatic pressure directly regulates eukaryotic cell volume, cortical tension, and intracellular ion concentration[13]. The application of positive pressure inhibits exocytosis in patch-clamped nerve cells[14], induces volumetric contraction by cytoskeletal rearrangements[15], and causes ion transport[16] including by effects on volume-regulated channels[13]. For platelets, whose behavior is intricately linked to geometry, sphericalization and cytoskeletal expansion characterize the first steps of activation preceding coagulation[17]. Thus, expansive depressurization, particularly of a cyclical nature, may drive platelet activation by influencing the cytoskeleton, ion transport, and exocytotic surface expansion.

In these experiments, platelets are subjected to a more intense depressurization of 460mmHg to establish an upper bound of effects from this isolated stimulus. To exaggerate the repeated acclimation and stimulation characteristic of dialytic recirculation, chamber depressurization occurred periodically over 0.7s at maximum pump evacuation followed by instantaneous re-pressurization to atmospheric levels and 0.7s of rest. Activation was measured by surface expression of PAC1, the activated GPIIb/IIIa integrin complex to fibrinogen, and P-Selectin (CD62P), which is localized to internal granules and externally presented upon degranulation. Because of differences measured in these historically interchangeable biomarkers of platelet activation[18], expression was also measured as a function of ADP exposure for pressure-stimulated and unstimulated (0 minute) samples. Experiments were repeated on

platelets from dialysis patient donors before and after hemodialysis to measure differences in clinical settings. Common expression trends reveal a novel and universal basis for pressure-driven degranulation distinct from shear-based activation, while contrasting population baselines substantiate response variability owing to uremic dysfunction. Depending on the proteomic and transcriptomic contents of circulating platelets, this could exacerbate platelet contributions to fibrotic pathologies and cardiovascular dysregulation in vulnerable patient demographics[6].

Table 3.1. Subject demographics.

Control demographics (n=1)	
Age, years - median (range)	25.31 (25.17-25.32)
Gender ratio - [male/female]	1/0
Ethnicity	
Mixed	1
Patient demographics (n=4)	
Age, years - median (range)	68.75 (46.73-78.79)
Gender ratio - [male/female]	3/1
Ethnicity	
African American	2
Asian American	1
Caucasian	1
Prior time on dialysis, months - median (range)	24.16 (3.78-96.14)
Cause of renal failure	
Hypertension	3
Diabetes mellitus	1
Unknown	0
Comorbidities	
Anemia	2
Hyperlipidemia	1
CHF	2
Hepatitis	0
Hypothyroidism	1
Medication	
Lipid-lowering drugs	2
Platelet inhibitor	2
RAS Inhibitors	1
Unknown	0

Methods

Blood Collection & Platelet Isolation

Hemodialysis blood samples were collected immediately before vascular access and after tubing removal from four patients at DaVita Oakland. All patients were dialyzed using NIPRO single-use, hollow-fiber ELISIO filters. Four control blood samples with no history of smoking, drug abuse, current medications, or comorbidities were collected at the University of California, Berkeley Tang Center. **Table 3.1** summarizes subject demographics. All samples were collected in ACD-A Vacutainers and processed immediately by centrifugation at 200g for 10min to collect the top 90% of platelet-rich plasma (PRP). Collected PRP was centrifuged again for 5min at 200g to remove remaining erythrocyte and leukocyte contamination and gently pipetted into a 60mL plastic syringe in a BSL2 biosafety cabinet for immediate use. Participants provided informed consent under protocols approved by the U.C. Berkeley IRB and in compliance with the Declaration of Helsinki.

Cyclical Depressurization & Sample Collection

The PRP-loaded syringe was evacuated isochorically by 460mmHg using a rigid spacer and 12V/12W diaphragm vacuum pump under constant maximum operation (**Figure 3.1A**). The chamber was re-pressurized to atmospheric using a 12V solenoid valve given an electrical cycle of 700ms impulse followed by 700ms release (**Figure 3.1B**). Chamber pressure was measured by a vacuum transducer (Omega, PX141) elevated to water-level. Valve, pump, sensor, and stepper motor-operated spacer were controlled by NI myDAQ using LabVIEW. PRP was collected by gentle extrusion from the syringe at 0min (no stimulation) through 180min of cyclical depressurization into sterile polypropylene and left at dark room-temperature (RT) until final time-point collection.

Flow Cytometry & Controls

Upon final collection, sub-samples were siphoned and exposed to ADP at 2.5 x 10-4M for 5min at RT. Then, antibodies for CD41 (Thermo, MA180666), PAC1 (Thermo, BDB340507), and CD62P (Thermo, 12-0626-82) were added 1:2 to 5μL PRP at RT for 15min in a 96U plate, followed by addition of paraformaldehyde in calcium-free saline to 1%. Arg-Gly-Asp-Ser (RGDS) (Sigma, A9041) was added to a separate PAC1 stain mixture to 2 x 10-2M prior to platelet labeling as a competitive inhibitor to subtract nonspecific binding (**Figure 3.1D**). Isotype controls for FITC (Thermo, 11-4714-81) and PE (Thermo, 12-4714-82) were used for each sample to subtract nonspecific binding. Single-plex fluorescence was measured on an Attune NxT Flow Cytometer immediately after staining. The same fluorescence gates were used across all trials.

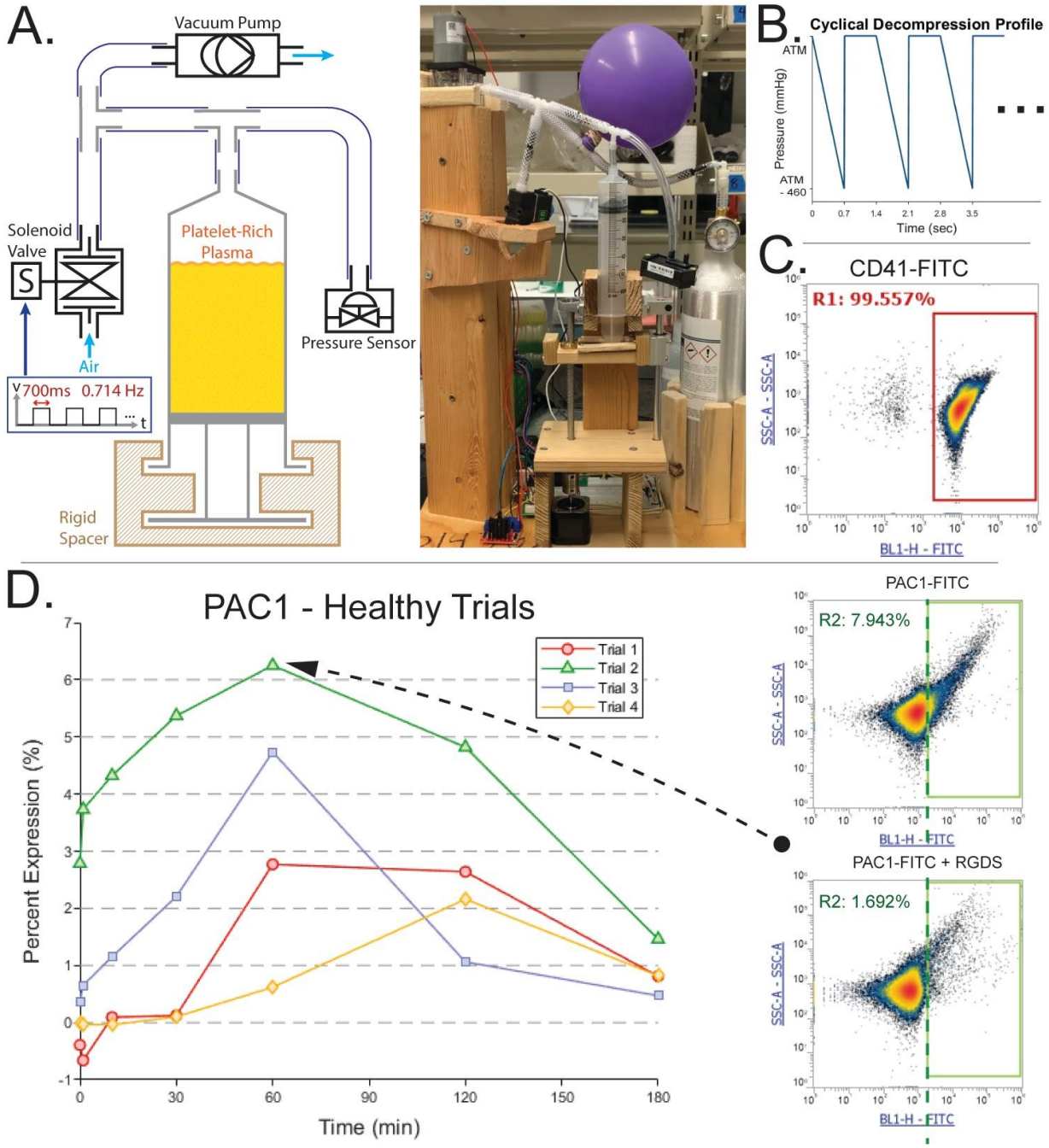

Figure 3.1. Experimental setup. (**A**) Machine for static depressurization of platelets suspended in plasma within a syringe. (**B**) Hydrostatic pressure profile experienced by platelets involving linear evacuation of 460mmHg from atmospheric pressure over 700ms followed by instantaneous release at 50% duty cycle. (**C**) CD41 positive gating using FITC isotype control indicates >99% pure platelet populations across samples. (**D**) Flow cytometry measurement example of PAC1 by subtraction of RGDS control.

Statistics

Measurement distributions were compared by two-sample t test, assuming unequal variance and two tails. Linear dependencies were assessed by Pearson correlation. Significance in all cases was defined by $p \leq 0.05$. Figure error bars represent 95% confidence intervals.

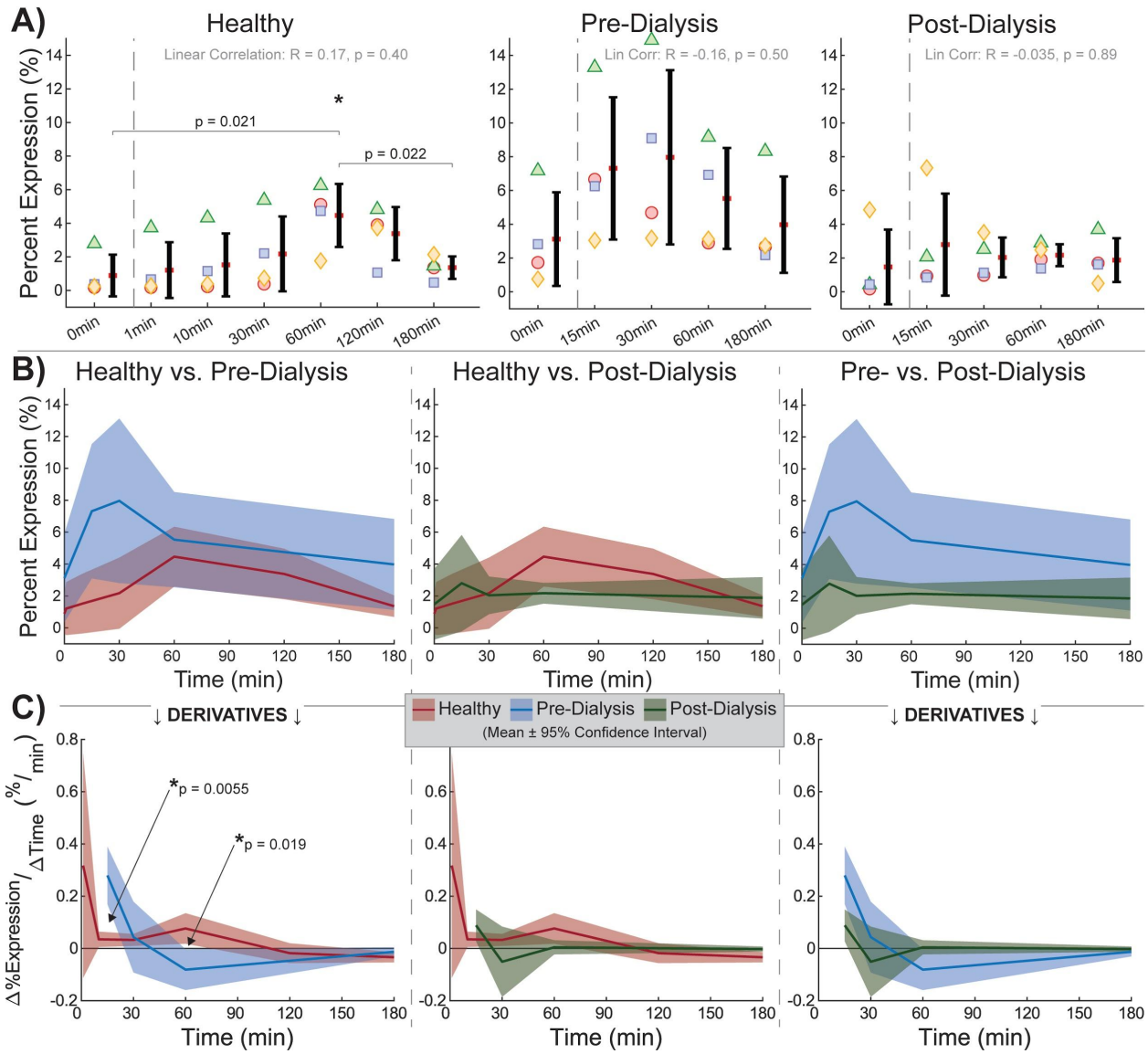

Figure 3.2. Platelet PAC1 expression. (**A**) No linear correlations observed in PAC1 as a function of pressure-cycling duration within healthy, pre-dialysis, and post-dialysis test groups. (**B**) No significant differences observed in percent expression between test groups at any time point. (**C**) Pre-dialysis platelets increase in expression faster early on and decrease faster later by trial-paired derivative analysis.

Results

Pure platelet populations across trials were confirmed by unimodal forward-scatter (FSC) against side-scatter (SSC) density and > 99% CD41 expression (**Figure 3.1C**). Cyclical depressurization alone yielded no response in platelet PAC1 expression (**Figure 3.2**). No linear trends were observed within healthy, pre-dialysis, and post-dialysis test groups (**Figure 3.2A**). No differences were found between any two test groups at any time point (**Figure 3.2B**). Derivative analysis of expression over time found no significant differences in rate of change between healthy and post-dialysis time points and pre- and post-dialysis time points, though pre-dialysis platelets had a more rapid expression increase at 15min and decrease at 60min compared to healthy platelets (**Figure 3.2C**). This difference in receptor rate of change is also observed by significantly elevated PAC1 expression at 60min compared to 0min and 180min in healthy trials (**Figure 3.2A**). In the absence of a universal PAC1 trend observed as a function of pressure-cycling duration, expression data was aggregated by test group across all time points to assess baseline differences attributable to population (**Figure 3.3**). Healthy and post-dialysis samples had nearly identical ranges (2.1±1.9 vs 2.1±1.8, mean±SD), while pre-dialysis measurements were significantly elevated and significantly more varied (SD = 3.9). Thus, overall PAC1 elevation in pre-dialysis samples may be attributed to uremia, while baseline expression levels in the same dialysis patients are comparable to a healthy range after uremic clearance.

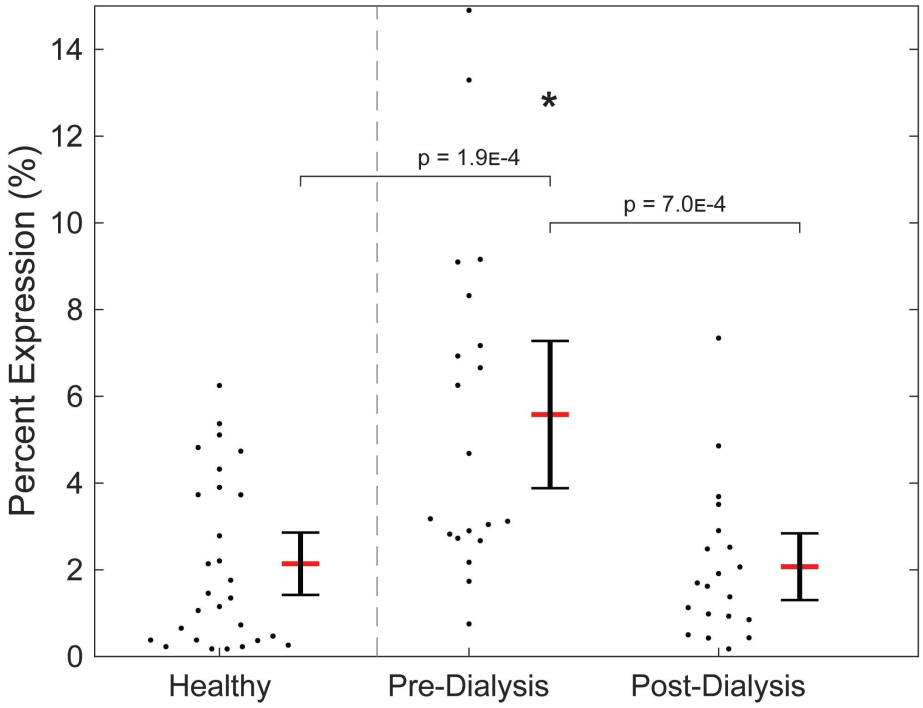

Figure 3.3. Test group-aggregated PAC1 expression. Pre-dialysis platelets had elevated expression compared to healthy and post-dialysis platelets, which had similar ranges.

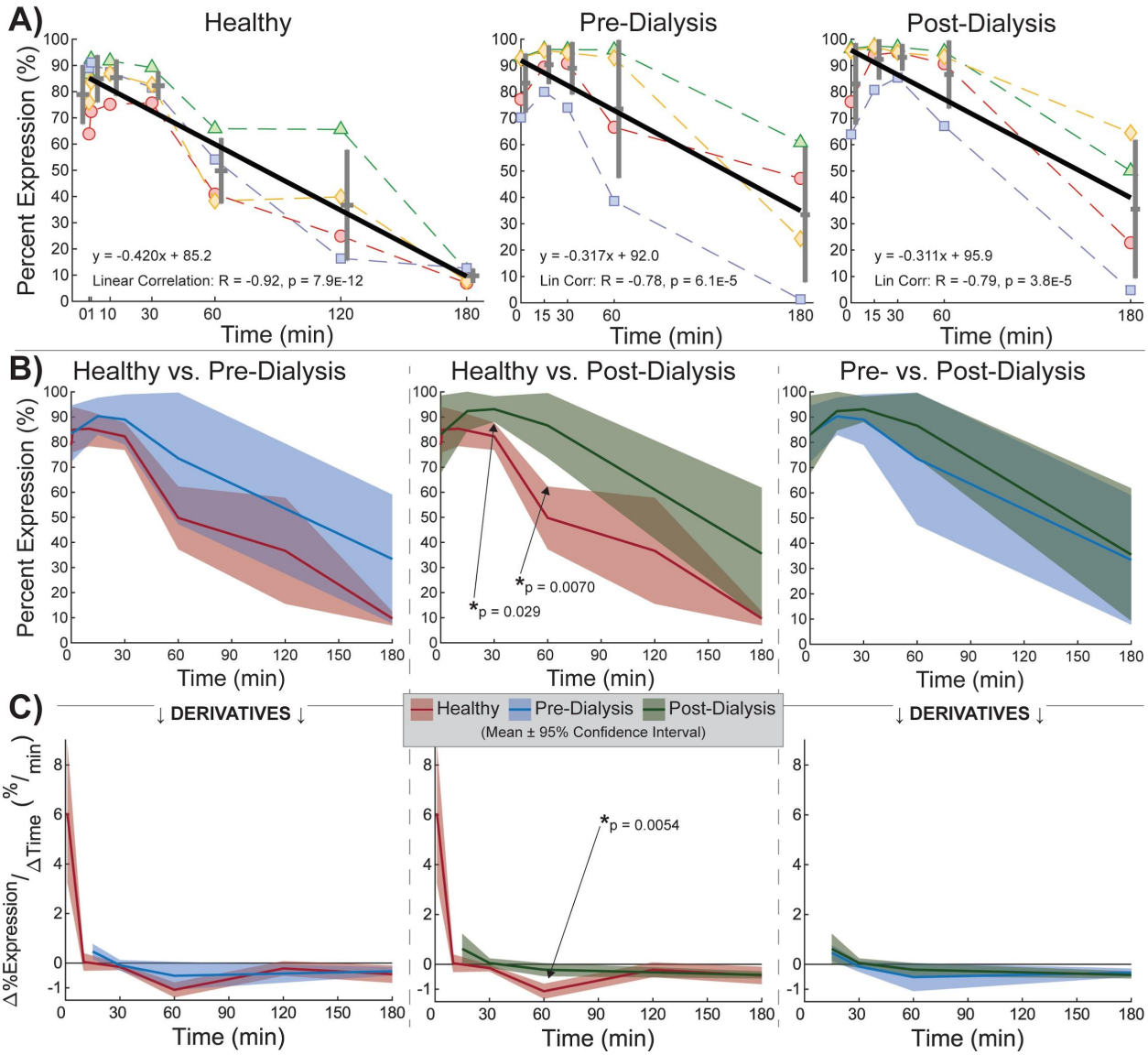

Figure 3.4. PAC1 expression for samples subsequently stimulated with ADP. (**A**) Expression correlated negatively to pressure-cycling duration in all test groups, with healthy platelets diminishing fastest. (**B** & **C**) Faster reduction in healthy platelet PAC1 expression observed by significant differences in percent expression (**B**) and derivative expression (**C**) at middle time points.

When subsequently stimulated with ADP, platelets reliably decreased in PAC1 expression with increasing duration of pressure-stimulation. Negative linear correlations were detected in all test groups (**Figure 3.4A**). However, healthy platelets demonstrated a greater reduction in expression overall (R = -0.92) compared to pre-dialysis (R = -0.78) and post-dialysis (R = -0.79) platelets. In the healthy test group, platelets at 60min (p = 0.015), 120min (p = 0.014), and 180min (p =

2.4E-5) expressed PAC1 at significantly lower levels compared to pressure-unstimulated platelets at 0min. In comparison, pre-dialysis ($p = 0.013$) and post-dialysis ($p = 0.022$) platelets expressed significantly lower levels of PAC1 only after 180min of pressure cycling. The more rapid reduction in PAC1 expression in healthy platelets with longer pressure-cycling duration preceding identical exposure to ADP compared to dialysis platelets is further reflected in significantly lower expression at 30min and 60min (**Figure 3.4B**) and a significantly faster decrease in rate of change at 60min compared to the post-dialysis population (**Figure 3.4C**).

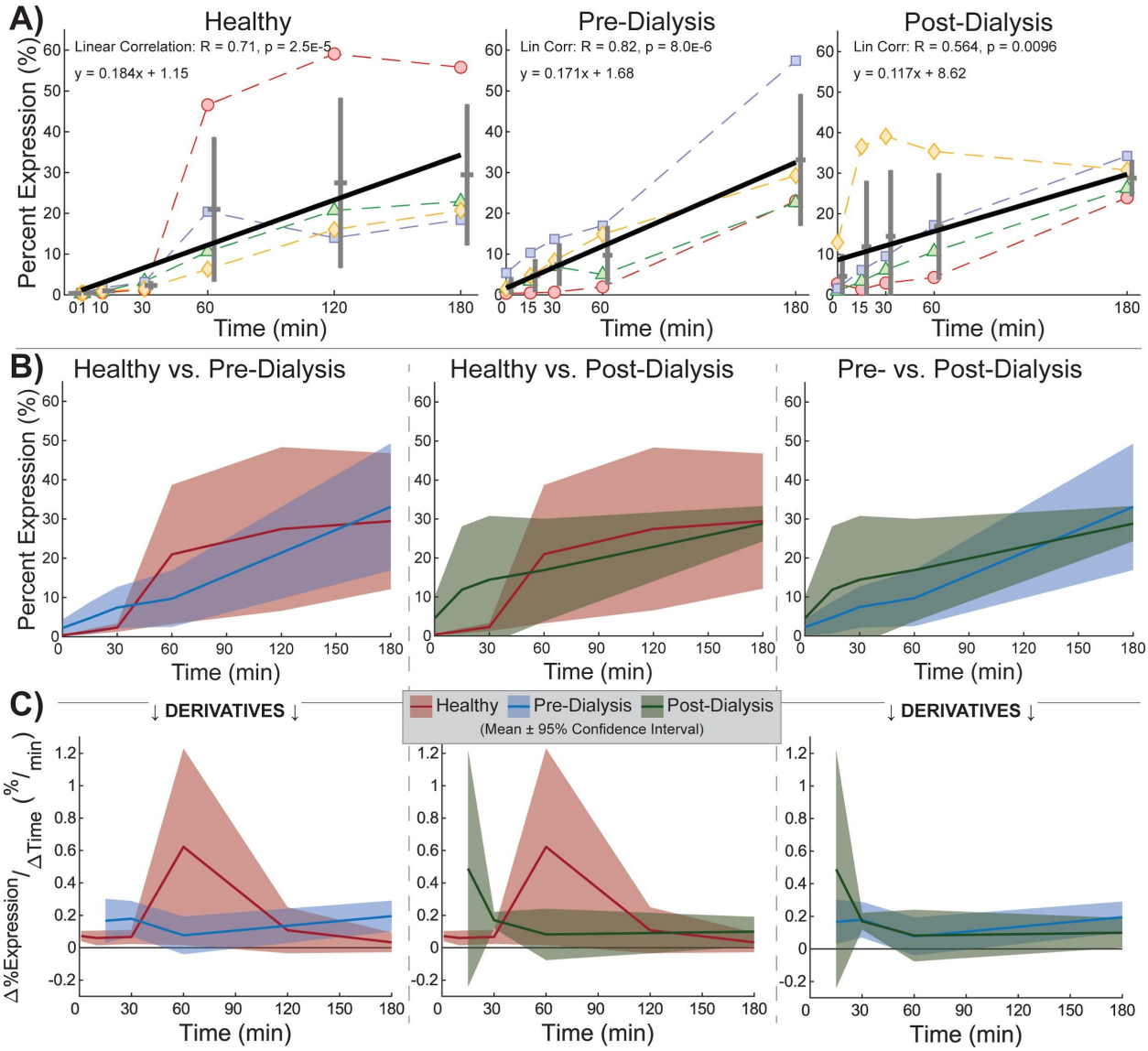

Figure 3.5. CD62P expression. (**A**) Expression correlated positively to pressure-cycling duration in all test groups. (**B** & **C**) No significant differences observed in percent expression (**B**) or derivative expression (**C**) between test groups at any time point.

Unlike PAC1, CD62P unilaterally increased in expression with cyclical depressurization. Positive linear trends were detected in all test groups (**Figure 3.5A**), with no differences measured between test groups at any time point (**Figure 3.5B**), and no differences calculated in derivative expression (**Figure 3.5C**). These trend consistencies led to the aggregation of expression data across all test groups to measure overall CD26P behavior as a function of pressure-cycling duration (**Figure 3.6**). Increased statistical strength (p = 6.9E-11) signifies that CD62P increases in expression with pressure stimulation as a universal platelet response that is agnostic to uremia. Because CD62P is originally stored in differentiated granules within platelets, these data support that repetitive depressurization induces degranulation.

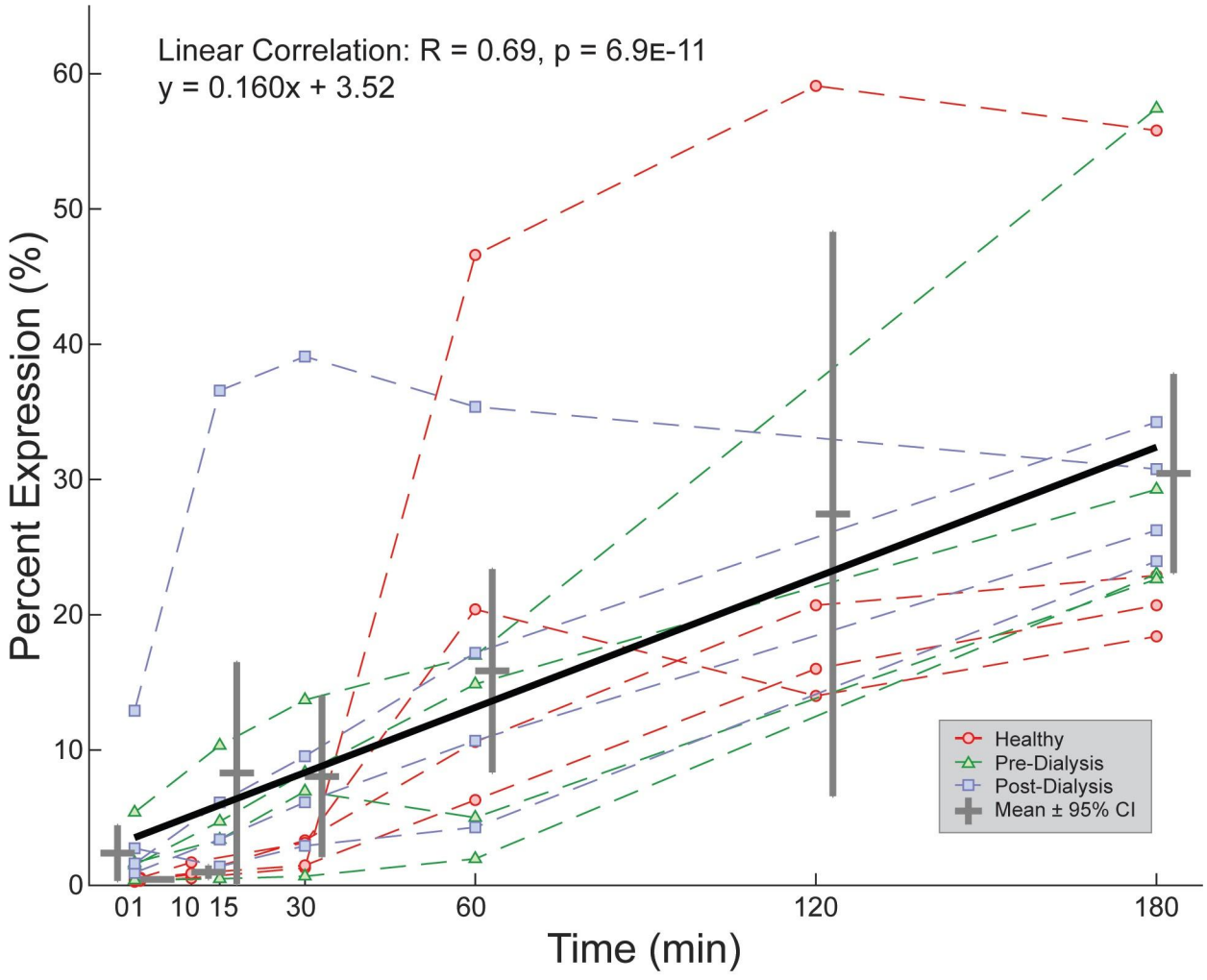

Figure 3.6. Total aggregated CD26P expression. Expression universally increases with pressure-cycling duration, regardless of uremic state.

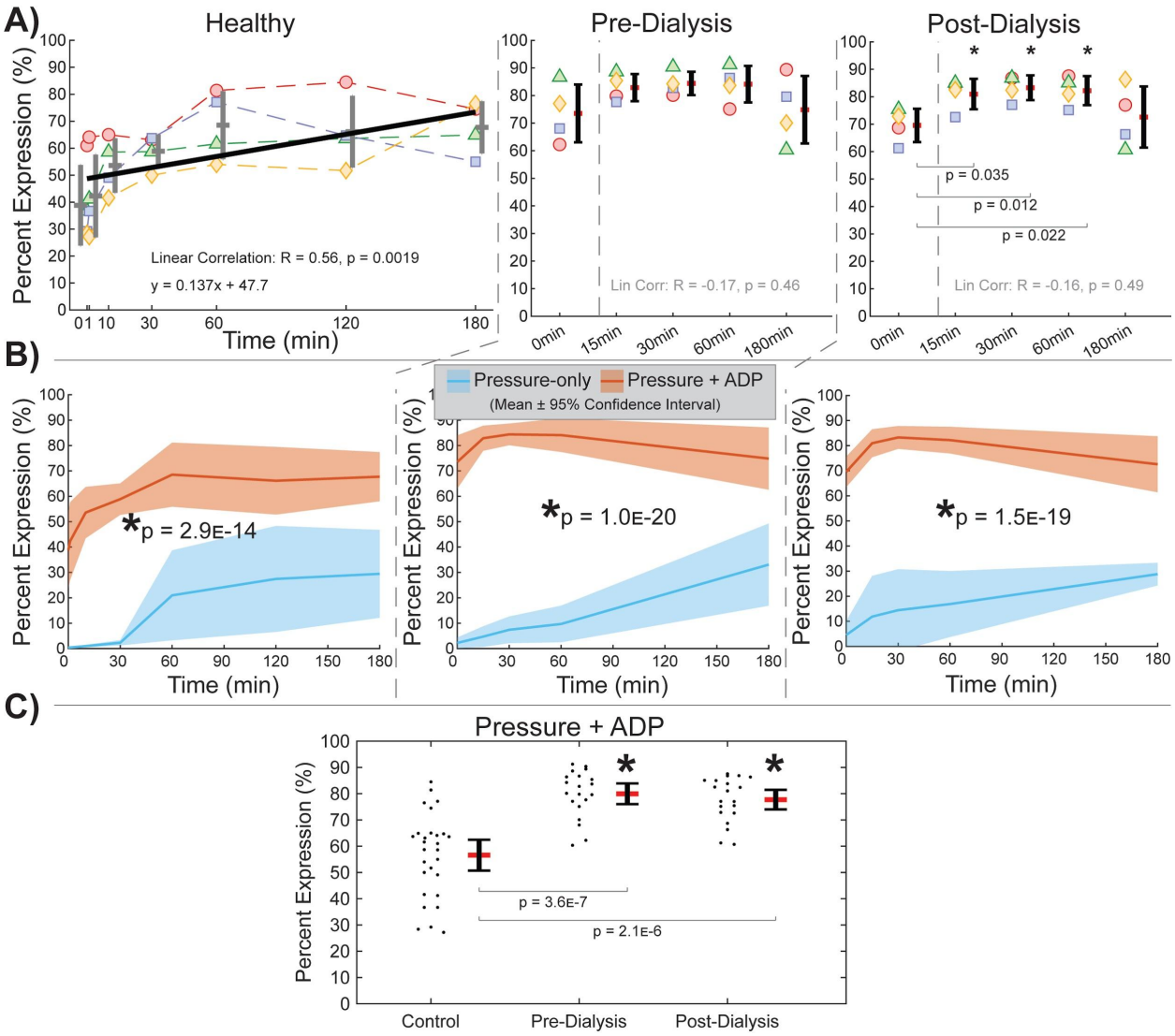

Figure 3.7. CD62P expression for samples subsequently stimulated with ADP. (**A**) A positive trend in healthy platelets indicates additive effects, while no trend in pre- or post-dialysis platelets is likely from heightened sensitivity to stimulation. (**B**) ADP increases expression for all test groups at all time points. (**C**) Healthy platelets have lower baseline expression levels than both pre- and post-dialysis platelets.

When subsequently stimulated with ADP, platelets expressed CD62P in greater proportion, with behavioral discrepancies observed between healthy and dialysis samples. A positive correlation was observed in the healthy test group, while no significant trend could be fitted to pre-dialysis or post-dialysis measurements (**Figure 3.7A**). However, pressure-and-ADP-stimulated platelets expressed greater CD62P at all durations of pressure stimulation compared to pressure-only stimulated platelets from the same test group (**Figure 3.7B**). Thus, while for healthy platelets ADP and depressurization may have additive effects on degranulation, dialysis patient platelets

may have heightened sensitivity to both pressure and ADP. The latter is supported by significantly higher expression levels in ADP-only (0 minute) stimulated platelets for both pre-dialysis ($p = 0.0098$) and post-dialysis ($p = 0.0097$) samples. Furthermore, significant elevation in middle time points for post-dialysis samples may corroborate additive interactions between pressure and ADP on degranulation, while the absence of significant differences between any time points in pre-dialysis samples may indicate a dependency in sensitivity on uremic state. Comparing test group aggregates confirms elevated baseline expression levels in dialysis samples (**Figure 3.7C**).

Discussion

Cyclical depressurization induced platelet degranulation without activating the GPIIb/IIIa integrin in a unique and unexplored mechanism of platelet stimulation. While CD62P increased linearly with duration of pressure cycling, PAC1 expression remained at base unstimulated rates. In comparison, when stimulating platelets by shear stress, both CD62P and PAC1 interchangeably predict platelet activation[18]. Interestingly, co-stimulation with ADP additively enhanced CD62P expression while decreasing PAC1 expression. When stimulated using ADP alone, platelets have been shown to retain PAC1 expression for up to 8hr[18]. Taken together, these data suggest that depressurization circumvents receptor signal transduction to induce exocytosis and further that this mechanism desensitizes platelets to chemical stimuli. In hemodialysis, this may contribute to bleeding disorders[2] while still exacerbating the circulation of platelet factors[6].

While CD62P profiles were universal, population-level differences observed between healthy, pre-dialysis, and post-dialysis PAC1 measurements indicate effects attributable to uremia and chronic kidney disease (CKD). Pre-dialysis platelets exhibited overall PAC1 elevation compared to healthy and post-dialysis platelets whose profiles were equivalent, indicating a baseline state of hyperactivity in dialysis patients that is corrected with uremic clearance and platelet renewal. Further, the significant early increase in paired pre-dialysis platelet PAC1 expression could signify a heightened sensitivity to pressure shock. However, the “acclimation” observed by a significant negative rate of change at 60min to average unstimulated levels may imply that perturbations on PAC1 caused by depressurization are not sustained, regardless of uremic state. Examining the combinatorial effects of ADP on top of pressure, both pre- and post-dialysis platelets showed a slower decline in PAC1 expression over time compared to healthy platelets considering comparable ranges at 0 minutes of pressure stimulation between all groups. As pressure-inhibition of GPIIb/IIIa may be beneficial in preventing capillary bed plugging[19,20], inclined retention of the activated integrin after agonist exposure demonstrates a troubling adaptive possibility in which CKD patient platelets remain preferentially adherent for longer.

Study limitations include low donor count, higher pressure drop used than experienced across hemodialysis, the use of a single pressure profile, number of platelet activation reporters, and additional agonists used. The experimental pressure drop of 480mmHg is over two-fold higher

than that experienced by platelets during hemodialysis, though remains relevant as a benchmark for the progression of blood ultrafiltration technology[7]. Future studies should probe the effects of varying pressure drop rate and frequency to establish bounds of safe usage. Further investigation of depressurization effects on phosphatidylserine and clotting factor binding would better characterize whether the same downstream procoagulant phenotype as from shear is produced[19,21]. Similarly, sensitivity to other agonists including thrombin would round out the resulting coagulative profile[1,17].

Theory

The Starling Equation describes an outward volumetric flux, J, across a membrane driven by hydrostatic pressure P and osmotic pressure π.

$$J_v = L_p S\left(\left[P_{in} - P_{out}\right] - \sigma\left[\pi_{in} - \pi_{out}\right]\right),$$

where L_p, S, and σ are constants.

A sudden reduction in P_{out} by external hydrostatic depressurization would generate a solvent convective force outwards unless met with a net ion influx, increasing π_{in}, thereby expanding cortical volume. In these experiments, no population-level changes in platelet diameter were evident by forward scatter distributions, so any potential volumetric changes to pressure shock were not sustained after stimulation. Thus, either absorptive ion influx was followed by equivalent contracting ion outflux upon vacuum release, or filtrative solvent outflow caused localized forces at the platelet membrane followed by reabsorption. In both cases, the cytoskeleton is strained, and both geometric rearrangements are evident in the classic clotting response. In fact, in response to agonist-induced activation, platelets first become spherical by the influx of calcium and secondly hydraulically generate podia[17]. While neither platelet shape nor volume were actively tracked throughout the applied pressure cycle, the feasibility of inducing these same swelling and protruding forces without a surface receptor agonist may explain the here-mentioned observations of downstream degranulation by CD62P presentation without initiation by integrin signal transduction measured by PAC1.

The theorized cortical forces across platelet membranes may be symptomatic of other non-contact platelet stimuli beyond the repetitive frictional pressure shock characteristic of hemodialytic filtration. Taking the other driver of flux from the Starling Equation, osmotic shock likely also induces platelet degranulation by the same principles. Early studies reported platelet morphological expansion[22], aggregation[23], and free ion flux[24] in both hyper- and hypotonic solutions with implications on blood storage. Considering the drastic shifts in osmolarity experienced in the renal medulla and procoagulant platelet phenotypes observed in representative hyperosmotic solutions[21], agonist-free platelet degranulation may contribute to worsening CKD in dialysis patients exhibiting pro-fibrotic platelet disposition[6].

Works Cited

1. Sánchez-González DJ, Méndez-Bolaina E, Trejo-Bahena NI. Platelet-rich plasma peptides: Key for regeneration. *International Journal of Peptides*. 2012;2012. doi:10.1155/2012/532519
2. Daugirdas JT, Bernardo AA. Hemodialysis effect on platelet count and function and hemodialysis- associated thrombocytopenia. *Kidney International*. 2012;82(2):147-157. doi:10.1038/ki.2012.130
3. Ding J, Chen Z, Niu S, et al. Quantification of Shear-Induced Platelet Activation: High Shear Stresses for Short Exposure Time. *Artificial Organs*. 2015;39(7):576-583. doi:10.1111/aor.12438
4. Nomura S, Hamamoto K, Kawakatsu T, et al. Analysis of platelet abnormalities in uremia with and without Glanzmann's thrombasthenia. *Nephron*. 1994;68(4):442-448. doi:10.1159/000188305
5. Tsun Wong AK. Platelet biology: The role of shear. *Expert Review of Hematology*. 2013;6(2):205-212. doi:10.1586/ehm.13.5
6. Velasquez-Mao AJ, Velasquez MA, Hui Z, Armas-Ayon D, Wang J, Vandsburger MH. Hemodialysis exacerbates proteolytic imbalance and pro-fibrotic platelet dysfunction. *Scientific Reports*. 2021;11(1):1-14. doi:10.1038/s41598-021-91416-8
7. Ronco C, Brendolan A, Lupi A, Metry G, Levin NW. Effects of a reduced inner diameter of hollow fibers in hemodialyzers. *Kidney International*. 2000;58(2):809-817. doi:10.1046/j.1523-1755.2000.00230.x
8. Field CL, Tablin F. Response of Northern Elephant Seal platelets to pressure and temperature changes: A comparison with human platelets. *Comparative Biochemistry and Physiology - A Molecular and Integrative Physiology*. 2012;162(4):289-295. doi:10.1016/j.cbpa.2012.01.023
9. Hultgren HN. High altitude pulmonary edema. *Biomedicine of high terrestrial elevations*. Published online 1969:131-141.
10. Bärtsch P, Mairbäurl H, Maggiorini M, Swenson ER. Physiological aspects of high-altitude pulmonary edema. *Journal of Applied Physiology*. 2005;98(3):1101-1110. doi:10.1152/japplphysiol.01167.2004
11. Murayama M. Ex vivo human platelet aggregation induced by decompression during reduced barometric pressure, hydrostatic, and hydrodynamic (Bernoulli) effect. *Thrombosis research*. 1984;33(5):477-485.
12. Pickles DM, Ogston D, Macdonald AG. Effects of hydrostatic pressure and inert gases on platelet aggregation in vitro. *Journal of Applied Physiology*. 1990;69(6):2239-2247. doi:10.1152/jappl.1990.69.6.2239
13. Liu S, Tao R, Wang M, et al. Regulation of cell behavior by hydrostatic pressure. *Applied Mechanics Reviews*. 2019;71(4):1-13. doi:10.1115/1.4043947

14. Heinemann SH, Conti F, Stühmer W, Neher E. Effects of hydrostatic pressure on membrane processes: Sodium channels, calcium channels, and exocytosis. *Journal of General Physiology*. 1987;90(6):765-778. doi:10.1085/jgp.90.6.765
15. Myers KA, Rattner JB, Shrive NG, et al. Hydrostatic pressure sensation in cells: Integration into the tensegrity model. *Biochemistry and Cell Biology*. 2007;85(5):543-551. doi:10.1139/O07-108
16. Hui TH, Zhou ZL, Qian J, Lin Y, Ngan AHW, Gao H. Volumetric deformation of live cells induced by pressure-activated cross-membrane ion transport. *Physical Review Letters*. 2014;113(11):1-5. doi:10.1103/PhysRevLett.113.118101
17. Shin EK, Park H, Noh JY, Lim KM, Chung JH. Platelet shape changes and cytoskeleton dynamics as novel therapeutic targets for anti-thrombotic drugs. *Biomolecules and Therapeutics*. 2017;25(3):223-230. doi:10.4062/biomolther.2016.138
18. Lu Q, Malinauskas RA. Comparison of Two Platelet Activation Markers Using Flow Cytometry After In Vitro Shear Stress Exposure of Whole Human Blood. *Artificial Organs*. 2011;35(2):137-144. doi:10.1111/j.1525-1594.2010.01051.x
19. Cheng H, Yan R, Li S, et al. Shear-induced interaction of platelets with von Willebrand factor results in glycoprotein Ibα shedding. *American Journal of Physiology - Heart and Circulatory Physiology*. 2009;297(6):2128-2135. doi:10.1152/ajpheart.00107.2009
20. Tyml K. Critical Role for Oxidative Stress, Platelets, and Coagulation in Capillary Blood Flow Impairment in Sepsis. *Microcirculation*. 2011;18(2):152-162. doi:10.1111/j.1549-8719.2010.00080.x
21. Gatidis S, Borst O, Föller M, Lang F. Effect of osmotic shock and urea on phosphatidylserine scrambling in thrombocyte cell membranes. *American Journal of Physiology - Cell Physiology*. 2010;299(1):111-118. doi:10.1152/ajpcell.00477.2009
22. Law P. The tolerance of human platelets to osmotic stress. *Experimental Hematology*. 1983;11(5):351-357.
23. Fantl P. Osmotic stability of blood platelets. *The Journal of Physiology*. 1968;198(1):1-16. doi:10.1113/jphysiol.1968.sp008590
24. Lundberg A, Meryman H, Estwick N. of human platelets media to at 37 and -SC and hypotonic. *American Journal of Physiology-Legacy Content*. 2021;222(5):1100-1106.

Chapter 4

Plasma and platelet culture of iPSC-derived cardiomyocytes: tracking cardiac tissue remodeling by hemodialysis patient blood

Introduction

Chronic kidney disease (CKD) is intricately linked to high rates of cardiovascular disease (CVD)[1], with CVD rather than end stage renal disease (ESRD) as the leading cause of death in advanced CKD[2]. Cardiorenal syndrome most commonly presents as uremic cardiomyopathy involving diastolic dysfunction, left ventricular hypertrophy (LVH), and diffuse fibrosis leading to congestive heart failure[3]. However while hemodynamic overload constitutes the primary mode of structural failure, all manifestations of cardiovascular disease (CVD) in ESRD including macrovascular stiffening like coronary artery disease leading to fatal arrhythmias[2], vascular calcification driven by arterial osteogenesis[4], and a self-reinforcing cycle of microvascular dysfunction and myocardial interstitial fibrosis[5,6] are characterized by a concerted program of complex cardiovascular remodeling.

Pathogenesis is explainable in part by uremia[7], but the more complex mechanisms involved in selective structural modeling and cell transition are enacted by larger molecules that are minimally cleared by hemodialysis (HD). To name a few, fibroblast growth factor 23 (FGF23) protectively overproduced by bone in response to hyperphosphatemia induces vascular calcification and fibrotic proliferation[7,8], transforming growth factor beta-1 (TGF-β1) mediates extracellular matrix accumulation[9], and matrix metalloproteinases (MMP) and tissue inhibitors of MMP (TIMP) overexpression facilitates rapid tissue turnover[10]. Furthermore, not only do non-dialyzable proteins pose a currently unsolved challenge for HD, more recent study shows that HD itself exacerbates pathological cardiac remodeling. For one, dialysis filter membranes elicit coagulative and immune phase responses because of inadequate biocompatibility[11]. Next, chronic and sustained platelet and leukocyte activation shortens circulatory lifecycles and exhausts coagulative and immunogenic capabilities, leading to long term dysfunction and adaptive secretory phenotypes[11]. Finally, the fundamental fluidic stimuli of ultrafiltration mechanically induce degranulation, misdirecting secretory mechanisms intended for paracrine signaling at sites of injury to become more endocrine in nature[12,13].

In vitro tissue culture models offer a unique opportunity to observe granular structure protein changes caused by circulating pathogenic proteins and platelets. In these experiments, human cardiac tissues derived from induced pluripotent stem cells (iPSC) fluorescently tagged for troponin were cultured with plasma and platelets from dialysis patient donors pre- and post-HD, healthy donor plasma and platelets, and ordinary maintenance medium with B27 and insulin for 28 days. Tissues were imaged by fluorescent microscopy and video recorded daily to visually track muscular network remodeling and changes in contractile performance over time. At the

beginning and end of the experimental culture period, tissues were sacrificed for proteomic assessment of matrix and cell type proportion. Differences in structural plasticity, contractile maturity, and endpoint composition elucidate tissue changes by acute and chronic ESRD circulations and unique platelet phenotypes. Developments appear to be directed by tissue growth in plasma, non-proliferative remodeling in platelet media, and consequently more fibrotic by dialysis derived blood products. Particular fibrogenesis observed in post-HD platelet cultured cardiomyocytes (CM) mechanistically corroborates clinical outcomes observed by platelet activation on left ventricular remodeling in the REMODELING trial[14]. Furthermore, healthy derived blood products induced stronger and more diffuse cardiac networks, showing promise for future use in improving maturity in cardiac tissue culture.

Methods

Blood Collection and Fractionation

Hemodialysis blood samples were collected immediately before vascular access and after tubing removal from three patients at DaVita Oakland. All patients were dialyzed using NIPRO single-use, hollow-fiber ELISIO filters. Three healthy blood samples with no history of smoking, drug abuse, current medications, or morbidities were collected at the University of California, Berkeley Tang Center. Platelet samples were isolated from blood collected in ACD-A Vacutainers by centrifugation at 200g for 10min to collect the top 90% of platelet-rich plasma (PRP), centrifugation for 5min at 200g to remove remaining erythrocyte and leukocyte contamination, and finally by precipitation at 15Kg for 15min and resuspended in RPMI 1640 medium. Plasma samples were isolated from blood collected in Vacutainers containing no additive to induce coagulation, centrifugation at 200g for 10min to collect the aqueous phase, and double centrifugation at 15Kg for 15min to remove hematocyte contamination. Resuspended platelets and plasma were aliquoted for single use in a sterile biosafety cabinet and stored at -80°C. Participants provided informed consent under protocols approved by the U.C. Berkeley IRB and in compliance with the Declaration of Helsinki.

iPSC Culture and Cardiac Differentiation

Cells were received from the U.C. Berkeley Cell Culture Facility's Allen Institute for Cell Science genome-engineered human iPSC collection, fluorescently tagged for Troponin (mEGFP-TNNI1, AICS-0037). iPSC cultures were maintained in feeder-free monolayer using Essential 8 Medium (ThermoFisher, A1517001) on hESC-qualified Matrigel (Corning, 354277) and passaged using TrypLE (ThermoFisher, 12605010) and ROCK inhibitor (Tocris, 1254). CM tissues were differentiated through adaptation of previously published protocols[15] on 12-well plates by GSK3 and Wnt inhibition using 12μm CHIR99021 (Sigma, SML1046) and 8μm IWP4 (Sigma, SML1114) in RPMI 1640 medium with B27 minus insulin (ThermoFisher, A1895601). Cultures were maintained on day 6 of differentiation and beyond using RPMI 1640 medium with

B27 supplement complete with insulin (ThermoFisher, 17504044). Spontaneous contraction was observed 8 days after GSK3 inhibition.

Cardiac Tissue Culture

Contracting cardiac cultures were maintained in RPMI 1640 medium with B27 and insulin every other day for 14 days to allow for tissues to stabilize, after which tissues were cultured daily with thawed plasma, RPMI suspended platelets supplemented with B27 and insulin, or continued ordinary medium (RPMI 1640 with B27 and insulin) for 28 days. CM tissues were lysed immediately before experimental culture with plasma or platelets by scraping and dry transfer into tubes containing TRIzol LS (ThermoFisher, 10296010) to prevent test group exposure to volatile phenols. After 28 days, all remaining tissues were lysed in-plate after medium aspiration using TRIzol LS. Tissue samples in TRIzol were dissolved by incubation at room temperature with gentle shaking for 30min and stored at -80°C until protein isolation.

Microscopy and Visual Analysis

Tissues were imaged and video recorded daily for the first 10 days of experimental culture and every other day thereafter in the U.C. Berkeley QB3 Cell and Tissue Analysis Facility using an ImageXpress Micro at 37°C and 5% CO_2 in the same well locations at 10x objective magnification. Fluorescent images for GFP were filtered for noise and digital artifacts and quantified for pixel intensity using MATLAB. Brightfield videos were measured for frame-to-frame displacement using the MATLAB computer vision toolbox.

Table 4.1. Antibodies used for Western Blot analysis.

Target	Size (kDa)	Classification	Supplier	Catalog
cTnI	24, 60	Cardiomyocyte	Thermo	MA1-22700
cTnT	42	Cardiomyocyte	Thermo	MA1-24621
FAP	55, 130	Matrix Remodeling	Thermo	PA5-51057
PDGFRA	55	CM Differentiation	Thermo	PA5-16571
POSTN	40, 58	Matrix Remodeling	Thermo	PA5-69142
TCF21	20	CF Differentiation	Thermo	PA5-68595
WISP1	30, 60	CF Differentiation	Thermo	PA5-13231
a-SMA	42	Loading Control	Thermo	MA1-10046
b-Act	47	Loading Control	Thermo	MA1-140
b-Tub	55	Loading Control	Thermo	MA5-16308
GAPDH	40	Loading Control	Thermo	MA5-15738
Donkey anti-Mouse, AFp488		Secondary Ab	Thermo	A32766
Donkey anti-Rabbit, AFp800		Secondary Ab	Thermo	A32808

Western Blot

Protein was precipitated from Trizol using acetone at − 20 °C followed by centrifugation at 12Kg and 4°C. The protein pellet was washed with 0.3 M guanidine hydrochloride in 95% ethanol before dissolution in 1% SDS in ultrapure water with 8M urea. Solubilized protein was aliquoted and stored for single use at − 20 °C for up to 1 month, according to concentrations measured by BCA assay. Protein samples were denatured by LDS and reduced, electrophoresed at 20 µg loads, and transferred to PVDF membranes by Power Blotter. Membranes were probed for multiplexed targets using fluorescent antibodies (**Table 4.1**) and imaged using an iBright FL1500 Imaging System. Band densitometry was performed using ImageJ.

Statistics

Group differences, paired changes, and time aggregated differences to day 0 offsets were assessed by t test. Image analysis normalization was subtractive rather than fractioned to account for activity external to the observed fields of view. Paired analysis of plasma-platelet Western Blot expression was normalized relative to the larger band to eliminate outlier effects on means by high multiples of low-signal bands and band nonexistence. **Figure 4.4** tabulates predictive strength p, and significant relationships are colored green and red by positive and negative column test group means relative to row group means. Significance in all cases was determined by $p \leq 0.05$. Figure error bars represent 95% confidence intervals.

Results

I. Media Characterization

Plasma and platelet-rich media used for cardiomyocyte (CM) culture were characterized for key biomarkers indicative of inflammation, platelet activation, and pro-fibrotic tissue remodeling in end-stage renal disease (ESRD) (**Figure 4.1**). The broad inflammatory indicator C-reactive protein (CRP) was strongly represented in plasma but not platelet-rich media, indicating the removal of non-platelet released factors during platelet isolation. Conversely, platelet-sourced proteins platelet factor 4 (PF4) and pro-platelet basic protein (PPBP) were measured in comparable abundance in plasma and platelet-rich media for each donor type. Pro-fibrotic tissue regulators MMP-2, -3, and -9, and TIMP-2 were generally found more abundantly in plasma than platelet-rich media, while specific elevations in pre- and post-dialysis over healthy platelets signify subtype-specific phenotypes linked to comorbidity.

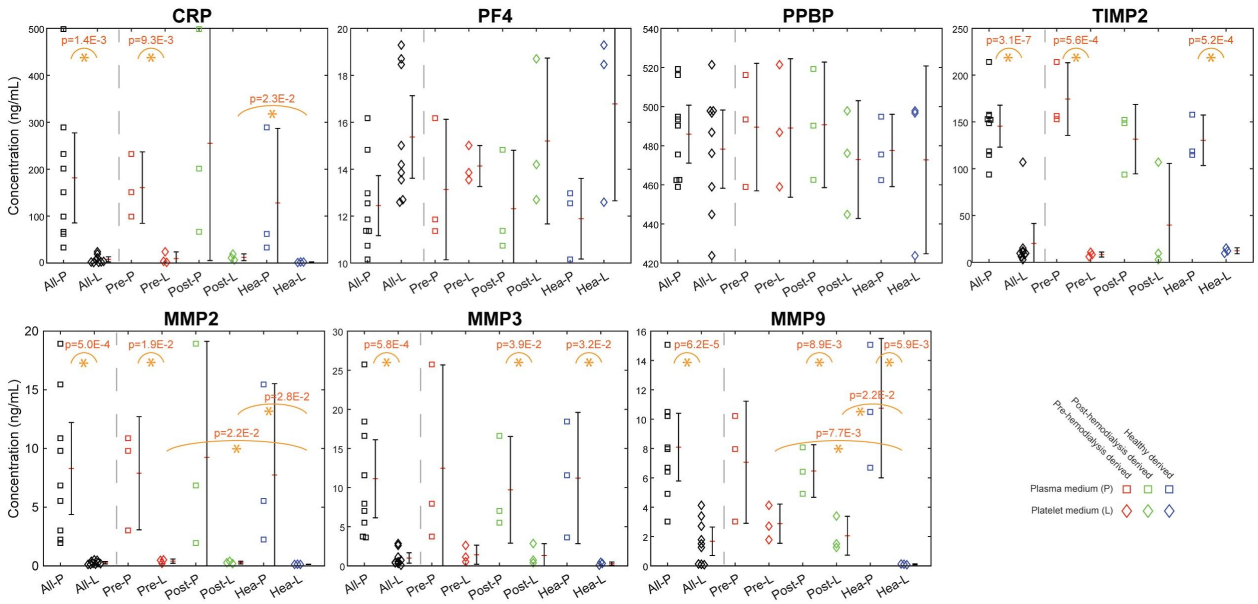

Figure 4.1. Characterization of plasma and platelet-rich media used for cardiomyocyte culture. Platelet media had lesser concentrations of inflammatory CRP and pro-fibrotic MMPs and TIMPs, equal concentrations of platelet released factors PF4 and PPBP, and exhibited MMP2 and MMP9 concentration differences by donor type owing to adaptive ESRD platelet phenotypes. Adjacent ranges represent mean (red) ± 95% confidence interval.

II. Tissue Time Lapse Analysis

The different media formulations and donor types caused clear observable differences in cardiac tissue development regarding troponin network remodeling, cell proliferation, and contractile performance (**Figure 4.2**). While CM cultured in control media changed minimally, CM cultured in donor plasma unilaterally increased in cell confluency and troponin network density. Among donor plasmas, healthy-derived most consistently improved contractile isotropy and network density, with one imaged well of six growing significantly thicker than the observed depth of focus, depicted (**Figure 4.2**, bottom left). In contrast, CM cultured in platelet-rich media developed with greater variance, exhibiting more localized changes in confluency and matrix remodeling.

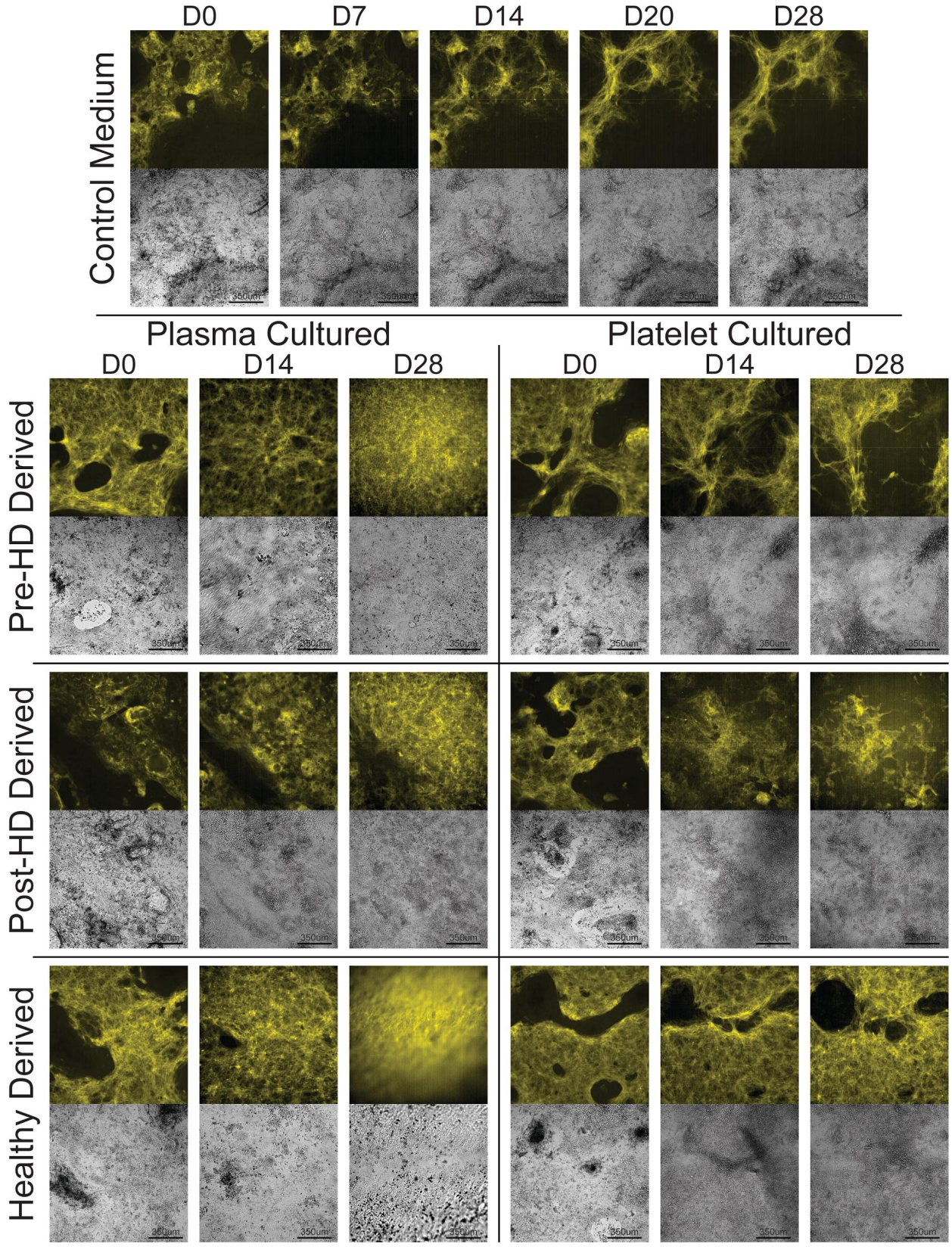
D0
D7
D14
D20
D28
Control Medium
Plasma Cultured
Platelet Cultured
D0
D14
D28
D0
D14
D28
Pre-HD Derived
Post-HD Derived
Healthy Derived
350um

Figure 4.2. Fluorescent (mEGFP-TNNI1) and brightfield images of cardiac tissues over time. Control medium caused minimal change, plasma induced strong proliferation and remodeling, and platelets induced non-proliferative remodeling. Healthy derived media yielded a more regenerative response, post-HD yielded a more fibrotic phenotype, and uremic pre-HD exhibited comparatively less remodeling.

Quantitative analysis of normalized pixel intensity corroborates observed tissue changes (**Figure 4.3**). Troponin network surface area coverage represented by pixel fraction post noise filtration measures network spread and fiber diffusion (**Figure 4.3A**). Subtractively normalized to day 0 , time aggregated CM images increased in coverage fraction when cultured with all plasma groups but did not change when cultured with either platelets or control medium. For each donor type, plasma populations exhibited greater tissue spread compared to their respective platelet cultures (pre-HD: p=5.7E-11, post-HD: p=2.8E-16, healthy: 2.8E-9, aggregate: p=6.8E-32) and control (aggregate: p=3.2E-19) as assessed by t test. When normalized to previous day measurements, pre- and post-HD plasma induced daily increases in coverage while healthy plasma did not (p=0.052). The inconsistent expansion of healthy plasma-cultured CM supports observations of prolonged tissue stagnation followed suddenly by tissue thickening and network percolation at day 23 of culture. However, while healthy plasma induced growth may follow a more stepwise than linear function, macroscopic muscular maturation exceeded those of the pre- and post-HD plasma cultured CM by late-stage contractile strength.

Further interrogation of signal distribution shifts, asymmetry, and peak parameters yields greater insight to the biological mechanisms of observed tissue pattern changes. Plasma in aggregate did not cause peak translation (p=0.63) with the exception of healthy plasma which caused a left shift compared to day 0 of culture (**Figure 4.3B**). All platelet groups on the other hand induced a left peak shift, with control culture experiencing a greater significant shift toward decreasing intensity than platelet groups in aggregate (p=5.2E-5). A contrast between plasma and platelet cultured CM was observed only for the pre-HD donor type (p=8.5E-4), likely owing to the interplays of uremia and platelet dysfunction. Independent of peak translation, changing signal profile asymmetry illustrated macroscopic tissue changes (**Figure 4.3C**). All platelet groups and the control medium induced a right skew, while post-HD plasma and aggregate plasma induced a left skew. Comparing media compositions per donor type, platelets all induced a greater right skew than their plasma counterparts (pre-HD: p=5.4E-6, post-HD: 1.9E-7, healthy: p=8.7E-7, aggregate: p=6.3E-16). Similarly, control media induced a greater right skew than all plasma groups (aggregate: p=1.2E-6). While both platelet and control media induced left shifts and right skews, the greater shift observed in control samples indicates tissue degeneration as contraction dissipates over time. For platelets, these trends indicate tissue remodeling in the direction of reducing prominence of high intensity features. For healthy plasma, the left shift with unchanged skew points to the muscular network becoming more diffuse considering tissue growth and

contractile maturation. Taken together, these data signify that blood derived products abate the natural decay experienced by ordinarily cultured CM, that plasma induces tissue growth by mechanisms other than how platelets induce matrix turnover, and that the more diffuse network generated by healthy plasma is preferable over the tissue growth caused by uremic and dialyzed plasma.

Developments in intensity signal peak aspect ratio as measured by peak height and full-width at half max (FWHM) differentiated effects by donor type, with post-HD plasma-platelet differences opposing those of pre-HD and healthy sample relationships. Peak height increased for all test groups, with pre-HD (p=9.0E-4) and healthy (p=8.1E-3) plasma causing greater peak increases than platelets, and post-HD platelets causing a greater peak increase than plasma (p=1.9E-4) (**Figure 4.3D**). Control medium facilitated greater peak increases than all blood derived groups (p=2.2E-3 against pre-HD plasma, p=2.1E-10 against pre-HD platelets, p=8.7E-7 against post-HD plasma, p=4.8E-2 against post-HD platelets, p=2.9E-3 against healthy plasma, p=7.3E-8 against healthy platelets), illustrating the effects of tissue degeneration considering the large leftward shift in signal intensity. Normalization to network coverage to correct for proliferation eliminated significant differences between platelet and plasma induced peak changes for pre-HD (p=0.82) and healthy (p=0.29) samples, but not for post-HD samples (p=6.8E-10). Post-HD platelets caused greater normalized peak increases than all other blood derived test groups (p=3.4E-10 against post-HD plasma, p=2.6E-7 against pre-HD platelets, p=5.5E-8 against healthy platelets) but a smaller normalized peak increase than control medium (p=8.0E-3). The similar but muted effects of post-HD platelets compared to control medium indicate tissue restructuring leading to control-like performance decay. The distinction of post-HD platelets on tissue performance compared to all other blood-derived test groups supports that HD platelets are pro-fibrotic in the long term owing to chronic adaptation given that HD clearance renews platelets for megakaryocyte derived products. Peak width increased for all groups except for control medium and post-HD platelets (**Figure 4.3E**). That neither control nor post-HD platelet meda change peak width suggests that observed peak changes describe performative decay, while peak width increases in the other test groups may be attributed to proliferation and network spread. Normalization to coverage eliminates peak width changes by pre-HD and healthy plasma. Platelets cause greater normalized width changes than plasma for pre-HD (p=3.5E-3) and healthy (p=1.3E-10) derived samples, while the opposite holds for post-HD samples (p=1.6E-4). That healthy platelets don't have fibrotic factors and pre-HD platelets have uremic dysfunction, while post-HD plasma has acute response factors to filtration and post-HD platelets have a pro-fibrotic phenotype may explain these opposite trends observed.

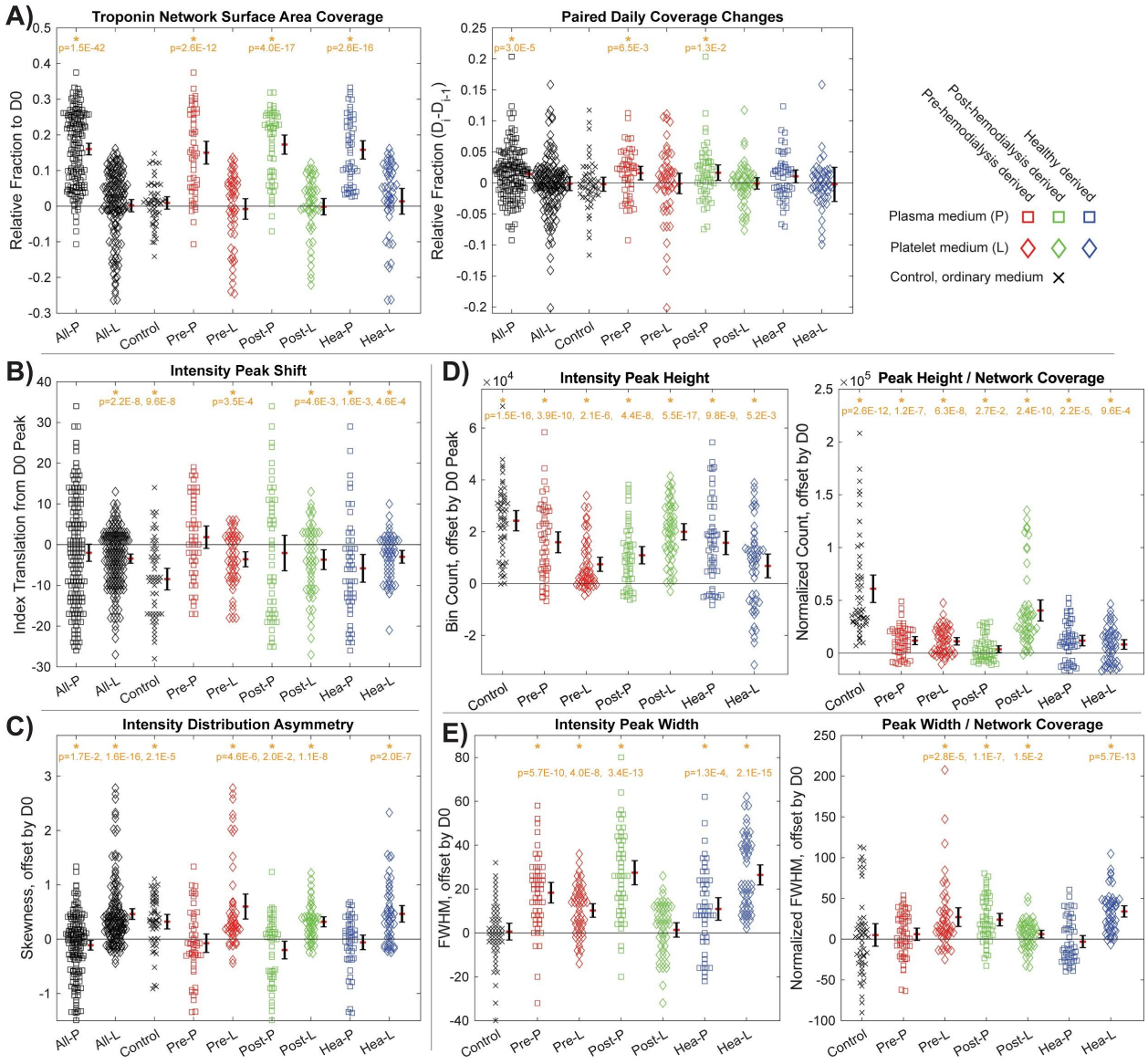

Figure 4.3. Pixel analysis of troponin networks by fluorescent signal post-filtration, time aggregated by experimental group. (**A**) Coverage measured by threshold signal-containing pixel fraction shows increased spread in plasma but not platelet or control cultured tissues. (**B**) Signal translation measured by delta peak fluorescence intensity shows leftward shift in platelet and control cultured tissues indicative of reduced prominence of bundled features. (**C**) Distribution asymmetry measured by histogram skew shows rightward skew developments in platelet and control cultured tissues indicative of tissue degeneration. (**D**) Signal peak height shows a reinforcement of observed trends by test group, highlighting decay in control and post-HD platelet media. (**E**) Signal peak width measured by full width at half maximum bin count shows differing plasma-platelet trends by donor type, implying distinct bioactivities by proliferation, decay, and remodeling. Adjacent ranges represent mean (red) ± 95% confidence interval.

III. Endpoint Tissue Characterization

CM tissues were sacrificed at day 0 prior to culture with donor derived media, and all tissues cultured with plasma, platelet, and control media were lysed after 28 days to analyze tissue composition (**Figure 4.4**). Western blots for matrix indicators reveal remodeling in all blood product cultured tissues and developments toward more fibrotic phenotypes (**Figure 4.4A**). All blood product cultured tissues had less periostin (POSTN), a matrix protein, than control medium cultured CM at days 0 and 28, suggesting that platelets and plasma drive matrix remodeling to reduce POSTN composition in cardiac tissues. Healthy plasma ($p=7.2E-3$), pre-HD platelets ($p=2.1E-2$), and post-HD platelets (3.1E-2) yielded greater POSTN compared to healthy platelets. Healthy derived samples uniquely exhibited POSTN differences between platelet and plasma cultured CM, indicating different remodeling mechanisms between fractionated blood components. Pre- and post-HD samples on the other hand did not exhibit POSTN differences between fractionated components, indicating that remodeling is driven by platelet-released factors present in both platelet and plasma media. Further, differences between HD and healthy derived platelet media support a diseased platelet phenotype in ESRD patients. Fibroblast activation protein (FAP), a remodeling indicator, increased for all groups relative to day 0 except for post-HD and healthy platelets, representing proliferative differences between platelets and plasma. The increase in FAP in control cultured tissues after 28 days shows a natural degeneration to a more fibrotic phenotype accompanying weakening contraction. FAP in day 28 control tissues exceeded that in platelet groups, highlighting that platelets actively remodel tissue by means other than natural tissue degeneration. Direct comparison between plasma and platelet cultured CM bands indicates lower expression yielded by platelets for all test groups, reinforcing different bioactivities between plasma, platelet, and control media.

Direct measurement of cardiac troponin (cTn) shows that cardiac maturity is improved by plasma over platelets and by healthy over dialysis derived samples (**Figure 4.4B**). cTnI for plasma cultured CM was in aggregate greater than platelet cultured CM, driven by significant differences observed between healthy test groups. cTnT for pre-HD plasma was less than day 0 and day 28 controls while pre-HD platelets generated CM with comparable cTnT to controls, indicating that uremic plasma hindered cardiac maturity by factors not sourced to platelets. Conversely, post-HD plasma improved cardiac maturity by non-platelet factors as indicated by greater cTnT by plasma than day 0 but not day 28 controls and no platelet differences to controls. Finally, both healthy plasma and platelets improved cardiac maturity as indicated by greater cTnT produced by both compared to controls. When normalized to healthy plasma, no difference in performance was observed between healthy plasma and platelet media, while healthy plasma generated more cTnT than all dialysis-derived blood products. Similarly, when normalized to healthy platelets, healthy platelets performed better than pre-HD platelets. Taking together that healthy derived media yielded tissues with greater cTnT proportion and that healthy platelets yielded smaller POSTN and FAP proportions than both dialysis donor types, healthy platelets appear to have a more regenerative phenotype than dialysis platelets, and healthy blood products

may induce a more desirable mode of tissue remodeling than that observed in dialysis product cultured CM.

Measurement of CM and cardiac fibroblast (CF) differentiation markers further distinguish fibrotic phenotypes independent of proliferative effects (**Figure 4.4C**). PDGFRA decays in nearly all groups relative to day 0 control but more so in day 28 control tissues than all blood derived test groups, showing that propensity for CM differentiation declines over time but that both platelet and plasma factors reduce natural decline in spontaneously contractile CM[16]. Differentiation factor TCF21 distinguishes platelets as more fibrotic than plasma and control media, while post-HD plasma induces greater fibrotic changes than healthy plasma. All blood derived media and 28 day control media culture yielded greater TCF21 than day 0 controls. Platelets induced even greater TCF21 production than control media and plasma, shown by stronger bands relative to day 28 control tissues and stronger bands relative to respective plasma samples by paired analysis for post-HD, healthy, and in aggregate. Thus, while CM may develop to be more fibrotic over time regardless of culture medium, platelets cause an even greater fibrotic phenotype in CM tissues by concentration of differentiation factors. By similar comparison, post-HD plasma yielded a more fibrotic tissue phenotype than healthy plasma by TCF21 concentration. Induction of WISP1, a mediator of growth in CF and survival in CM, measured proliferative disposition in tissue cultures. Compared to day 0 controls, pre-HD plasma yielded less WISP1 while platelets yielded more, post-HD plasma and platelets yielded more WISP1, and healthy plasma yielded more WISP1 while platelets yielded less. Compared to day 28 controls, pre-HD plasma but not platelets yielded less WISP1, both post-HD media yielded more, and healthy plasma yielded more while platelets yielded less. Day 28 control levels were comparable to day 0, corroborating minimal changes observed in tissue spread and matrix orientation in control medium over time. When normalized for inter-blot comparison, post-HD platelets generated greater WISP1 than healthy platelets, post-HD and healthy plasma generated greater WISP1 than pre-HD plasma, and pre-HD platelets generated greater WISP1 than pre-HD plasma. Taken together, these data support that post-HD and healthy plasma induce proliferation by different mechanisms and that healthy and HD platelets phenotypically differ in composition. WISP1 induction by pre-HD platelets but not uremic plasma and both filtered plasma and renewed platelets post-HD imply that proliferative remodeling in dialysis patients is driven by platelet released factors. In contrast, healthy platelets do not drive proliferation, while healthy plasma likely induces WISP1 by other potentially more regenerative factors.

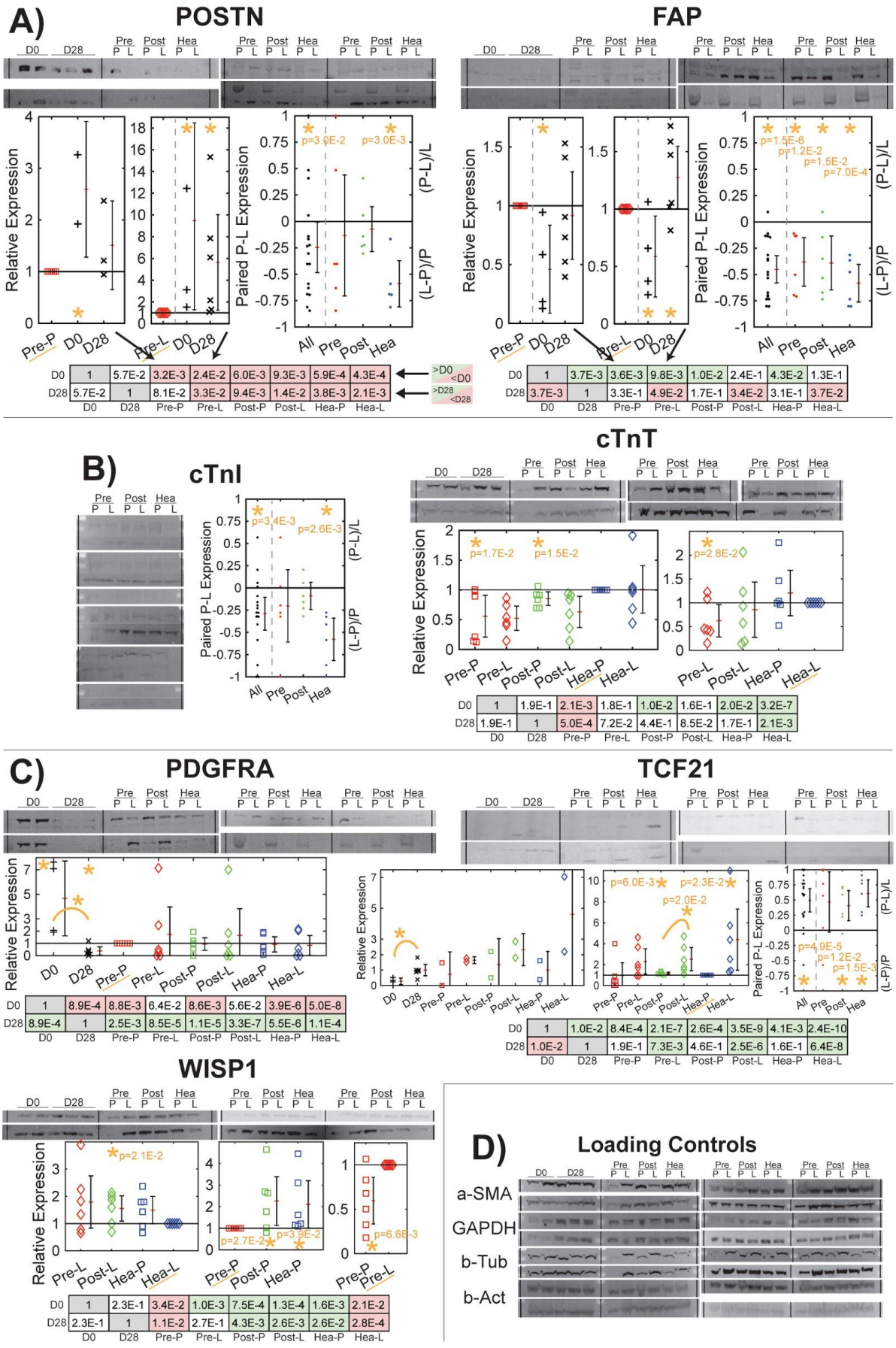

D0 = ordinary medium, day 0 control (+). D28 = ordinary medium, day 28 control (x). P = plasma cultured (¤). L = platelet co-cultured (◊).
Pre = pre-hemodialysis derived (red). Post = post-hemodialysis derived (green). Hea = healthy sample derived (blue).

Figure 4.4. Endpoint characterization of relative matricellular protein composition by Western Blot, normalized to total protein loaded. (**A**) Remodeling proteins show POSTN dilution over time with greater plasma-platelet differences by healthy blood, and increasing FAP in control and plasma but not platelet media. (**B**) Cardiac proteins show a significant increase in maturity by healthy plasma via cTnI and greater cTnT in healthy derived than dialysis derived media. (**C**) Differentiation indicators show increasing specialization by PDGFRA, greater cardiac fibroblast phenotypes in platelet media by TCF21, and unique fibrotic proliferation in post-HD media sourced to platelets. (**D**) Loading controls for all samples. Adjacent ranges represent mean (red) ± 95% confidence interval.

Discussion

This study is the first to document the visual transition of CM cultures to a more fibrotic phenotype in dialysis patient blood and to stronger, more mature tissues in healthy blood. Cardiac tissue developments in plasma and platelet media compared to stagnancy in control medium highlight unique bioactivities by donor type and contributions by platelets. Tissue strengthening with healthy plasma defined a regenerative response not observed in relatively inert culture with healthy platelets. In contrast, tissue spread with degenerative remodeling characterized a fibrotic response in dialysis plasma, with greater cell transition observed in post-HD plasma cultures owing to increased concentration of large proteins. Furthermore, observation of similar remodeling in particularly post-HD platelet cultures strongly supports the notion of an adaptive pathogenic platelet phenotype in CKD. These observations strengthen the causal link between chronic CKD and acute HD induced platelet dysfunction and the deteriorative fibrogenesis of cardiac tissue.

An understanding of the underlying media conditions sheds mechanistic insight not only on the tangible impact of HD patient platelets on CM, but also on uremic and post-clearance plasma on worsening cardiac functional outcomes. Pre-HD derived samples had uremic accumulation and associated platelet dysfunction. Post-HD samples were cleared uremically except for large molecules, had refreshed platelet populations, and contained acute response factors to dialyzer interactions. Healthy samples contained baseline tissue factor levels and an ordinary platelet phenotype. Beyond biomarkers for CM maturity, measurement of classical CF indicators FAP, POSTN, TCF21, and WISP1 indicated CF-like cells differentiating remodeling activities between tissue groups[17,18]. Consistent PDGFRA decay and FAP growth across all tissues indicated increasing specialization and remodeling with time. POSTN dilution across blood-cultured tissues indicated de novo production of other matricellular proteins with remodeling. Regarding differing bioactivities between plasma and platelets, coverage, peak shift, and signal asymmetry identified proliferative tissue spread unique to plasma cultures, while cTnI and TCF21 indicated greater CM specialization by plasma and greater CF specialization by platelets, respectively. Granularity by donor type observed by cTnT, WISP1, and signal peak

height and width further indicated greater cardiac maturation in healthy derived media and greater fibrotic shift in dialysis derived media.

Beyond mechanistic contributions to the pathogenesis of CVD in HD patients, study findings have implications for in vitro cardiac culture. As a mode of toxicity screening, the culture of iPSC derived CM with unmodified plasma and resuspended platelets validates patient blood samples as exposure conditions representative of a disease state. The use of patient blood in culture media enables the assessment of specific tissue changes without the need for preliminary identification of molecular perpetrators of disease. Observations of consistent cardiac tissue maturation in healthy plasma and tissue remodeling by platelets suggest potential for incorporation in the future toolkit of CM culture. Platelets could drive structural remodeling without inducing proliferation, while plasma may yield tissues with stronger and more concerted contraction for macroscopic tissue study. The latter may additionally contribute to bridging the therapeutic application of tissue engineering in autologous organ replacement and repair. For example, the use of healthy donor plasma can supplement the development of an ex vivo cardiac patch for surgical repair of congenital defects[19]. However, mechanisms warranting further investigation include the expression of FAP, which is typically low-to-nonexistent in healthy hearts[20], and matricellular expression of POSTN which indicates fibroblast activation when produced de novo[18] even though it was proportionally diluted over time in all test cultures relative to day 0 controls. Broader application of the plasma and platelet toolkit warrants further study on viability, complexity, and consistency effects in the in vitro culture of other organ system formats.

Study limitations include non-comprehensive media characterization, trial number, CM tissue variation upon starting experimental culture, and day-to-day imaging condition variability. While media characterization was limited, key markers symptomatic of the pro-fibrotic milieu in ESRD sufficiently determined representative differences attributable to uremia, acute response to HD, chronic elevation by morbidity, and platelet sourced factors[10]. The effects of low trial number were most notably exhibited in the low statistical power between donor types in media characterization, with three donations collected per test group (pre-HD, post-HD, and healthy). The experiment using all collected blood samples was duplicated, yielding a total of six independent trials per test condition. Experimental culture with blood derived media was initiated fourteen days after cardiac differentiation when tissues achieved proliferative and contractile stability. Even though only spontaneously contracting CM were tested, cultures exhibited a fair degree of variation in isotropy and clustering. Inconsistency of contractile features made comparative visual analysis difficult. In lieu of a universally applicable methodology for tracking muscular alignment, signal histogram analysis was employed broadly as a catch-all for assessing wholesale complexity. Similarly, daily intermittent imaging variability and tissue thickening made the application of fractal analysis impossible for inter-tissue comparison, given limited image depth of focus. Consequent to daily image condition variation, t

test comparisons against day 0 were found to be more insightful than linear correlation against time.

Future improvement may focus on further sample fractionation, model improvement, functional endpoint characterization, and the broader study of effects on other tissues. In this study, platelet effects on cardiac tissues were subtractively determined from plasma. Combination culture with platelets and plasma may enhance observed remodeling events, while further plasma fractionation could explicate granular matricellular effects by molecular size. Scaffolding[21], controlled release of cardiac differentiators[22], improved seeding by acoustics[23], and conditioning through mechanical and electrical pacing[24] could improve starting point cardiac tissue consistency. The use of patient-derived iPSC[25] and CM co-culture with CF[26] could generate a more clinically relevant platform for studying fibrotic remodeling. Functional characterization of stiffness, conduction, and contractile strength should accompany assessment of maturity and remodeling outcomes[27,28]. Study expansion to renal and bone tissues would enhance systemic understanding of CKD progression[29] and renal osteodystrophy[30].

Works Cited

1. M. G. Shlipak, L. F. Fried, M. Cushman, T. A. Manolio, D. Peterson, C. Stehman-Breen, A. Bleyer, A. Newman, D. Siscovick, B. Psaty, Cardiovascular mortality risk in chronic kidney disease: Comparison of traditional and novel risk factors. J. Am. Med. Assoc. 293, 1737–1745 (2005).
2. Jankowski J, Floege J, Fliser D, Böhm M, Marx N. Cardiovascular Disease in Chronic Kidney Disease: Pathophysiological Insights and Therapeutic Options. Circulation. 2021 Mar 16;143(11):1157-72.
3. Wang X, Shapiro JI. Evolving concepts in the pathogenesis of uraemic cardiomyopathy. Nature Reviews Nephrology. 2019 Mar;15(3):159-75.
4. Mizobuchi M, Towler D, Slatopolsky E. Vascular calcification: the killer of patients with chronic kidney disease. Journal of the American Society of Nephrology. 2009 Jul 1;20(7):1453-64.
5. Radhakrishnan A, Pickup LC, Price AM, Law JP, Edwards NC, Steeds RP, Ferro CJ, Townend JN. Coronary microvascular dysfunction: a key step in the development of uraemic cardiomyopathy?. Heart. 2019 Sep 1;105(17):1302-9.
6. González A, Schelbert EB, Díez J, Butler J. Myocardial interstitial fibrosis in heart failure: biological and translational perspectives. Journal of the American College of Cardiology. 2018 Apr 17;71(15):1696-706.
7. Lekawanvijit S. Cardiotoxicity of uremic toxins: a driver of cardiorenal syndrome. Toxins. 2018 Sep;10(9):352.
8. Jimbo R, Kawakami-Mori F, Mu S, Hirohama D, Majtan B, Shimizu Y, Yatomi Y, Fukumoto S, Fujita T, Shimosawa T. Fibroblast growth factor 23 accelerates

phosphate-induced vascular calcification in the absence of Klotho deficiency. Kidney international. 2014 May 1;85(5):1103-11.
9. Fassett RG, Venuthurupalli SK, Gobe GC, Coombes JS, Cooper MA, Hoy WE. Biomarkers in chronic kidney disease: a review. Kidney international. 2011 Oct 2;80(8):806-21.
10. Velasquez-Mao AJ, Velasquez MA, Hui Z, Armas-Ayon D, Wang J, Vandsburger MH. Hemodialysis exacerbates proteolytic imbalance and pro-fibrotic platelet dysfunction. Scientific reports. 2021 Jun 3;11(1):1-4.
11. Kokubo K, Kurihara Y, Kobayashi K, Tsukao H, Kobayashi H. Evaluation of the biocompatibility of dialysis membranes. Blood purification. 2015;40(4):293-7.
12. Velasquez-Mao AJ, Velasquez MA, Vandsburger MH. Cyclical depressurization degranulates platelets in an agonist-free mechanism of platelet activation. **IN REVIEW**.
13. Tsun Wong AK. Platelet biology: the role of shear. Expert review of hematology. 2013 Apr 1;6(2):205-12.
14. Park Y, Tantry US, Koh JS, Ahn JH, Kang MG, Kim KH, Jang JY, Park HW, Park JR, Hwang SJ, Park KS. Novel role of platelet reactivity in adverse left ventricular remodelling after ST-segment elevation myocardial infarction: the REMODELING trial. Thrombosis and haemostasis. 2017;117(05):911-22.
15. Lian X, Zhang J, Azarin SM, Zhu K, Hazeltine LB, Bao X, Hsiao C, Kamp TJ, Palecek SP. Directed cardiomyocyte differentiation from human pluripotent stem cells by modulating Wnt/β-catenin signaling under fully defined conditions. Nature protocols. 2013 Jan;8(1):162-75.
16. Kim BJ, Kim YH, Lee YA, Jung SE, Hong YH, Lee EJ, Kim BG, Hwang S, Do JT, Pang MG, Ryu BY. Platelet-derived growth factor receptor-alpha positive cardiac progenitor cells derived from multipotent germline stem cells are capable of cardiomyogenesis in vitro and in vivo. Oncotarget. 2017 May 2;8(18):29643.
17. Ivey MJ, Tallquist MD. Defining the cardiac fibroblast. Circulation Journal. 2016:CJ-16.
18. Gibb AA, Lazaropoulos MP, Elrod JW. Myofibroblasts and fibrosis: mitochondrial and metabolic control of cellular differentiation. Circulation Research. 2020 Jul 17;127(3):427-47.
19. Velasquez-Mao AJ, Tsao CJ, Monroe MN, Legras X, Bissig-Choisat B, Bissig KD, Ruano R, Jacot JG. Differentiation of spontaneously contracting cardiomyocytes from non-virally reprogrammed human amniotic fluid stem cells. PLoS One. 2017 May 17;12(5):e0177824.
20. Hoffmann DB, Fraccarollo D, Galuppo P, Frantz S, Bauersachs J, Tillmanns J. Genetic ablation of fibroblast activation protein alpha attenuates left ventricular dilation after myocardial infarction. PloS one. 2021 Mar 5;16(3):e0248196.
21. Madden LR, Mortisen DJ, Sussman EM, Dupras SK, Fugate JA, Cuy JL, Hauch KD, Laflamme MA, Murry CE, Ratner BD. Proangiogenic scaffolds as functional templates for cardiac tissue engineering. Proceedings of the National Academy of Sciences. 2010 Aug 24;107(34):15211-6.

22. Tsao CJ, Taraballi F, Pandolfi L, Velasquez-Mao AJ, Ruano R, Tasciotti E, Jacot JG. Controlled release of small molecules for cardiac differentiation of pluripotent stem cells. Tissue Engineering Part A. 2018 Dec 1;24(23-24):1798-807.
23. Serpooshan V, Chen P, Wu H, Lee S, Sharma A, Hu DA, Venkatraman S, Ganesan AV, Usta OB, Yarmush M, Yang F. Bioacoustic-enabled patterning of human iPSC-derived cardiomyocytes into 3D cardiac tissue. Biomaterials. 2017 Jul 1;131:47-57.
24. Ruan JL, Tulloch NL, Razumova MV, Saiget M, Muskheli V, Pabon L, Reinecke H, Regnier M, Murry CE. Mechanical stress conditioning and electrical stimulation promote contractility and force maturation of induced pluripotent stem cell-derived human cardiac tissue. Circulation. 2016 Nov 15;134(20):1557-67.
25. Sacchetto C, Vitiello L, de Windt LJ, Rampazzo A, Calore M. Modeling cardiovascular diseases with hipsc-derived cardiomyocytes in 2D and 3D cultures. International journal of molecular sciences. 2020 Jan;21(9):3404.
26. Rupert CE, Kim TY, Choi BR, Coulombe KL. Human cardiac fibroblast number and activation state modulate electromechanical function of hiPSC-cardiomyocytes in engineered myocardium. Stem cells international. 2020 Jul 16;2020.
27. Babaei B, Velasquez-Mao AJ, Pryse KM, McConnaughey WB, Elson EL, Genin GM. Energy dissipation in quasi-linear viscoelastic tissues, cells, and extracellular matrix. Journal of the mechanical behavior of biomedical materials. 2018 Aug 1;84:198-207.
28. Babaei B, Velasquez-Mao AJ, Thomopoulos S, Elson EL, Abramowitch SD, Genin GM. Discrete quasi-linear viscoelastic damping analysis of connective tissues, and the biomechanics of stretching. Journal of the mechanical behavior of biomedical materials. 2017 May 1;69:193-202.
29. Zhou D, Liu Y. Understanding the mechanisms of kidney fibrosis. Nature Reviews Nephrology. 2016 Feb;12(2):68-70.
30. Slatopolsky E, Gonzalez E, Martin K. Proceedings: Pathogenesis and Treatment of Renal Osteodystrophy. Blood purification. 2003;21(4-5):318-26.

Chapter 5

Conclusions and Future Direction

Platelets play a significant role in the progression of cardiovascular disease in chronic kidney disease. Platelet secretomes exhibit distinctly pro-fibrotic phenotypes in hemodialysis patients regardless of uremic state. In fact, post-clearance platelets exhibit greater capacity for promoting fibrosis in that platelet reticulation refreshes RNA and granule proteins that drive fibrogenesis and matrix remodeling. Chronic progression towards pro-fibrotic platelet phenotypes is proposed to be caused by shortened circulatory halflives and accumulating circulation of platelet released factors, in addition to prolonged uremic effects, in a vicious self-reinforcing cycle. Faster prescribed blood filtration rates and prior time on dialysis comprised risk factors for platelet secretome dysfunction. To explain the former, higher shear and faster pressure loss to friction implicit to the use of faster flow rates stimulate platelet activation. However, between shear and pressure, the latter induces degranulation without the need for surface receptor signal transduction. This mechanotransductive mechanism harmfully misdirects secretory mechanisms intended for paracrine signaling at sites of injury to become more endocrine in nature. The harmful effects of platelet secretome dysfunction on cardiac tissue can be directly observed by network remodeling of troponin and myofibroblast activation.

Findings have direct implications for the future of dialysis, design of blood-contacting medical devices, and tissue engineering. Most immediately, results scientifically support the prescription of slower flow rates in dialysis. Next, while more frequent dialysis may aid the management of uremia, it may not delay multiple organ fallout because of the counterproductivity of the therapy itself as it stands for platelet dysregulation. Platelet characterization should be used to personalize medical treatment to more optimally balance uremic clearance with platelet and leukocyte dysregulation. Ideally, minimally disruptive dialysis with potential co-medication could enable more frequent management of uremia without platelet disruption. Bio-inert fluidics design in dialyzers needs to be considered with the same or greater fervor as the biocompatibility of materials used. Beyond hemodialysis, the thresholds for bio-active friction losses and precipitous pressure changes should be more thoroughly investigated and incorporated in the design of all blood contacting medical devices, like ECMO which is also well known to induce platelet dysfunction. Separately, models developed have promising implications for the toolbox of in vitro cardiac culture. Donor blood culture could be used to screen for toxicity without the need for biopsy or preliminary identification of molecular perpetrators of disease. Meanwhile, platelet culture could be used as a tool for studying or inducing tissue remodeling, and the use of healthy donor plasma could bridge the maturation and therapeutic applicability of autologous organ repair.

Future use of platelets as therapeutic agents and diagnostic tools for left ventricular remodeling, microvascular dysfunction, and myocardial interstitial fibrosis could aid the prevention of congestive heart failure.